Zeitabhängige Untersuchungen zu reaktiven Streuprozessen

Dissertation

zur Erlangung des Grades eines Doktors

der Naturwissenschaften

vorgelegt von

M. Sc. Ioan Cristian Morari

aus Prundu Bârgăului, Rumänien

eingereicht beim Fachbereich 8

der Universität-Siegen

Siegen 2001

Contents

Abbreviations and notations

TDSE - Time-Dependent Schrödinger Equation
PES - Potential Energy Surface
WP - WavePacket
SF - Space-Fixed (coordinate system)
BF - Body-Fixed (coordinate system)
DVR - Discrete Variable Representation
FBR - Finite Basis Representation
FFT - Fast Fourier Transform
DIM - Diatomics In Molecules
R, r, θ - Jacobi coordinates
P_m^l - associated Legendre functions
Φ_n - Chebyshev polynomials
$\hat{J}$ - the total angular momentum operator for the A-BC system
J - the total angular momentum quantum number of an A-BC system
j - the diatomic angular momentum quantum number of the diatomic (BC) molecule
v - vibrational quantum number of the BC molecule
l - the relative angular momentum quantum number for A - BC system
Ω - the projection of $\hat{J}$ onto the BF axis quantum number
M - the projection of $\hat{J}$ onto the SF axis quantum number

Atomic units

The most important atomic units are summarised in the table below [1]:

Observable	Atomic unit
Energy	27.21183 eV (1 hartree - E_h)
Length	0.529177×10^{-10} m (1 bohr - a_0)
Time	2.418884×10^{-17} s
Mass	9.109381×10^{-31} kg

[1] The latest set of constants '1998 CODATA recomended values' is available at http://physics.nist.gov/cuu/Constants/.

1 Introduction

Molecular dynamics involves the study of the molecular mechanism of elementary physical and chemical processes [1]. It is concerned with both intramolecular and intermolecular collisions and with the means of promoting such collisions like using the molecule-photon interaction. Chemical dynamics is one major discipline of this field since chemical change is brought by the motion of electrons and nuclei within reacting molecules.

In order to investigate chemical processes, "observables" such as "size" and "shape" of molecules may be of great interest. A quantitative measure for the "size" of molecules can be introduced, namely the *collision cross section*, an observable which is energy dependent. In the same way the *differential collision cross section* can be considered as a parameter describing the "shape" of molecules.

Investigations of collision cross sections can be done experimentally or theoretically as well. With the crossed-beam approach a direct study of bimolecular reactions is possible [2, 3, 4]. Ultrafast laser pulses in the femtosecond regime allow the study of elementary processes of the fast, direct type, before the surrounding molecules can interfere [5, 6, 7].

Theoretical methods fall in two large categories [1]: modelling and simulating a molecular system. The purpose of modelling is to gain insight into the mechanism of molecular phenomena. A simple calculation pointing to a possible theoretical interpretation is usually adequate. The aim of simulation is to give a quantitative correspondence of theory to experiment. Once the potential surface is known, several theoretical methods can be used in order to perform the simulation of the collision experiment.

The classical trajectory approaches [8] consist in solving Newton's equations of motion for the molecular system. A deficiency of classical methods is that basic quantum effects like tunneling or the zero-point motion cannot be described. These effects are extremely important for chemical reactions.

The aim of semiclassical methods is to correct this by including the most important quantum effects within the classical description of the dynamics (maintaining the simple implementation of classical mechanics) [9, 10, 11, 12]. For example, the wavepacket can be constrained to be of Gaussian form during the propagation [13, 14, 15].

Exact quantum mechanical calculations can provide good simulations of scattering experiments. Because of the non-local character of quantum wavepackets, a global simultaneous description of whole phase space is required. This leads to storage problems in the implementation. In the frame of exact quantum mechanical calculations, there are two basic approaches: the time-dependent and the time-independent ones.

The stationary coupled channel (CC) [16, 17] approach is based on the solution of

stationary scattering equations [18]. The computational effort within this method scales with the number of channels cubed. This is a serious computational bottleneck for systems with many channels.

Time-dependent quantum mechanical methods are based on the Schrödinger equation (TDSE)

$$i\hbar\frac{\partial\psi}{\partial t} = \hat{H}\psi,$$

where $\hat{H}$ is the Hamilton operator of the system and ψ is the nuclear wavefunction [2].

The central quantity to obtain in quantum dynamical treatments of chemical reactions is usually the quantum mechanical probability amplitude, represented by the scattering S-matrix (which will be discussed in the next section). Time-dependent methods are efficient for computing initial state-selected reaction probabilities. In this case, one column of the S-matrix can be obtained for a range of collision energies. Time-independent methods have the advantage that, at a given scattering energy, the whole S-matrix can be obtained directly (all state-to-state reaction probabilities are obtained in a single calculation). The extension to higher system (tetra atomic collisions) can be easily done within the time-dependent frame [19].

The purpose of the present work is to investigate chemical reactions by performing time-dependent quantum mechanical calculations for systems involving three atoms ("A-BC systems"). Reaction probabilities have to be computed in a given energy range, then cross sections and reaction rates can be calculated.

The time-dependent quantum mechanical approach to scattering processes has received considerable attention in recent years, although initial efforts were made several decades ago. Mazur and Rubin [20] solved the time-dependent Schrödinger equation for a collinear exchange reaction of type:

$$\mathrm{A{+}BC} \rightarrow \mathrm{AB} + \mathrm{C},$$

as early as in 1959. There was not much activity in this direction for the following decade, till the work of McCullough and Wyatt [21] in 1969 for collinear ($H + H_2$) collisions. In addition to computing averaged reaction probabilities, they mapped quantal flux patterns for the ($H + H_2$) reaction and explained the dynamics in terms of quantal whirlpools. They used an implicit propagation scheme for solving the TDSE. Unfortunately, the method involved tedious matrix inversion procedures and was computationally very expansive. Subsequently, a number of efficient numerical algorithms have been introduced for solving the TDSE resulting in a resurgence of activity in this area.

The introduction of the fast Fourier transform (FFT) method by Kosloff and Kosloff [22] for computing the action of the kinetic energy part of the Hamiltonian on the wave

[2] A detailed presentation of these methods follows in **Section 4**.

function was a significant development in the area of time-dependent quantum mechanics (TDQM).

The discrete variable representation (DVR) was introduced in the area of molecular dynamics by Light *et al.* [23, 24] for solving the time-independent Schrödinger equation (1982). The idea of DVR representation for the potential matrix elements originates from works of Dickinson and Certain [25]. In 1984 Tal-Ezer and Kosloff [26] introduced a global propagation scheme based on the Chebyshev polynomial expansion of the evolution operator. This propagation scheme was improved by Mandelshtam and Taylor in 1995 [27, 28]. In 1998 Gray and Balint-Kurti introduced a new algorithm for propagating only the real part of the wave function [29].

Converged six-dimensional (6D) reactive scattering calculations of four-atom systems have been reported using the TDQM method [30, 31].

The outline of the present work is the following: a set of basic definitions forms the second section. The third section is devoted to a more detailed insight into the mathematical aspects of scattering theory (time-dependent and time-independent formulations). In the fourth section a presentation of the A-BC system in terms of quantum mechanics is given (Hamiltonian operator, basis functions which are well suited for describing the system, etc.). The implementation of time-dependent methods for A-BC systems is described in the fifth section. Finally, in the sixth section, the results obtained with the implementation, described in section 5, are presented.

2 General definitions

When an atom A approaches a molecule BC, there are several possibilities for the evolution of the system. The first situation can be represented as:

$$\text{A+BC}(v,j) \rightarrow \text{A} + \text{BC}\ (v,j),$$

where v and j are the vibrational and rotational quantum numbers of the diatomic molecule BC. This is the situation of *elastic scattering* when the internal state of the molecule BC does not change.

The second situation is called *inelastic scattering*:

$$\text{A+BC}(v,j) \rightarrow \text{A} + \text{BC}\ (v',j'),$$

when the reactants and the products are the same but the internal quantum states (v',j') of the products have been changed. Finally, we can have the following situation:

$$\text{A+BC}(v_1,j_1) \rightarrow \text{AB}(v_2,j_2)+\text{C},$$

or

$$\text{A+BC}(v_1,j_1) \rightarrow \text{AC}(v_3,j_3) + \text{B}.$$

The index "1" means "ro-vibrational states of the reactants" and index "2" (or "3") means "ro-vibrational states of products". The atom "A" and the molecule "BC" are the *reactants* while the molecule "AB" and the atom "C" (respectively the molecule "AC and the atom"B") are the *products*. The two possible final arrangements are the two *reaction channels* of the reaction.

At small energies the collisions are mostly of purely elastic nature. By increasing the energy, first the rotational levels of the BC molecule are excited. If the collision energy still increases, the activated chemical reaction might occur with different reaction channels according to the topology of the potential energy surface. At even higher energies (e.g. comparable with the well of the PES) the complete dissociation happens:

$$\text{A+BC} \rightarrow \text{A} + \text{B} + \text{C}.$$

By using the time-dependent techniques, we want to investigate the cross sections for the (A+BC) type reaction in a energy range $\Delta E \approx 1$ eV (e.g. between 0.5 eV and 1.6 eV in the case of $\text{D+H}_2 \rightarrow$ DH +H reaction) where ro-vibrational excitations and chemical reactions take place.

2.1 The cross section

The differential cross section [33] is defined for elastic, inelastic or reactive scattering according to the rule

$$\frac{d\sigma}{d\Omega}d\Omega = \frac{number\ of\ particles\ scattered\ into\ d\Omega\ per\ unit\ time}{number\ of\ incident\ particles\ crossing\ unit\ area\ per\ unit\ time}. \quad (1)$$

This leads to

$$\frac{d\sigma}{d\Omega}d\Omega = \frac{r^2|j_{scatt}|}{|j_{incid}|}d\Omega, \quad (2)$$

where r is the distance between the physical system and the measurement apparatus, j_{scatt} is the scattered flux of particles in the $d\Omega$ solid angle, and j_{incid} is the incident flux of particles.

To give a clear picture of the theoretical formulation for the cross section, a model is helpful. This model must be able to describe the following:

- The projectile-target interaction (model potential)
- The interaction between internal degrees of freedom for projectile or target (for system which are not point-like)
- The asymptotic 'in' (entrance) and 'out' (exit) states

We can start classically with the simple model of a *point* which collides with a *sphere*. Then the cross section σ will be the surface of a cut through the center of the sphere, $\sigma = \pi R^2$, where R is the radius of the sphere. A model with two spheres will improve this formulation to the new cross section $\sigma = \pi(R + r)^2$, where R and r are the radii of the target and projectile. For the angular dependence θ this can be expressed in the differential form

$$d\sigma(\theta) = 2\pi b db. \quad (3)$$

b is the *impact parameter* and db is the width of the annulus which scatters particles at the angle θ.

We can improve this model by imaging that the spheres are not hard, but they allow some "tunnelling effects". According to Levine and Bernstein [34], by using this model, the differential cross section can be written as

$$d\sigma = 2\pi P(b) b db, \quad (4)$$

where $P(b)$ is the *opacity of the target* (it is defined as the fraction of particles at impact parameter b that leads to a scattering process).

A hard sphere model leads to a step function for $P(b)$ which is 1 from 0 to R (target radius) and 0 from R to infinity. More realistic classical and quantum models consider

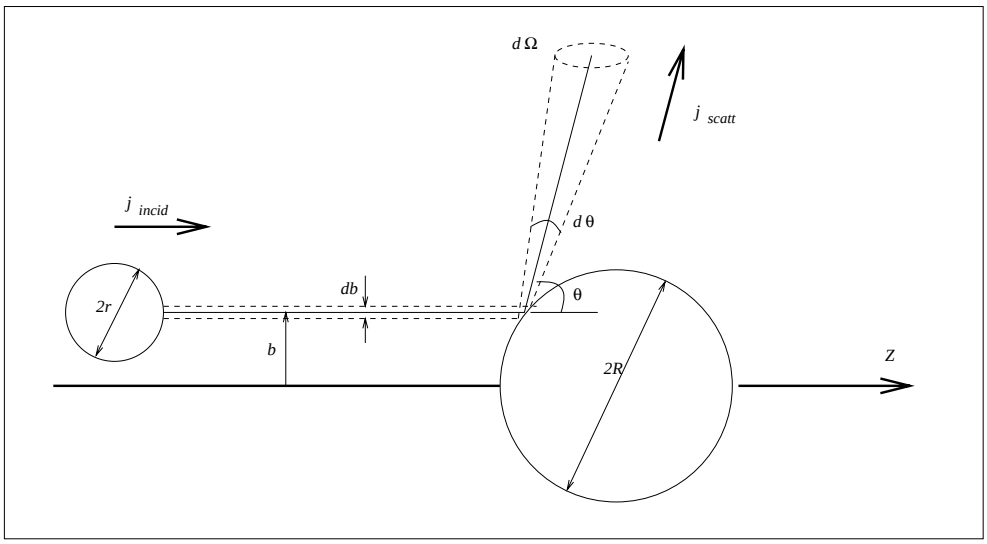

Figure 1: Different parameters for the collision of two hard spheres are given. b is the impact parameter, r and R are the radii of projectile and target; j_{incid} is the incident flux of particles, j_{scatt} is the scattered flux of particles; θ is the scattering angle and $d\Omega$ is the solid angle in which the particles with impact parameters between $b - db/2$ and $b + db/2$ are scattered.

smooth expressions for $P(b)$. In the realistic case, $P(b)$ is a smooth function which decrease from $P(b) = P_0$, $P_0 \leq 1$ (close to the target) to $P(b) = 0$ (far away form the target) - see Figure 2.

The total cross section is defined as

$$\sigma^{tot} = \int_0^\infty 2\pi b P(b) db. \tag{5}$$

The expression above can be rewritten in the momentum space as

$$\sigma^{tot} = \int 2\pi b P^l dl, \tag{6}$$

where l is the relative angular momentum and P^l is the reaction probability corresponding to a given l. By taking into account the physical meaning of the angular momentum and its classical definition ($\vec{l} = \vec{r} \times \vec{p}$, $\vec{r}$ is the distance vector and $\vec{p}$ is the momentum vector) and comparing with the quantum definition of the angular momentum [35] we can write

$$bk \approx l + \frac{1}{2} \;\; or \;\; b \approx \frac{1}{k}(l + \frac{1}{2}), \tag{7}$$

with $\vec{k}$ the wave number of the projectile ($\vec{p} = \hbar\vec{k}$). By switching from continuum to discrete representation we get for Eq. (6) the following expression [34]:

$$\sigma^{tot} = \frac{\pi}{k^2} \sum_{l=0}^{\infty} (2l + 1) P^l. \tag{8}$$

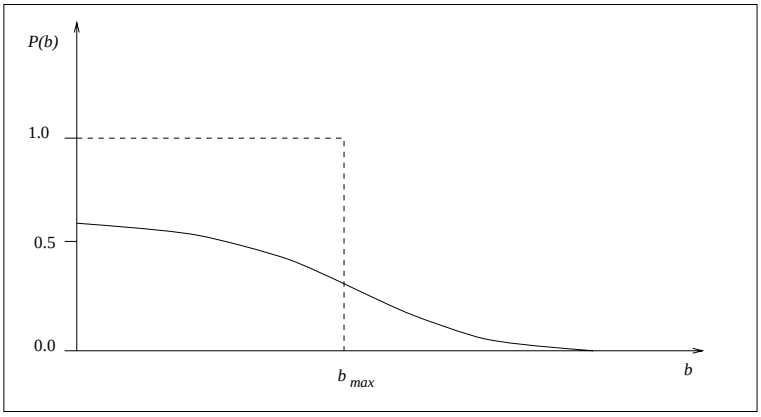

Figure 2: The shape of the opacity function $P(b)$ for a hard sphere model (dashed line) and for a realistic model (continuous line). $b_{max} = R + r$ is the largest impact parameter allowed by the hard spheres model.

In this formulation the relative angular momentum has only discrete values. P^l are now the *reaction probabilities* at a given angular momentum l, and the total cross section σ^{tot} is described entirely in a quantum mechanical formulation.

2.2 The S-matrix

In order to compute the reaction probabilities P^l in Eq. (8) we introduce the S-matrix [36]:

$$S_{out,in} = \langle \psi^+_{out} | \psi^-_{in} \rangle. \tag{9}$$

$|\psi^-_{in}\rangle$ is the quantum state of the system at an initial time in the entrance channel and $\langle \psi^+_{out}|$ is the quantum state of the system at a final time in the exit channel.

In order to compute the total cross section, using Eq. (8), we need to know the reaction probabilities P^l. This time-dependency of the S-matrix can be made explicit by formulating it in the operator style [37]

$$S = \lim_{t \to \infty, t' \to -\infty} U(t, t'), \tag{10}$$

where $U(t, t')$ is the *evolution operator* [1, 33].

Until now we did not discuss the internal structures of the target, respectively of the projectile. Formally this can be introduced straightforwardly into the formulation above. The S-matrix and the reaction probabilities will be indexed by those quantum numbers corresponding to the internal degrees of freedom, of the target and projectile, respectively. For the case of a diatomic molecule we have to take into account the rotational and the vibrational quantum numbers $(v,\ j)$.

The total angular momentum $\hat{J}$ of the atom-molecule system is

$$\hat{J} = \hat{l} + \hat{j}, \tag{11}$$

where $\hat{j}$ is the rotational angular momentum of the target and $\hat{l}$ is the relative angular momentum for the target-projectile system.

In terms of the S-matrix the **state-to-state reaction probability** can be written as

$$P^J_{v'j',vj} \equiv (2j+1)^{-1} \sum_{\Omega,\Omega'} |S^J_{v'j'\Omega',vj\Omega}|^2 \tag{12}$$

or:

$$P^J_{v'j',vj} = (2j+1)^{-1} \sum_{l,l'} |S^J_{v'j'l',vjl}|^2. \tag{13}$$

$2j+1$ is the degeneracy of the initial rotational level. l and l' are the relative angular momentum quantum numbers of the two components of the system before and after the reaction, Ω and Ω' are the projections of $\hat{J}$ onto the Z axis of the coordinate system before and after the collision.

The general expression for the reaction probability can be considered as a sum over reaction probabilities at different "impact parameters" [38]

$$P(E) = \sum_{J=0,1,..}^{\infty} (2J+1) P^J(E), \tag{14}$$

where J is the total angular momentum quantum number, and E is the collision energy. J plays the role of the "impact parameter" in the quantum mechanical formulation. The partial wave reaction probability $P^J(E)$ can be written as

$$P^J(E) = \sum_{v,j,\Omega} \sum_{v',j',\Omega'} P^J_{v'j'\Omega',vj\Omega}(E), \quad J = 0, 1, ... \tag{15}$$

where $P^J_{v'j'\Omega',vj\Omega}$ is the detailed state-to-state reaction probability between initial and final ro-vibrational states.

For the Hamiltonian we use in the case of A-BC system, J is a good quantum number. This property allow us to do separate calculations for each P^J, $J = 0, 1, 2, ...$ in order to compute the total cross section given in Eq. 8 [34, 36].

On the other hand, different Ω channels in the wavefunction do couple together. As a result, more functions or grid points are needed to store the complete information about the wavefunction. By increasing the number of grid points in the angular part we need more core memory. Therefore several approximate methods are proposed for computing the reaction probabilities for $J > 0$.

The J-shift approach is a very useful approximation for the J dependence of $P^J(E)$ [38]. The reaction probability $P^{J>0}$ is written as a function of the reaction probability for $J = 0$

$$P^J(E) \approx P^{J=0}(E - E_J^*), \tag{16}$$

where $E_J^* = B^* J(J+1)$ is the rotational energy at the transition state. The physical meaning of this approach is related to the presence in the Hamiltonian of *the effective potential* term $V_{eff} = V_0 J(J+1)$, where V_0 is a constant, depending on the total moment of inertia of the system. It is assumed that the reaction probability for a given J is roughly the reaction probability for $J = 0$ shifted in energy by a quantity which is equal with the centrifugal barrier for the given J.

According to Bowmann [38], the J-shift is a good approach as long as the coupling between the different Ω channels in the wavefunction is small.

Several cross sections are defined as follows: the integral cross section given in Eq. (8) became

$$\sigma^{tot}_{v'j',vj} = \frac{\pi}{k^2_{vj}} \sum_J (2J+1) P^J_{v'j',vj}(E). \tag{17}$$

The differential cross section:

$$\sigma_{v'j'\Omega',vj\Omega}(\theta) = \frac{1}{4k^2_{vj\Omega}} |\sum_J (2J+1) d^J_{\Omega\Omega'}(\theta) T^J_{v'j'\Omega',vj\Omega}|^2. \tag{18}$$

$d^J_{\Omega\Omega'}$ are the Wigner functions [35], $\theta \in [0, \pi]$ is the scattering angle, and the T^J operator is given as [33]

$$T^J_{v'j'\Omega',vj\Omega} = 1 - S^J_{v'j'\Omega',vj\Omega}. \tag{19}$$

2.3 The reaction rate

Once the cross sections for a given reaction and a given energy range are known, we can compute the reaction rate constant [34, 39]. It is defined as the speed of formation of the products. The rate constant $k(T)$ can be computed by using the model of kinetic theory for gases. Maxwell's distribution of the velocities $f(v)$ in an ideal gas is [40]

$$f(v)dv = 4\pi v^2 (\mu/2\pi kT)^{(3/2)} exp(-\mu v^2/2k_B T)dv. \tag{20}$$

T is the temperature, μ - the reduced mass, v is the velocity and k_B is the Boltzmann constant ($k_B = 1.380658 \times 10^{-23}$ J/K).

Thermal motion leads to collisions between molecules, hence to chemical reactions, depending on the energy of collision. A simple model leads to the *Arrhenius-type* reaction rate, [34] in which the cross section σ_{tot} is considered to be of the form

$$\sigma^{tot} = \pi b^2_{max} = \begin{cases} 0, & E_{col} \leq E_0 \\ \pi d^2 (1 - E_0/E_{col}), & E_{col} \geq E_0 \end{cases} \tag{21}$$

where d is the "radius" of a molecule, E_{col} is the collision energy and E_0 is the threshold energy for the reaction. By integrating with respect to collision energy the product of this with the Maxwell distribution of the velocities in a gas we get

$$k(T) = Ae^{-\frac{E_0}{k_B T}}, \quad A = A(\sqrt{T}). \tag{22}$$

If we take into account that the cross section is energy dependent, this simple model cannot be used any more. The integral over $f(v)$ given by Eq. 20 in the gas will lead to a new formulation of the reaction rate in the gas phase

$$k_\alpha(T) = \sqrt{\frac{8}{\pi\mu(k_B T)^3}} \int_0^\infty E_{col}\sigma_\alpha(E_{col})e^{-E_{col}/k_B T} dE_{col}. \tag{23}$$

α is the electronic state, and σ_α^{col} is the cross section. The rate constant can be evaluated if we know the values of the cross sections in an energy range of the order of eV. To reach a convenient accuracy in the integration, we need information about the cross sections at relatively many energies. These requirements can be fulfilled by the time-dependent formulation of scattering theory.

3 Scattering theory

This section is devoted to the mathematical aspects of the scattering theory. The two paradigms - time-dependent and time-independent formulation of scattering theory are presented.

First we remark that the equations describing the scattering processes can be splitted, from the mathematical point of view, into two categories: boundary condition problems and initial value problems. Time-independent solutions fall in the first category [41, 42]. Substitution of different expansions of the wavefunction (like plane or spherical waves) into the time-independent Schrödinger equation lead to coupled channels equations which are typically ordinary differential equations. These equations can be solved by various finite difference methods [43].

Time-dependent methods are initial value problems. When the time-dependent methods are used to calculate time-independent observables the role of time lies mainly in the fact that the problem becomes an initial value one, and a single calculation provides information over a wide range of energies. One can prepare the initial wavefunction for a specified set of initial conditions. Next, the initial wavepacket is propagated forward in time. During the propagation the reaction attributes are extracted out of the wavepacket. This can be done for example by projecting the final wavefunction onto individual ro-vibrational states or by computing the flux through a dividing line or a surface far away from the interaction region.

3.1 Time-independent formalism

3.1.1 The Lippman - Schwinger equation

For a simple model (structureless particle) we assume that the Hamiltonian can be written as [33]

$$\hat{H} = \hat{H}_0 + \hat{V}, \tag{24}$$

with

$$\hat{H}_0 = \frac{\hat{p}^2}{2\mu}$$

being the kinetic energy operator.

In absence of a scatterer (potential $\hat{V} = 0$) an energy eigenstate would be a free-particle state. The presence of a potential causes the energy eigenstate to be different from a free-particle state. If the scattering process is elastic we are interested in obtaining a solution of the full Hamiltonian Schrödinger equation with the same energy eigenvalue. If $|\phi\rangle$ is the solution of the free-particle Hamiltonian

$$\hat{H}_0|\phi\rangle = E|\phi\rangle \tag{25}$$

and $|\psi\rangle$ is the solution for the full Hamiltonian

$$(\hat{H}_0 + \hat{V})|\psi\rangle = E|\psi\rangle, \tag{26}$$

then we look for a solution of Eq. (26) satisfying the condition: $|\psi\rangle \to |\phi\rangle$, when $\hat{V} \to 0$. The desired solution is

$$|\psi\rangle = \frac{1}{E - \hat{H}_0}\hat{V}|\psi\rangle + |\phi\rangle. \tag{27}$$

Asymptotic states in the scattering process will be of the form

$$|\psi^{\pm}\rangle = |\phi\rangle + \frac{1}{E - \hat{H}_0 \pm i\epsilon}\hat{V}|\psi^{\pm}\rangle, \tag{28}$$

where

$$\hat{G}^{\pm} = \frac{1}{E - \hat{H}_0 \pm i\epsilon}$$

is the Green function of the system.

Several strategies can be used to solve Eq. (28) (the Lippman-Schwinger equation).

We define the transition operator, $\hat{T}$ as follows:

$$\hat{V}|\psi^{\pm}\rangle = \hat{T}|\phi\rangle; \tag{29}$$

where $\hat{T}$ can be derived from Eq. (28)

$$\hat{T} = \hat{V} + \hat{V}\hat{G}^{\pm}\hat{T} = \hat{V}\sum_{n=0}^{\infty}(\hat{G}^{\pm}\hat{V})^n. \tag{30}$$

The spatial representation for the solution of the Lippman - Schwinger equation is given as

$$\langle\vec{x}|\psi^{\pm}\rangle = \langle\vec{x}|\phi\rangle + \int d^3\vec{x}'\langle\vec{x}|\hat{G}^{\pm}|\vec{x}'\rangle\langle\vec{x}'|\hat{V}|\psi^{\pm}\rangle \tag{31}$$

with

$$\langle\vec{x}|\phi\rangle = \frac{e^{i\vec{p}\vec{x}/\hbar}}{2\pi\hbar^{3/2}}.$$

Using the complex integration one finds that the matrix element of the Green's operator in the spatial representation has the form

$$\langle\vec{x}|\hat{G}^{\pm}|\vec{x}'\rangle = -\frac{2m}{4\pi^2\hbar^2}\frac{1}{|\vec{x} - \vec{x}'|}e^{i|\vec{x}-\vec{x}'|k}. \tag{32}$$

It is possible to give an iterative solution for Eq. (31). The idea is to start from an initial guess for $|\psi^{\pm}>$ then to refine by a self-consistent procedure. If we take $< \vec{x}|\psi^{+} > \to < \vec{x}|\phi >$ and we keep the first term in the expansion we get the *Born approximation* described in the textbook of Sakurai [33].

For the simplest case we considered (a structureless particle), the asymptotic form of the Lippman-Schwinger equation can be written as

$$\psi^{\pm}(\vec{x}) = \frac{1}{(2\pi)^{3/2}}[e^{i\vec{k}\vec{x}} + \frac{e^{ikx}}{x} f(\vec{k}', \vec{k})], \tag{33}$$

with $x = |\vec{x}|$ and

$$f(\vec{k}', \vec{k}) = -\frac{1}{4\pi}(2\pi)^3 \frac{2m}{\hbar^2} \langle \vec{k}' | \hat{T} | \vec{k} \rangle$$

given as the *scattering amplitude*. $\vec{k}$, $\vec{k}'$ are the momenta before and after scattering. According to Eq. (33) the solution of the Lippman-Schwinger equation is the overlap between a plane wave and a spherical (scattered) wave at infinity [33, 36].

According to Eq. (33) the differential cross section can be expressed in terms of a scattering amplitude as

$$\frac{d\sigma}{d\Omega} = |f(\vec{k}', \vec{k})|^2. \tag{34}$$

In the case of a central field, Eq. (33) can be rewritten using the expansion of the plane wave in Bessel functions $j_l(kr)$

$$e^{i\vec{k}\vec{r}} = \sum_l (2l+1) i^l j_l(kr) P_l(\hat{k}\hat{r}). \tag{35}$$

$P_l(\hat{k}\hat{r})$ are the Legendre polynomials, $k = |\vec{k}|$ and $r = |\vec{r}|$. By comparing Eqs. (33) and (35) the scattering amplitude is given as

$$f(\vec{k}', \vec{k}) = \sum_l (2l+1) f_l(k) P_l(cos\theta). \tag{36}$$

All the relations above concern the simple model of an elastic scattering for a structureless particle. In the case of molecules, the equations have in principle the same structure, but additional indices are required for the internal degrees of freedom. The overlap between a plane wave and a scattering wave (see Eq. (33)), becomes in case of an atom-diatom scattering for $R \to \infty$ [34, 44]:

$$G(R) \to \frac{1}{\sqrt{k_{j'v'}}} \delta_{j'j} \delta_{l'l} \delta_{v'v} [e^{-i(k_{jv}R - l\pi/2)} - S^J_{j'l'v',jlv} e^{i(k_{j'v'}R - l'\pi/2)}]. \tag{37}$$

$G(R)$ is the radial part of the wavefunction for the A-BC system, expressed in Jacobi coordinates (see page 26), with R the distance between the single atom and the center of mass of the BC molecule, k is the atom-diatom relative momentum, j is the label for the rotational quantum number, l is the relative angular momentum quantum number, v is the label for the vibrational quantum number. S^J is the S-matrix for the total angular momentum J. Primed indices mean "after reaction".

3.1.2 Time-independent wavepackets

There is another possibility to formulate scattering theory, with time-independent wavepackets [45, 46]. It is based on the time to energy Fourier transform of the equation

$$\Psi(t) = exp(-i\hat{H}t/\hbar)\Psi(0) \tag{38}$$

where $\Psi(0)$ is the wavepacket at time $t = 0$, leading to

$$\Psi(E,T) = \frac{1}{2\pi\hbar}\int_0^T dt exp(iEt/\hbar)exp(-i\hat{H}t/\hbar)\Psi(0) \tag{39}$$

where $\hat{H} = \hat{H}_0 + \hat{V}$ is the total hamiltonian, $\hat{H}_0$ is the kinetic energy, $\hat{V}$ is the potential energy.

The scattering equations describe the scattering at a well defined energy E as in the section before, but they involve an initial $\mathcal{L}^2$ wavepacket which contains a whole range of energies (time independent wavepacket Schrödinger equation) [45, 46]

$$(E - \hat{H})\Psi(E, T \to \infty) = \frac{i}{2\pi}\Psi(0). \tag{40}$$

The inhomogeneous Schrödinger equation for the scattered wave can be written

$$(E - \hat{H}_0)\Psi^+(E) = \hat{V}\Phi(E) \tag{41}$$

with

$$\Psi^+(E) = \Phi(E) + \frac{1}{E - \hat{H}_0 + i\epsilon}\hat{V}\Phi(E), \tag{42}$$

and $\hat{H}_0$ the unperturbed Hamiltonian. The unperturbed initial state $\Phi(E)$ satisfies

$$(E - \hat{H}_0)\Phi(E) = 0. \tag{43}$$

The time-independent wavepacket Lippman-Schwinger equation is

$$\Psi(E) = \frac{i}{2\pi(E - \hat{H} + i\epsilon)}\Psi(0). \tag{44}$$

In solving this equation, the following method is used: according to [45, 46], $\Psi(E)$ can be computed by using a Chebyshev expansion (see next section). We note:

$$\frac{i}{E - \hat{H} \pm i\epsilon} = \frac{i}{\Delta H}\frac{1}{\tilde{E} - \hat{H}_{norm} \pm i\eta}. \tag{45}$$

$\hat{H}_{norm} = (\hat{H} - \tilde{H})/\Delta H$, $\tilde{H} = \frac{1}{2}(H_{max} + H_{min})$ and $\Delta H = \frac{1}{2}(H_{max} - H_{min})$.
$\tilde{E} = (E - \tilde{H})/\Delta H$ and η is $\epsilon/\Delta H$. The Green's function is expanded in a set of Chebyshev polynomials

$$\frac{1}{(\tilde{E} - \hat{H}_{norm} \pm i\epsilon)} = \sum_{n=0}^{\infty} a_n(\alpha_\pm)\Phi_n(\hat{H}_{norm}), \tag{46}$$

$$\alpha_{\pm} = \tilde{E} \pm i\eta = \alpha_0 \pm i\eta, \tag{47}$$

$$a_n(\alpha_{\pm}) = i \int_{-1}^{1} ds \frac{\Phi_n(s)}{(\alpha_{\pm} - s)\sqrt{1 - s^2}}, \tag{48}$$

and the final solution for $\Psi(E)$ can be computed by applying this expansion (which includes only linear operators, so there are no problems in doing it directly) on the initial asymptotic state $\Psi(0)$.

3.2 Time-dependent formalism

For many physical situations the use of time-dependent methods is more convenient compared to the time-independent ones. Because time-dependent methods are initial value problems they are easier to implement. The time-dependent picture enables a simpler treatment of rearrangement problems in reactive scattering, compared to the time-independent methods. Besides these technical advantages, time-dependent methods lead to a better interpretation of the physical mechanism under discussion. The time variable also enables a description of externally driven systems (like molecules subject to strong laser fields) by introducing time-dependent Hamiltonians. The time-dependent approach is analogous to the classical mechanical description in that one obtains a physical picture of the underlying dynamics, but within the quantal framework.

Starting point in developing these methods is the time-dependent Schrödinger equation [1, 47]

$$i\hbar \frac{\partial \Psi(t)}{\partial t} = \hat{H}\Psi(t), \tag{49}$$

where $\hat{H}$ is the Hamiltonian operator of the system. This is a first-order differential equation in time, hence it has the following *formal solution* for time-independent $\hat{H}$

$$\Psi(t) = \hat{U}(t)\Psi(0) = exp\left(-\frac{i\hat{H}t}{\hbar}\right)\Psi(0), \tag{50}$$

where $\hat{U}(t)$ is the time evolution operator for the Schrödinger equation. Since this operator is not a linear one it cannot act directly on the initial state. We need a linear expansion of this operator, namely a polynomial one. According to Kosloff [48] this expansion can be optimally done by using a *Chebyshev polynomial expansion*

$$exp\left(-\frac{i\hat{H}t}{\hbar}\right) \approx \sum_{n=0}^{N} a_n S_n\left(-\frac{i\hat{H}t}{\hbar}\right). \tag{51}$$

S_n are complex Chebyshev polynomials [3] of order n.

[3] See the Appendix for the definition of the real Chebyshev polynomials.

To ensure the convergence of the expansion we have to renormalise the Hamiltonian operator to:

$$\hat{H}_{norm} = \frac{2(\hat{H} - \Delta E/2 - V_{min})}{\Delta E} \tag{52}$$

where ΔE is the energy range of the "real" Hamiltonian $\hat{H}$ and V_{min} is the lowest potential value.

Using this form for the evolution operator the time development of the wavefunction will be

$$\Psi(t+\Delta t) = exp\left(-\frac{i(\Delta E/2 + V_{min})\Delta t}{\hbar}\right) \sum_{n=0}^{N} a_n \left(\frac{\Delta t \Delta E}{2\hbar}\right) S_n\left(-i\hat{H}_{Norm}\right) \Psi(t), \tag{53}$$

$$\Delta E = E_{max} - E_{min} = T_{max} + V_{max} - V_{min}.$$

The coefficients a_n are Bessel functions [4]

$$a_0(\alpha) = J_0(\alpha), \quad a_n(\alpha) = 2J_n(\alpha), \ n = 1, ..., N.$$

The argument of the Bessel functions $(\Delta E \Delta t/2\hbar)$ is related to the volume of the time-energy phase space that is contained in the problem. The number of terms N needed to converge the expansion is determined by this volume. This is related to the asymptotic properties of Bessel functions: when the order n becomes larger than the argument α of the Bessel function $J_n(\alpha)$ decreases exponentially fast [48].

The energy domain ΔE is defined by imposing a cutoff for the kinetic (T_{cutoff}) and potential (V_{cutoff}) energy. The conditions are

$$T^{max}_{kinetic} < T_{cutoff}, \tag{54}$$

and

$$V^{max} < V^{max}_{cutoff}, \quad V^{min} > V^{min}_{cutoff}. \tag{55}$$

The energy domain has the expression

$$\Delta E = T_{cutoff} + V^{max}_{cutoff} - V^{min}_{cutoff}. \tag{56}$$

Computation of different complex Chebyshev polynomials is done by using the recurrence formula

$$\phi_{n+1}(x) = 2x\phi_n(x) + \phi_{n-1}(x) \tag{57}$$

with $\phi_n = S_n(-i\hat{H}_{norm})\Psi(0)$, $x = -i\hat{H}_{Norm}$. The initial values are $\phi_0 = \Psi(0)$ and $\phi_1 = x\Psi(0)$.

[4] Property: the Fourier transform of the $(1-x^2)^{-1/2}\Phi_n(x)$ is $(-1)^n i^n J_n(k)$. $\Phi_n(x)$ are the real Chebyshev polynomials, $J_n(k)$ are the Bessel functions [49].

An **improved version** of Chebyshev expansion was developed by Mandelshtam and Taylor [27, 28]. It includes in the propagation a damping factor, which cancels the wavefunction at the end of the grid. The evolution operator is expanded as

$$\hat{U}(t) = \sum_{n=0} a_n(t) Q_n(\hat{H}_{norm}; \gamma). \tag{58}$$

with $a_n(t) = (2 - \delta_{n0}) e^{-i\tilde{H}t/\hbar}(-i)^n J_n(\Delta E t/\hbar)$, $\tilde{H} = \frac{1}{2}(H_{max} + H_{min})$, and where the operators $Q_n(\hat{H}_{norm}; \gamma)$ can be viewed as an analytical continuation of real Chebyshev polynomials $\Phi_n(\hat{H}_{norm})$. $Q_n(\hat{H}_{norm}, \gamma)$ satisfies the recurrence relation

$$e^{-\gamma} Q_{n-1}(\hat{H}_{norm}; \gamma) + e^{\gamma} Q_{n+1}(\hat{H}_{norm}; \gamma) - 2\hat{H}_{norm} Q_n(\hat{H}_{norm}; \gamma) = 0, \tag{59}$$

$$Q_0(\hat{H}_{norm}; \gamma) = \hat{I}, \;\; Q_1(\hat{H}_{norm}; \gamma) = e^{-\gamma} \hat{H}_{norm}, \tag{60}$$

where $e^{-\gamma}$ is a damping factor with typically $\gamma = (x - x_0)^2$, where x_0 is the point where the absorption starts: $x > x_0$. By using these equations we can do the absorption of the wavepacket at the grid edge during the propagation. When the absorbing potentials of the type presented in Eq. (76) are used, the time step has not to be too large (typically, around 250 a.u.). When the Eqs. (58) and (59) are used, the complete propagation time can be $\Delta t \approx 6000$ a.u. (for D + H_2 collision) or larger.

Once the evolution operator is linearly expanded we can compute the action of the Hamiltonian operator on the wavepacket in order to propagate it.

3.2.1 The discrete variable representation

In the *finite basis representation* (FBR) the wavefunction is expanded using a set of basis functions

$$\Psi(x) \approx \tilde{\Psi}(x) = \sum_{n=0}^{N} a_n \phi_n(x). \tag{61}$$

The spectral coefficients a_n (orthonormalized basis set) are given as

$$a_n(t) = \int \phi_n(x) \Psi(x, t) dx. \tag{62}$$

The aim is to minimize the "rest-function" $R(x; a_0, a_1, ...a_n)$

$$R(x; a_0, a_1, \ldots a_n) = \hat{H}\tilde{\Psi}(x) - \hat{H}\Psi(x). \tag{63}$$

This idea leads to the Rayleigh-Ritz method for finding the coefficients of the finite basis representation.

In the *discrete variable representation* (DVR) method [23, 24] the basic idea is to expand the wavefunction in an orthonormal basis set $\{\phi_n(x); n = 1, N\}$, and to use a quadrature rule (usually Gaussian) consisting of a set of quadrature points $\{x_n; n = 1, N\}$ and weights $\{w_n;\ n = 1, N\}$ to define the inner product of the basis vectors.

The DVR method is based on the Gaussian quadrature [43, 51] formula

$$\int_a^b f(x)\,dx = \sum_{n=0}^{N} \omega_n f(x_n). \tag{64}$$

The wavefunction is expanded as

$$\Psi(x) \approx \tilde{\Psi}(x_j) = \sum_{n=0}^{N} a_n \phi_n(x_j). \tag{65}$$

At the grid points an *exact solution* is requested: $R(x_j; a_0, \ldots a_n) = 0$.

The spectral coefficients a_n are

$$a_n(t) = \sum_{m}^{N} \omega_m \phi_n^*(x_m)\Psi(x_m, t). \tag{66}$$

In terms of an N-points quadrature, Eq. (61) can be rewritten as

$$\Psi(x,t) = \sum_{m}^{N}\sum_{n}^{N} \omega_n \phi_m^*(x_n)\Psi(x_n,t)\phi_m(x) = \sum_{n}^{N} \Psi_n \psi_n(x), \tag{67}$$

where

$$\psi_n(x) = \sqrt{\omega_n} \sum_{m}^{N} \phi_m^*(x_n)\phi_m(x) \tag{68}$$

form a set of orthogonal basis functions in the discrete representation. The expansion coefficient is given as

$$\Psi_n = \sqrt{\omega_n}\Psi(x_n, t). \tag{69}$$

The $n-th$ order derivative of the wavefunction is obtained as

$$\frac{\partial^n \Psi(x)}{\partial x^n} = \sum_{j}^{N} \Psi_j \frac{\partial^n \psi_j(x)}{\partial x^n}. \tag{70}$$

The transformation between DVR and its associated FBR [23] is

$$U_{nj}^{\dagger} = \sqrt{\omega_j}\,\phi_n^*(x_j). \tag{71}$$

$\hat{U}$ is an *unitary operator* if the DVR points are the zeroes of the FBR basis set

$$\hat{U}^{\dagger}\hat{U} = \hat{U}\hat{U}^{\dagger} = \mathbf{1}. \tag{72}$$

A local operator (e.g. the potential $\hat{V}$) is diagonal in a DVR representation. For the kinetic energy part, it is convenient to use the FBR representation. The complete expression of the Hamiltonian can be putted in the form

$$\hat{\mathbf{H}}^{DVR} = \hat{\mathbf{U}}\,\hat{\mathbf{T}}^{FBR}\,\hat{\mathbf{U}}^{\dagger} + \hat{\mathbf{V}}^{DVR}. \tag{73}$$

The connection of these initial value problems with the boundary condition problems is performed by using **optical potentials** [1, 52]. If the wavefunction is propagated on a finite grid of "n" points, at the "n+1" position it will be suddenly set to zero. This is equivalent to the presence of an infinite potential at the grid edge and will cause a reflection of the wavepacket back into the interaction region. To ensure that the wavefunction is zero at the grid edge (hence, it satisfies the appropriate boundary conditions) we must include an absorbing potential in the region before the end of the grid. The optical potential is a negative imaginary potential, and has the property to absorb the wavefunction. The propagation of the wavepacket is done using a perturbed Hamiltonian $\tilde{H}$ of type

$$\tilde{H} = \hat{H} - i\hat{V}_I. \tag{74}$$

Several forms can be chosen for the absorbing potential. The simplest is a triangular form which in one dimension is given as

$$\hat{V}_I(X) = V_{I0}\frac{X - (X_{max} - \Delta X)}{\Delta X}. \tag{75}$$

X_{max} is the maximum value of a grid in the "X" direction, ΔX is the width of the absorbing region and V_{I0} is a prefactor. According to Balint-Kurti [53], an optimized version of the optical potential is

$$\hat{V}_I(X) = Ae^{-2/\tilde{X}}, \tag{76}$$

with

$$\tilde{X} = \frac{X - (X_{max} - \Delta X)}{\Delta X}. \tag{77}$$

The absorption during the propagation itself was already mentioned in the previous section (see Eqs. (58 - 59)). Mandelshtam and Taylor's version, presented in Eqs. (58 - 59) has the advantage that it is stable for very long propagation time steps.

3.2.2 Time evolution using only the real part of the wavepacket

An optimized version of the Chebyshev propagation scheme was proposed by Gray and Balint-Kurti [29]. It consists in propagating and extracting information only from the real part of the wavepacket. For a given wavepacket $\psi(x,t)$ we can write

$$\psi(x, t+\tau) = -\psi(x, t-\tau) + 2cos(\frac{\hat{H}\tau}{\hbar})\psi(x,t). \tag{78}$$

$\hat{H}$ is the Hamilton operator and τ is a time-step. We make the notations

$$q(x,t) = Re[\psi(x,t)],\ \ p(x,t) = Im[\psi(x,t)] \tag{79}$$

and similar to Eq. (78) we get

$$q(x,t+\tau) = -q(x,t-\tau) + 2cos(\frac{\hat{H}\tau}{\hbar})q(x,t), \tag{80}$$

with the initial conditions $\psi(t=0) = q(0) + ip(0)$.

The evolution of only the real part of the wavepacket is governed by

$$q(x,\tau) = cos(\frac{\hat{H}\tau}{\hbar})q(x,t=0) + sin(\frac{\hat{H}\tau}{\hbar})p(x,t=0). \tag{81}$$

The absorption is realized by using a damping factor $\hat{A}$ in the style of the Mandelshtam and Taylor propagation [27, 28]

$$q(x,t+\tau) = \hat{A}[-\hat{A}q(x,t-\tau) + 2cos(\frac{\hat{H}\tau}{\hbar})q(x,t)]. \tag{82}$$

Because time does not enter in any fundamental way into the observables which are to be calculated, it is allowed to substitute a modified time evolution equation for the time-dependent Schrödinger equation. Replacing $\hat{H}$ with $f(\hat{H})$ we obtain

$$i\hbar\frac{\partial\psi(x,t)}{\partial t} = f(\hat{H})\psi(x,t). \tag{83}$$

f is a continuous smooth function. *Note:* ψ satisfying Eq. (83) is not the same ψ that satisfies the usual time-dependent Schrödinger equation. However, similar information can be extracted form it. As long as the function $f(E)$ is a one-to-one mapping, each eigenvalue of $\hat{H}$ will be mapped into one unique value $f(E)$. A particular function of interest is

$$f(\hat{H}) = -\frac{1}{\tau}cos^{-1}(\hat{H}_s), \tag{84}$$

with

$$\hat{H}_s = a_s\hat{H} + b_s. \tag{85}$$

$\hat{H}_s$ is a scaled Hamiltonian operator [5] such that its eigenvalues lie between -1 and 1. If E_{min} and E_{max} are the lower and upper bounds of the spectrum of $\hat{H}$, then

$$a_s = 2/\Delta E, \quad b_s = -1 - a_s E_{min}.$$

The analog of Eq. (78) for Eqs. (83 -85)may be written in the simplified form

$$\psi(x,t+\tau) = -\psi(x,t-\tau) + 2\hat{H}_s\psi(x,t). \tag{86}$$

[5]The same scaled operator is used in the Chebyshev expansion of the evolution operator $e^{-i\hat{H}t}$.

Repeated application of this three-term recursion propagates the real part of the wavepacket forward in time steps τ. The dynamics is *independent* of the value of τ, which allow us to take a single long time-step in the propagation. In addition, absorbing conditions must be set at the grid edges. The damped recursion for the wavepacket will be of the form

$$q(x, t + \tau) = \hat{A}(-\hat{A}q(x, t - \tau) + 2\hat{H}_s q(x, t)). \tag{87}$$

By making use of this formulation, we need just half of the storage space in the core memory, compared with what we need in the case of the full complex representation. The execution of the program can be speeded up because all the mathematical operations involve real numbers.

4 The A-BC system

4.1 Coordinate systems

Quantum mechanical reactive scattering provides the fundamental, rigorous and the most complete description of a chemical reaction allowed by the basic laws of nature. Unfortunately it is also the most complicated to deal with because of the lack of one physically appropriate set of coordinates for "translation" and internal degrees of freedom. Figure 3 shows the possible choices of coordinates for a collinear A + BC → AB +C reaction.

As long as only an inelastic scattering process (e.g. vibrational excitation) is investigated

$$\text{A+BC}(v) \rightarrow \text{A+BC}(v'),$$

the **Jacobi coordinates** (r_a, R_a) are the natural choice (see the next section). For elastic scattering the wavefunction for relative motion behaves, at large separation, as an incident plus a scattered wave (see Eq. (37)). The scattered part is a sum over many final states, each term being a product of a scattered wave for the relative motion and an internal state wavefunction. If we use the Jacobi coordinates the expansion of the function has the form

$$\psi_{v'} = \sum_v \phi_v(r_a) f_{v \leftarrow v'}(R_a), \tag{88}$$

where ϕ_v are the vibrational eigenfunctions for diatom BC and v denotes the vibrational states. $f_{v \leftarrow v'}(R_a)$ is the translational part of the wavefunction.

Although the Jacobi coordinates (R_a, r_a) are natural for describing the reactants (A+BC) they are not so well suited for describing the products (AB+C). One way of dealing with this problem is to use a curvilinear coordinate system (**"natural collision coordinates"**) in which we have a smooth path from reactants to products (Figure 3 -B). The reaction coordinate s is the path along the indicated curve (i.e. the reaction path) and u is the coordinate orthogonal to s. In this case the wavefunction is expanded as

$$\psi_{v'} = \sum_v \psi_v(u; s) f_{v \leftarrow v'}(s). \tag{89}$$

A third choice of coordinates are the various types of **hyperspherical coordinates**, which in the collinear case reduce to the usual polar coordinates (the distance from the origin to the given point ρ, and the angle between the ρ vector direction and X axis - θ). The wavefunction is then expanded as

$$\psi_{v'} = \sum_v \phi(\theta; \rho) f_{v \leftarrow v'}(\rho). \tag{90}$$

The translational functions ($f_{v \leftarrow v'}$) satisfy coupled ordinary differential equations.

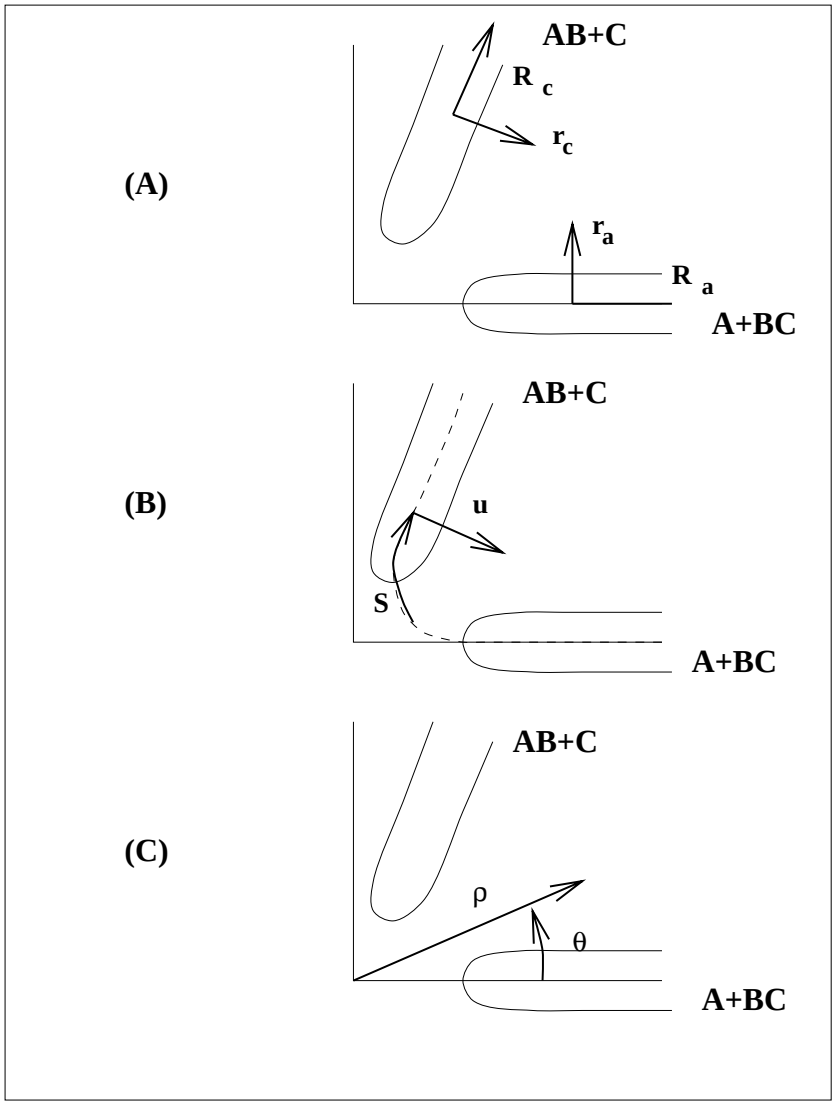

Figure 3: Schematic depiction of a collinear A+BC → AB +C PES and different ways of choosing the coordinates: (*A*) - Jacobi coordinates for arrangement a(A+BC) and c(C+AB); (*B*) - reaction path coordinates ("natural coordinates"); (*C*) - hyperspherical coordinates (here simply polar coordinates).

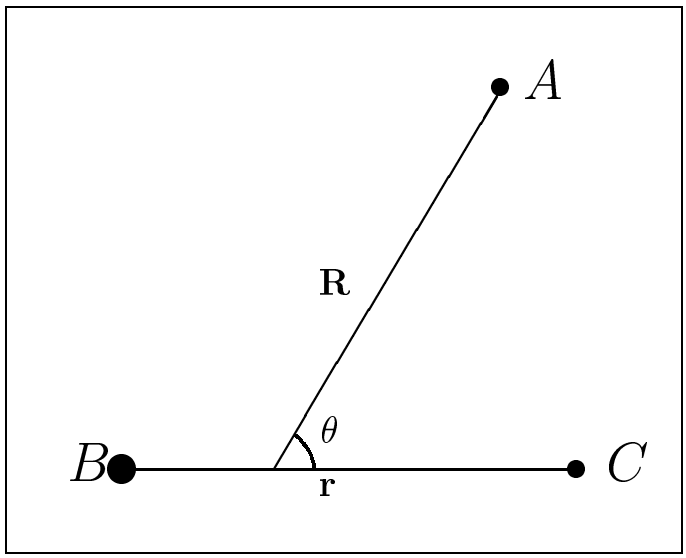

Figure 4: Jacobi coordinates

4.1.1 Jacobi coordinates

This set of internal coordinates is defined for a 3-atom system as the distance r between the two atoms that forms the diatomic molecule B-C, the distance R between the center of mass of diatomic BC and the free atom A and the angle between these two directions (θ) [44] (see Figure 4). As pointed out above, these coordinates are ideal for describing inelastic scattering.

The reactive problems are solved using Jacobi coordinates for various arrangements a(A+BC), b(B+AC), c(C+ AB). These coordinate sets can be used simultaneously, during the propagation, or one transforms the wavepacket from one set of coordinates to another. According to Miller [54] a general expansion of the wavefunction can include all the various arrangements. For the collinear case (see Figure 3) we have

$$\psi_{\gamma_1,n_1} = \sum_n \phi_n^a(r_a) f_{an\leftarrow\gamma_1 n_1}(R_a) + \sum_n \phi_n^c(r_c) f_{cn\leftarrow\gamma_1 n_1}(R_c) \tag{91}$$

γ is a symbol for the different possible arrangements (a(A+BC), c(C+AB)). ϕ_n^a and ϕ_n^c are the vibrational eigenstates of diatoms BC and AB, respectively.

The idea of this approach is similar to that in electronic structure calculations by using multicenter expansions for molecular orbitals (LCAO - method). In case of a diatomic molecule the molecular orbital $\chi(r)$ for an electron is expanded in basis functions using the coordinates (r_a, r_b) of the electron with respect to both nuclear centers a and b

$$\chi(r) = \sum_i a_i \phi_i^a(r_a) + \sum_i b_i \phi_i^b(r_b). \tag{92}$$

This means an expansion of the wavepacket in the entrance channel (A+BC) according to the coordinates defined by the exit channel (for example (C+AB)). This initial expansion is not as simple as in the case of inelastic scattering, on the other hand the final form of the wavepacket is easier to handle.

4.1.2 Space-fixed and body-fixed Jacobi coordinates

A 3-atom system has 9 degrees of freedom. Jacobi coordinates are responsible only for internal degrees of freedom of the system and in addition we have the rotation and translation motion (3+3 degrees of freedom). The molecule defined by three Jacobi coordinates must be "inserted" into a 3-D Cartesian coordinate system. According to Pack [44] there are two choices: a) a laboratory-fixed system axes (the so called "space-fixed coordinates" - SF) the wavefunction is defined within, b) one defines a "Z" axis along the R Jacobi coordinate (atom-diatom distance) and shifts the origin of the coordinate system to the center of mass of the complete A-BC system (the "body-fixed coordinate system" - BF) (Figure 5).

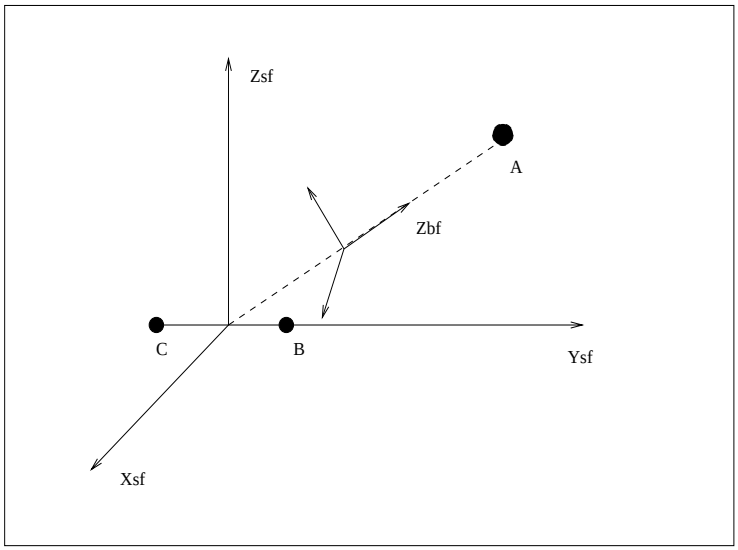

Figure 5: Space-fixed and body-fixed coordinates systems

The wavefunction of the system, including the rotational motion, (Figure 5) can be written by defining the angular momentum $\hat{l}$ of A relative to BC, the rotational angular momentum $\hat{j}$ of BC and the total angular momentum $\hat{J} = \hat{l} + \hat{j}$ of the system . If $Y_{l,m_l}(\hat{R}')$ is the spherical harmonic describing the relative angular momentum, and $Y_{j,m_j}(\hat{r}')$ is describing the rotational motion, the common set of eigenfunctions $\mathcal{Y}_{jl}^{JM}(\hat{r}', \hat{R}')$ for $\hat{J}^2$, $\hat{J}_z$, $\hat{l}^2$ and $\hat{j}^2$ [55, 44] is defined by coupling $Y_{l,m_l}(\hat{R}')$ and $Y_{j,m_j}(\hat{r}')$ via Clebsch-Gordan

coefficients

$$\mathcal{Y}_{jl}^{JM}(\hat{r}', \hat{R}') = \sum_{m_j=-j}^{j} \sum_{m_l=-l}^{l} C(jlJ; m_j, m_l, M) Y_{jm_j}(\hat{r}') Y_{lm_l}(\hat{R}'). \tag{93}$$

The complete wavefunction is given as

$$\Phi_{SF}^{JMjlv} \equiv \sum_{j''} \sum_{l''} \sum_{v''} R^{-1} G_{j''l''v''}^{Jjlv}(R) \chi_{j''v''}(r) \mathcal{Y}_{j''l''}^{JM}(\hat{r}', \hat{R}'), \tag{94}$$

where $G_{j''l''v''}^{Jjlv}(R)$ are the radial channel wavefunctions and $\chi_{j''v''}(r)$ are the diatomic wavefunctions. This expression is given in space-fixed formulation. To get a formulation for the body-fixed system a rotation with Euler angles $(\phi_r,\, \theta_r,\, 0)$ is needed

$$\Phi_{SF}^{JMjlv} = \sum_{\Omega'=-J}^{J} D_{M\Omega'}^{J}(\phi_r, \theta_r, 0) \Phi_{BF}^{J\Omega' jlv}. \tag{95}$$

ϕ_r and θ_r are the polar angular coordinates of atom-diatom direction in the space-fixed system.

4.2 The Hamiltonian of the A-BC system

According to Judson *et al.* [37] the **Hamiltonian operator** in *Jacobi coordinates* $(R,\ r,\ \theta)$ for the body-fixed frame representation is

$$\begin{aligned}\hat{H}^J = \Big\{ &-\frac{\hbar^2}{2\mu_{A-BC}} \frac{\partial^2}{\partial R^2} - \frac{\hbar^2}{2\mu_{BC}} \frac{\partial^2}{\partial r^2} + \frac{\hbar^2}{2\mu_{A-BC} R^2} [J(J+1) - 2\Omega^2 + j(j+1)] \\ &+ \frac{\hbar^2}{2\mu_{BC} r^2} j(j+1) + v(r) \Big\} \delta_{jj'} \delta_{\Omega\Omega'} + V^{\Omega}(R, r, \theta) \delta_{\Omega\Omega'} \\ &- \frac{\hbar^2}{2\mu_{A-BC} R^2} [\lambda_+(J, \Omega') \lambda_+(j, \Omega') \delta_{\Omega'+1,\Omega} \delta_{j,j'} + \lambda_-(J, \Omega') \lambda_-(j, \Omega') \delta_{\Omega'-1,\Omega} \delta_{j,j'}].\end{aligned} \tag{96}$$

The notations used above are: μ_{A-BC} is the reduced mass of A-BC system, μ_{BC} is the reduced mass of the diatomic molecule (BC), J is the total angular momentum quantum number j is the rotational angular momentum quantum number for the B-C molecule. $\lambda_\pm$ are the ladder operators for angular momentum, as defined in [35]. $V^{\Omega}(R, r, \theta)$ is the A-BC *potential energy* and $v(r)$ is the diatomic potential energy.

According to Leforestier [56] another expression of the Hamiltonian operator, equivalent to the one given above is

$$\hat{H}^J = -\frac{\hbar^2}{2\mu_{A-BC}} \frac{\partial^2}{\partial R^2} - \frac{\hbar^2}{2\mu_{BC}} \frac{\partial^2}{\partial r^2} - \frac{\hbar^2}{2I} \Big(\frac{1}{sin\theta} \frac{\partial}{\partial \theta} sin\theta \frac{\partial}{\partial \theta} - \frac{\hat{j}_z^2}{sin\theta^2} \Big) +$$

$$+\frac{\hbar^2}{2\mu_{A-BC}R^2}(\hat{J}^2 - 2\hat{J}_z\hat{j}_z - \hat{J}_+\hat{j}_- - \hat{J}_-\hat{j}_+) + V(R,r,\theta). \tag{97}$$

with

$$\frac{1}{I} = \frac{1}{\mu_{A-BC}R^2} + \frac{1}{\mu_{BC}r^2}, \tag{98}$$

and

$$V(R,r,\theta) = V^{\Omega}(R,r,\theta) + v(r). \tag{99}$$

To derive the expression in Eq. (96) we can use the general formulation from [57]. Acording to Nyman [19] the Hamiltonian of the system can be expressed as a sum of the kinetic energy operator $\hat{T}$ and the potential energy operator $\hat{V}$

$$\hat{H} = \hat{T} + \hat{V}. \tag{100}$$

The kinetic energy in terms of classical velocities can be written as

$$T = \frac{1}{2}p^T G(q) p \tag{101}$$

where p_i are the momenta conjugate to the chosen coordinates q_i and $G(q)$ is the $G-$matrix

$$G_{jk} = \sum_i \frac{1}{m_i}\frac{\partial q_j}{\partial x_i}\frac{\partial q_k}{\partial x_i} \tag{102}$$

where x_i denotes the Cartesian coordinates of atom i with mass m_i.

The quantum mechanical kinetic energy operator is

$$\hat{T} = -\frac{\hbar^2}{2}g^{-1/2}\sum_{ij}\frac{\partial}{\partial q_i}g^{1/2}G_{ij}\frac{\partial}{\partial q_j} \tag{103}$$

where g is the determinant $g = det|G^{-1}|$.

This method is very general and works for all kinds of coordinates.

Another choice is to start with the Hamiltonian for a 2-particle system [33]

$$\hat{H}_{BC} = -\frac{\hbar^2}{2\mu_{BC}}[\frac{1}{r^2}\frac{\partial}{\partial r}r^2\frac{\partial}{\partial r} - \frac{\hat{l}^2}{r^2}] + \hat{V}_{BC}, \tag{104}$$

where the first term is the Laplacian in spherical coordinates [51] and $\hat{l}$ is the relative angular momentum of the two particles (in units of $\hbar$)

$$\hat{l}^2 = -[\frac{1}{sin\theta}\frac{\partial}{\partial\theta}sin\theta\frac{\partial}{\partial\theta} + \frac{1}{sin^2\theta}\frac{\partial^2}{\partial\phi^2}]. \tag{105}$$

The idea is to write the three-particle Hamiltonian in a two-particle style: atom A and the "virtual particle" which is the center of mass of the BC molecule using the following notations: $\hat{j}$ is the rotational angular momentum of the BC molecule; $\hat{l}$ is the relative

angular momentum, (between A and center of mass of BC) and $\hat{J} = \hat{l} + \hat{j}$ is the total angular momentum of the system. The 3-particle Hamiltonian (Jacobi coordinates) of a body-fixed system can be written as

$$\hat{H}_{A(BC)} = -\frac{\hbar^2}{2\mu_{A-BC}}[\frac{\partial^2}{\partial R^2} - \frac{\hat{l}^2}{R^2}] + \hat{V}_{A(BC)}. \tag{106}$$

The Hamiltonian of the BC molecule is given by Eq. (104), with $\hat{j}$ instead of $\hat{l}$. By noting that $\hat{l} = \hat{J} - \hat{j}$ we can write the complete Hamiltonian in Jacobi coordinates as

$$\hat{H}_{A-BC} = -\frac{\hbar^2}{2\mu_{A-BC}}\frac{\partial^2}{\partial R^2} - \frac{\hbar^2}{2\mu_{BC}}\frac{\partial^2}{\partial r^2} + \frac{\hbar^2(\hat{J}-\hat{j})^2}{2\mu_{A-BC}R^2} + \frac{\hbar^2\hat{j}^2}{2\mu_{BC}r^2} + \hat{V}. \tag{107}$$

The potential energy $\hat{V}$ includes the contribution of the diatomic potential and the relative interaction atom-diatom.

For the operator expression $(\hat{J}-\hat{j})^2$ we get

$$(\hat{J}-\hat{j})^2 = \hat{J}^2 - \hat{J}\hat{j} - \hat{j}\hat{J} + \hat{j}^2. \tag{108}$$

By using the definition of the ladder operators [35]

$$\hat{J}_\pm = \hat{J}_x \pm i\hat{J}_y, \tag{109}$$

the commutation relations between the components of angular momentum, and the property that in the body-fixed coordinate system the projections of $\hat{J}$ and $\hat{j}$ onto the Z axis are equal [56]

$$\hat{J}_Z\Psi_{BF} = \hbar\Omega\Psi_{BF}, \tag{110}$$

and

$$\hat{j}_Z\Psi_{BF} = \hbar\Omega\Psi_{BF}, \tag{111}$$

we can write

$$\hat{J}^2 - \hat{J}\hat{j} - \hat{j}\hat{J} + \hat{j}^2 = \hat{J}^2 - 2\hat{J}_z^2 - \hat{J}_+\hat{j}_- - \hat{J}_-\hat{j}_+ + \hat{j}^2. \tag{112}$$

The final result is

$$\hat{H}_{A(BC)} = -\frac{\hbar^2}{2\mu_{A-BC}}\frac{\partial^2}{\partial R^2} - \frac{\hbar^2}{2\mu_{BC}}\frac{\partial^2}{\partial r^2} + \frac{\hbar^2}{2I}\hat{j}^2 + \frac{\hbar^2(\hat{J}^2-2\Omega^2)}{2\mu_{A-BC}R^2} - \frac{\hbar^2}{2\mu_{A-BC}R^2}(\hat{J}_+\hat{j}_- + \hat{J}_-\hat{j}_+) + \hat{V}(R,r,\theta), \tag{113}$$

The matrix expression of this operator in the DVR-FFT basis set described in previous section is given in Eq. (96). The expression given in Eq. (105) for the angular momentum can be used to express the Hamiltonian in the form [56]

$$\hat{H}^J = -\frac{\hbar^2}{2\mu_{A-BC}}\frac{\partial^2}{\partial R^2} - \frac{\hbar^2}{2\mu_{BC}}\frac{\partial^2}{\partial r^2} - \frac{\hbar^2}{2I}(\frac{1}{sin\theta}\frac{\partial}{\partial\theta}sin\theta\frac{\partial}{\partial\theta} - \frac{\hat{j}_z^2}{sin\theta^2})$$

$$+\frac{\hbar^2}{2\mu_{A-BC}R^2}(\hat{J}^2 - 2\Omega^2 - \hat{J}_+\hat{j}_- - \hat{J}_-\hat{j}_+) + \hat{V}(R,r,\theta) \tag{114}$$

4.2.1 Non-adiabatic PES

For many systems, particularly when one is studying photo-excitation processes, one has to take into account several electronic states that participate in the dynamics. In order to describe the coupling between different electronic states, we have to go beyond the Born-Oppenheimer approximation. This can be achieved by using the adiabatic (noncrossing) or the diabatic (crossing) representation [47]. In the first case the nuclear kinetic energy operator $\hat{T}_N(R)$ has a non diagonal representation and the potential energy operator, $\hat{V}(R)$, has a diagonal representation. In contrast, in the latter $\hat{T}_N(R)$ is represented by a diagonal matrix and the $\hat{V}(R)$ representation is nondiagonal.

For an A-BC system described by two coupled PES, we can write the time-dependent Schrödinger equation in the adiabatic representation as

$$i\hbar\frac{\partial}{\partial t}\begin{pmatrix}\psi_1(t)\\ \psi_2(t)\end{pmatrix} = -\frac{\hbar^2}{2\mu}\left\{\begin{pmatrix}\nabla_R^2+\hat{T}_{11} & \hat{T}_{12}\\ \hat{T}_{21} & \nabla_R^2+\hat{T}_{22}\end{pmatrix} + \begin{pmatrix}\hat{V}_1^a & 0\\ 0 & \hat{V}_2^a\end{pmatrix}\right\}\begin{pmatrix}\psi_1(t)\\ \psi_2(t)\end{pmatrix} \tag{115}$$

where $\hat{T}_{11(22)}$ and $\hat{T}_{12(21)}$ are defined as follows: $\hat{T}_{11} =< \phi_1^a|\nabla_R^2|\phi_1^a >$, $\hat{T}_{22} =< \phi_2^a|\nabla_R^2|\phi_2^a >$ $\hat{T}_{12} =< \phi_1^a|\nabla_R^2|\phi_2^a > +2 < \phi_1^a|\nabla_R|\phi_2^a > \nabla_R$, $\hat{T}_{21} =< \phi_2^a|\nabla_R^2|\phi_1^a > +2 < \phi_2^a|\nabla_R|\phi_1^a > \nabla_R$. $\mu = \mu_{A-BC}$ is the reduced mass of the A-BC system.

$\psi_{1(2)}$ and $\phi_{1(2)}$ are the nuclear and the adiabatic electronic eigenfunctions for the state 1(2) respectively. $\hat{V}_1^a$ and $\hat{V}_2^a$ are the adiabatic potential energy operators for states 1 and 2.

The perturbations arising from the off-diagonal matrix elements are referred to as non adiabatic perturbations. It is worth emphasizing that the off-diagonal matrix elements in this case are exclusively due to the nuclear kinetic operator.

In this representation the exact molecular wavefunction for a bound system is expanded as (Whetten *et al.* [58])

$$\Psi(\mathbf{q},\mathbf{Q}) = \sum_m \phi_m(\mathbf{q},\mathbf{Q})\psi_m(\mathbf{Q}), \tag{116}$$

where $\phi_m(\mathbf{q},\mathbf{Q})$ are the solutions of the electronic Schrödinger equation

$$\hat{H}_e(\mathbf{Q})\phi_m(\mathbf{q},\mathbf{Q}) = E_m(\mathbf{Q})\phi_m(\mathbf{q},\mathbf{Q}) \tag{117}$$

depending parametrically on the nuclear coordinates $\mathbf{Q}$. $\psi_m(\mathbf{Q})$ are the nuclear wavefunctions. The electronic eigenvalues $E_m(\mathbf{Q})$ define the usual adiabatic potential surfaces. $\mathbf{Q}$ and $\mathbf{q}$ are collective indices for nuclear and electronic coordinates.

For the same two-state system we can write the TDSE in the diabatic representation as

$$i\hbar\frac{\partial}{\partial t}\begin{pmatrix}\psi_1(t)\\ \psi_2(t)\end{pmatrix}=\left\{\begin{pmatrix}\hat{T}_1(R) & 0\\ 0 & \hat{T}_2(R)\end{pmatrix}+\begin{pmatrix}\hat{V}_{11} & \hat{V}_{12}\\ \hat{V}_{21} & \hat{V}_{22}\end{pmatrix}\right\}\begin{pmatrix}\psi_1(t)\\ \psi_2(t)\end{pmatrix}, \tag{118}$$

where $\hat{T}_1(R)$ and $\hat{T}_2(R)$ are the kinetic energy operators for nuclear motion on surfaces 1 and 2 respectively ($\hat{T}_{1(2)} = -\hbar^2/2\mu\nabla^2_{R_{1(2)}}$). $\hat{V}_{11(22)}$ and $\hat{V}_{12(21)}$ are the potential energy operators acting on the first, second potential energy surface and the coupling operator between them. Their matrix elements are: $< \phi^d_{1(2)}|\hat{H}_{el}|\phi^d_{1(2)} >$ for $V_{11(22)}$ and $< \phi^d_{1(2)}|\hat{H}_{el}|\phi^d_{2(1)} >$ for the coupling operator. $\phi^d_{1(2)}$ and $\psi_{1(2)}$ are the diabatic electronic and the nuclear wave functions. In this representation the off-diagonal matrix elements are due to the nuclear potential energy term (i.e. $\hat{H}_{el}$). Perturbations arising from these off-diagonal matrix elements are termed as electrostatic perturbations.

In the diabatic representation the exact molecular wavefunction for a bound system is expanded as (Whetten *et al.* [58])

$$\Psi(\mathbf{q},\mathbf{Q}) = \sum_m \phi_m(\mathbf{q},\mathbf{Q_0})\psi_m(\mathbf{Q}), \tag{119}$$

where $\phi_m(\mathbf{q},\mathbf{Q_0})$ are the solutions of the electronic Schrödinger equation at a chosen reference configuration $\mathbf{Q_0}$

$$\hat{H}_e(\mathbf{Q_0})\phi_m(\mathbf{q},\mathbf{Q_0}) = E^0_m(\mathbf{Q_0})\phi_m(\mathbf{q},\mathbf{Q_0}). \tag{120}$$

$\psi_m(\mathbf{Q})$ are the nuclear eigenfunctions.

In the adiabatic representation the potential energy surfaces may approach each other closely but they will not cross (avoided crossing). In the diabatic representation the PE curves do cross whenever degeneracies occur.

The two representations are related to each other via the following transformations

$$\begin{pmatrix}\phi^a_1\\ \phi^a_2\end{pmatrix}=\begin{pmatrix}cos\theta(R) & -sin\theta(R)\\ sin\theta(R) & cos\theta(R)\end{pmatrix}\begin{pmatrix}\phi^d_1\\ \phi^d_2\end{pmatrix}, \tag{121}$$

where the R-dependent angle θ is obtained from

$$\tan 2\theta(R) = 2V_{12}/(V_{11} - V_{22}). \tag{122}$$

The adiabatic PE curves are related to the diabatic PE curves through

$$V^a_{1,2} = \frac{1}{2}[(V_{11} + V_{22}) \pm \sqrt{(V_{11} - V_{22})^2 + 4V^2_{12}}] \tag{123}$$

(with: $V_{12} = V_{21}$).

4.2.2 Basis functions

According to Judson *et al.* [37] the wavepacket for the A+BC arrangement in the body-fixed frame Φ_{BF} can be expanded as

$$\Phi_{BF}(\hat{k}_0, v_0, j_0, m_0|R, r, t) = \frac{1}{rR}\sum_{J,j,\Omega}(2J+1)[D^J_{\Omega m_0}(\alpha,\beta,\gamma)]^* Y_{j\Omega}(\theta,0)\Psi^J_{BF}(j\Omega|v_0 j_0 m_0|R,r,t). \tag{124}$$

Ω is the projection of $\hat{J}$ (and $\hat{j}$) in the BF Z axis (defined to be R), v_0 and j_0 are the initial diatom vibrational and rotational states, m_0 is the initial projection of $\hat{j}$ in the SF Z axis. At the initial time t=0 the relative momentum $\vec{k}$ is parallel to both SF and BF Z axes. $\mathrm{D}^J_{\Omega m_0}(\alpha,\beta,\gamma)$ are the Wigner functions, with the Euler angles α,β,γ. $Y_{j\Omega}$ are the spherical harmonics. Ψ^J_{BF} are the channel wavepackets for each total J.

The total wavefunction obeys the Schrödinger equation

$$i\hbar\frac{\partial}{\partial t}\Phi_{BF} = \hat{H}\Phi_{BF} \tag{125}$$

where $\hat{H}$ is the total Hamiltonian of the system.

By projecting out the rotation matrices and spherical harmonics in Eq. (125) we can arrive at the following set of coupled equations for channel wavepackets [37]

$$i\hbar\frac{\partial}{\partial t}\Psi^J_{BF} = \sum_{j,\Omega}\hat{H}^J\Psi^J_{BF} \tag{126}$$

where $\hat{H}^J$ is given by Eq. (96).

Instead of propagating the full set of functions $\Psi^J_{BF}(j\Omega|v_0 j_0 m_0|R,r,t)$, given in Eq. (126) we form linear combinations of these with definite parity. Since parity is conserved, functions with definite parity can be propagated separately. The symmetrised functions are

$$\Psi^J_{\pm}(j\Omega|v_0 j_0 m_0|R,r,t) = \frac{1}{\sqrt{2}}(\Psi^J_{BF}(j\Omega|v_0 j_0 m_0|R,r,t) \pm (\Psi^J_{BF}(j-\Omega|v_0 j_0 m_0|R,r,t). \tag{127}$$

We need to propagate only the functions $\Psi^J_{\pm}(j\Omega|v_0 j_0 m_0|R,r,t)$ for $\Omega \geq 0$. The corresponding functions for $\Omega < 0$ are given by

$$\Psi^J_{\pm}(j-\Omega|v_0 j_0 m_0|R,r,t) = \pm\Psi^J_{\pm}(j\Omega|v_0 j_0 m_0|R,r,t). \tag{128}$$

According to Leforestier [56], the body-fixed function Ψ^J_{BF} can then be expanded in a FBR basis set ($e^{iK_m R}\times e^{ik_n r}\times P^{\Omega}_l(\theta)$) or in DVR [23, 24]. The FBR version is

$$\Psi^J_{\pm} = \sum_{m,n,l,\Omega} c_{m,n,l,\Omega} e^{iK_m R} e^{ik_n r} P^{\Omega}_l(\theta). \tag{129}$$

with K_m and k_n - momentum quantum numbers along R and r, $P_l^{\Omega}(\theta)$ are associated Legendre functions.

The second version is the expansion using a DVR [23, 24] grid ($R_m \times r_n \times \theta_l^{\Omega}$) [56]:

$$\Psi_{\pm}^{J} = \sum_{m,n,l,\Omega} \mathcal{C}_{m,n,l,\Omega} \Psi_R^J(R_m) \Psi_r^J(r_n) \Psi_\theta^J(\theta_l^{\Omega}). \tag{130}$$

In order to act with the Hamiltonian given by Eq. (96) on the wavepacket given by Eq. (130), we will separate the Hamiltonian into a sum of several operators; each operator will be treated independently in the most convenient representation.

4.2.3 The kinetic energy operator

The kinetic energy operator has the generic form

$$\hat{T}_{kin} = -\frac{\hbar^2}{2\mu}\frac{\partial^2}{\partial x^2}. \tag{131}$$

The most convenient basis set to describe this operator is formed from a set of *Fourier functions*

$$\phi_n(x) = \exp(2\pi i n x/L), \quad n = -(\frac{N}{2}-1), \ldots, 0, \ldots, \frac{N}{2}. \tag{132}$$

We need an equidistant grid to represent the wavefunction: $x_n = (n-1)\Delta x$, $n = 1, \ldots, N$. The kinetic energy in FBR representation can be written immediately as

$$T_n^{FBR} = \frac{\hbar^2}{2\mu}\frac{4\pi^2}{L^2}n^2. \tag{133}$$

The energy of a plane wave state is computed in the most easiest way using the momentum representation. We use the following practical algorithm to act with the kinetic part of the Hamiltonian on Ψ:

1. The wavefunction is transformed from the coordinate representation to the momentum representation using an FFT [6] algorithm.

2. From the momentum representation of the wavefunction the energy of each plane wave is computed according to the formula

$$E_k = \hbar^2 k^2/2\mu,$$

where k is the wavenumber corresponding to the given grid point.

3. The wavepacket is transformed back to the coordinate representation by an inverse FFT^{-1} transformation.

[6] Fast Fourier Transform [50]

4.2.4 The rotational operator

According to Judson *et al.* [37], Leforestier [56], the rotational operator for the diatomic molecule can be expressed as

$$\hat{T}_{rot} = \frac{\hbar^2}{2\mu_{BC}r^2}\hat{j}^2, \tag{134}$$

or equivalently

$$\hat{T}_{rot} = -\frac{\hbar^2}{2\mu_{BC}r^2}[\frac{1}{\sin\theta}\frac{\partial}{\partial\theta}\sin\theta\frac{\partial}{\partial\theta} - \frac{j_z^2}{\sin\theta^2}], \tag{135}$$

μ_{BC} is the reduced mass of the diatomic molecule.

$\hat{T}_{rot}$ has a diagonal form in a representation of *associated Legendre functions* [7]

$$P_j^{\Omega}(x) = (1-x^2)^{\Omega/2}\frac{d^{\Omega}}{dx^{\Omega}}P_j(x) \qquad \Omega = 0\ldots j. \tag{136}$$

j stands for the rotational quantum number and Ω for the projection of $\hat{j}$ (and $\hat{J}$) on the Z-axis of the body-fixed system. The rotational energy in FBR representation is

$$T_j^{FBR} = \frac{\hbar^2}{2\mu_{BC}r^2}j(j+1). \tag{137}$$

For a grid representation we take the interval $x \in [-1\ldots 1](x$ stands for $cos(\theta))$. The location of the grid points are defined by the Gauß-type quadrature rule for the associated Legendre functions (according to the DVR method [23, 24]).

The grid points are

$$\{x_{i,\Omega}\} \quad i = 1, 2...n_{\Omega}, \quad \Omega = 0, 1, ...j, \tag{138}$$

where n_{Ω} is the number of the grid points in the channel Ω. The location of these points is given by the relation

$$P_j^{\Omega}(x_{i,\Omega}) = 0 \quad i = 1, 2...n_{\Omega}, \tag{139}$$

where $P_j^{\Omega}(x)$ are the associated Legendre functions.

The weights for the associated Legendre quadrature can be computed using the Christoffel-Darboux formula [25]

$$\frac{1}{w_{i,\Omega}}\delta_{i,k} = \sum_{j=\Omega}^{\Omega+n_{\Omega}} P_j^{\Omega}(x_{i,\Omega})P_j^{\Omega}(x_{k,\Omega}). \tag{140}$$

In the equation above, $P_j^{\Omega}(x)$ are renormalized to 1.

The associated Legendre quadrature formula for the channel Ω is

$$\int_{-1}^{1} f(x)dx = \frac{1}{k_{\Omega}}\sum_i w_{i,\Omega}f(x_{i,\Omega}) \tag{141}$$

[7] See the Appendix 2.

with

$$k_\Omega = \sum_i w_{i,\Omega}. \tag{142}$$

Finally the transformation between DVR and the associated Legendre FBR representations is given by the following matrix (see Eq. (71))

$$(U^\Omega_{ji})^\dagger = \sqrt{w_{i,\Omega}} P^\Omega_j(x_{i,\Omega}), \quad j,i = 1,...,n_\Omega. \tag{143}$$

This means that in practice a set of matrices indexed by Ω has to be stored for a complete DVR - FBR transformation (one matrix for each Ω channel).

4.2.5 The coupling operator

The operator which couples different Ω channels is given by

$$\hat{T}_{coup} = \frac{\hbar^2}{2\mu_{A-BC}R^2} \hat{\lambda}_\pm(J,\Omega')\hat{\lambda}_\pm(j,\Omega')\delta_{\Omega'\pm1,\Omega}. \tag{144}$$

The same basis sets are used as given above (DVR and FBR type). The action of the ladder operators $\hat{\lambda}_\pm$ on the states follow the usual rules defined by the angular momentum theory [35]

$$\hat{\lambda}_\pm(J,\Omega')|\Psi^J_\pm(j\Omega')\rangle = [(J \pm \Omega' + 1)(J \mp \Omega']^{1/2}|\Psi^J_\pm(j\Omega' \pm 1)\rangle \tag{145}$$

(same for the $\hat{\lambda}_\pm(j,\Omega')$ operator).

$\hat{\lambda}_+(J,\Omega')$ couples the channel Ω' with the channel $\Omega = \Omega' + 1$, while $\hat{\lambda}_-(J,\Omega')$ couples the channel Ω' with the channel $\Omega = \Omega' - 1$ (see Eq. 96).

4.2.6 The potential energy

This operator is computed immediately in the DVR representation as the value of the function at the given point times the value of potential energy

$$\hat{V}_{DVR}|\psi> = V_{DVR}(x_i)\sqrt{w_i}\psi_{DVR}(x_i). \tag{146}$$

V_{DVR} is the complete contribution of the potential energy to the Hamiltonian and $V_{DVR}(x_i)$ is the local value of the potential at the given grid point x_i. w_i is the corresponding DVR weight.

The action of the Hamiltonian given in Eq. (96) on the wavepacket (Eq. (130)) can be summarized as follows: four independent modules are needed to compute the complete Hamiltonian. Module one computes the contribution of the kinetic energy. Module two computes the contribution of the rotational motion of the diatomic to the total energy. Module three computes the potential energy and finally module four computes the coupling between different channels describing the rotational motion of the diatomic.

4.3 Initial conditions for the wavepacket

According to Kosloff [1], Balakrishnan *et al.* [47] the initial wavepacket consists of a Gaussian function along the R coordinate multiplied with the wavefunction of ro-vibrational initial state of the diatomic molecule

$$\Psi(R, \mathbf{q}, t = 0) = \frac{1}{\sqrt[4]{\pi}\sqrt{\sigma}} exp\left(ik_0 R\right) exp\left(-\frac{(R - R_0)^2}{2\sigma^2}\right) \chi(\mathbf{q}). \tag{147}$$

R is the distance between the atom A and the BC system, $\mathbf{q}$ are the internal degrees of freedom for the BC molecule and $\chi(\mathbf{q})$ is the initial state of the diatomic.

For a wavepacket we have the Heisenberg relation

$$\Delta x \Delta p \geq \frac{\hbar}{2}.$$

The Gaussian wavepackets have the property that they minimize this relation [33]

$$\Delta x \Delta p = \frac{\hbar}{2}.$$

This property ensures that the wavepacket spreads as little as possible both in momentum and space representations. When it spreads very fast, large grids are needed to store the complete wavepacket. On the other hand the distance between two successive points of the grid must be small enough in order to give a correct description of the components of the wavepacket with a very large energy. In this case for the implementation we need a large amount of core memory.

4.4 Analysis of the propagated wavepacket

Several method were proposed in the literature for computing the S-matrix or the reaction probabilities from the wavepackets. The basic idea is to separate the representation grid into two pieces: one where the derivatives of the potential energy with respect to the distance atom-diatom are not negligible ("the interaction region") and the second where the potential energy is nearly constant ("the asymptotic region") - see Figure 6. In the asymptotic region the analysis is performed.

4.4.1 The split-function method

According to Heather and Metiu [59] at each time step of the propagation the wavepacket is written as a sum of two components

$$\Psi(R, q, t) = \Psi_i(R, q, t) + \Psi_f(R, q, t). \tag{148}$$

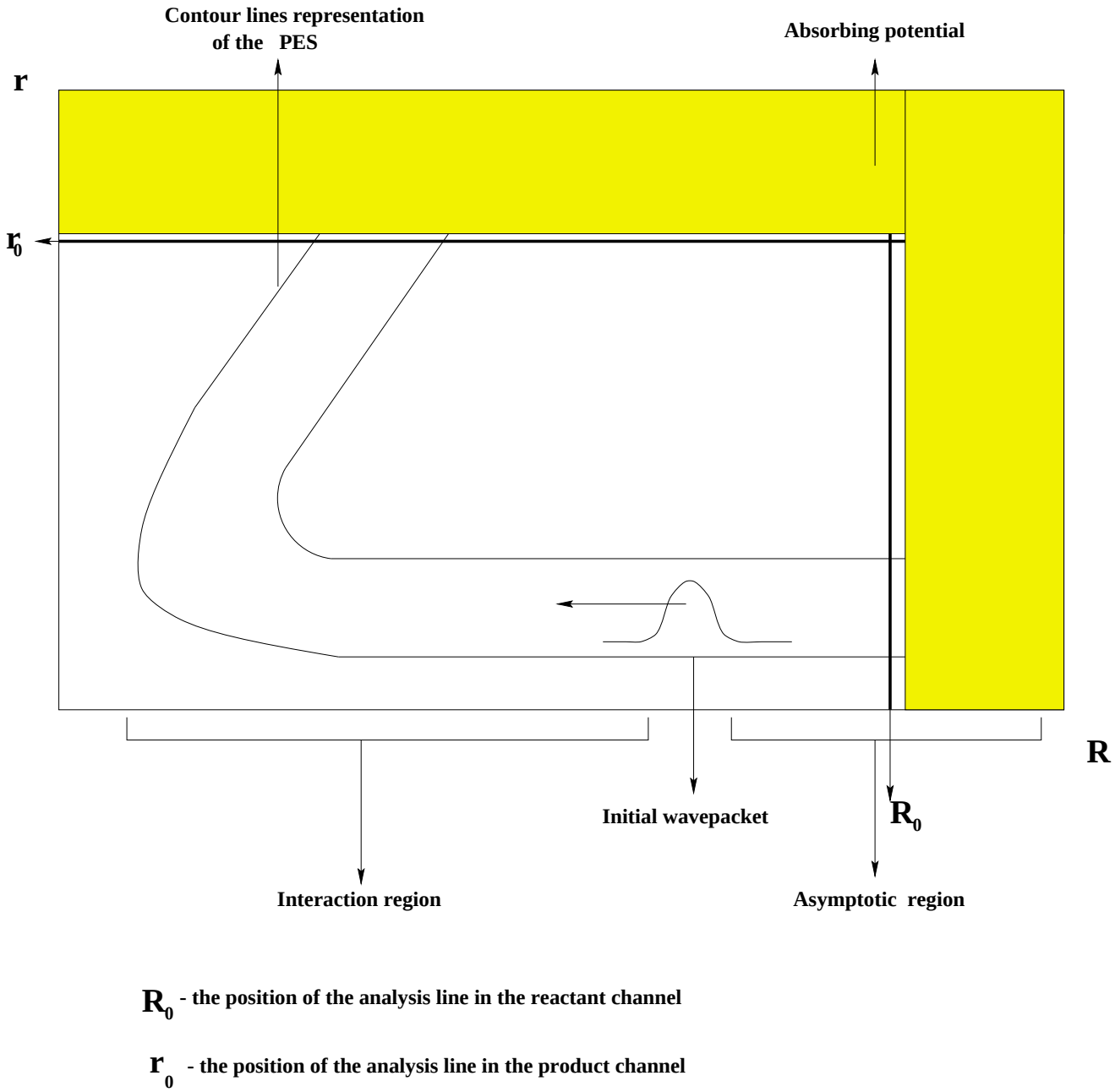

Figure 6: Analysis of the propagated wavepacket in Jacobi coordinates (R, r, θ) for a fixed value of the angle θ. The interaction region and the asymptotic region are shown. Analysis lines in both reactants and products coordinates are shown.

where $'i'$ denotes the interaction region and $'f'$ the asymptotic region. Since the time-dependent Schrödinger equation is linear we can propagate independently each term in Eq. (148). At each time step Ψ_f (=piece of the wavepacket located in the asymptotic region) is analyzed and Ψ_i (=piece of the wavepacket located in the interaction region) is propagated further by using the Chebyshev algorithm. Ψ_f is propagated as a free wavepacket just by multiplying it with the phase-factor $e^{-iE\delta\tau/\hbar}$, where $\delta\tau$ is the time step of the propagation.

The splitting is done using a function $f_p(R)$ which goes smoothly from 0 in the interaction region to 1 in the asymptotic region

$$\Psi(R,\mathbf{q},t) = (1 - f_p(R))\Psi(R,\mathbf{q},t) + f_p(R)\Psi(R,\mathbf{q},t). \tag{149}$$

The S-matrix components $S_{f,i}$ for entrance state i (configuration α= AB + C), final state f (configuration α'= A + BC) and the total energy E are [37, 52]

$$S_{f,i}(E) = \sqrt{\frac{k_i\mu_f}{k_f\mu_i}} \sum_{t_l} \frac{e^{\frac{iEt_l}{\hbar}}}{a_E} \left\langle \Phi_i(R,\mathbf{q}) | f\Psi(R,\mathbf{q},t_l) \right\rangle, \tag{150}$$

$$\Phi_i(R,\mathbf{q}) = e^{\frac{ik_iR}{\hbar}} \chi_i(\mathbf{q}). \tag{151}$$

k_i and k_f are initial and final relative momenta atom-diatom, μ_i and μ_f are effective masses of the system in the entrance, respectively exit channels. $\mathbf{q}$ is a collective index for the internal degrees of freedom of the diatomic molecule. $\chi_i(\mathbf{q})$ is the initial diatomic state and $f\Psi(R,\mathbf{q},t_l)$ is the component of the wavepacket which is splitted at the time step t_l. $\Psi_f(R,\mathbf{q},t) = f\Psi(R,\mathbf{q},t_l)$ is located in the asymptotic region of the grid.

The a_E factor is [52]

$$a_E = \int_0^\infty e^{\frac{ik_fR}{\hbar}} \eta_f(R, t=0) dR$$

where $\eta_f(R, t = 0)$ is the part which depends on R of the initial wavepacket (see Eq. (147)).

4.4.2 The half Fourier transform method

This idea for analysis of the propagated wavepacket is presented in the work of Balint-Kurti *et al.* [63, 64]. Its starting point is to compute at each time step the autocorrelation function, along a given analysis line - see Figure 6, lying in the asymptotic region

$$c(t) = \int_r dr \int_\theta \sin\theta d\theta \psi(r)\Psi(R = R_0, r, \theta, t). \tag{152}$$

R_0 defines the position of the 'analysis line'. $\psi(r)$ are the diatomic eigenfunctions. The half-Fourier transform of $c(t)$ becomes an energy dependent function

$$A(E) = \frac{1}{2\pi}\int_{t=0}^{\infty} dt e^{\frac{iEt}{\hbar}} c(t). \tag{153}$$

The S-matrix can be expressed as a function of A(E)

$$S(E) = (\frac{k_i k_f}{\mu_i \mu_f})^{1/2} \frac{e^{\frac{-ik_f R_0}{\hbar}}}{g(-k_i)} A(E). \tag{154}$$

k_i and k_f are initial and final relative momenta atom-diatom, μ_i and μ_f are effective masses of the system in the entrance, respectively exit channels and $g(k)$ is the Fourier transform of the initial wavepacket.

4.4.3 The flux analysis method

The idea of the flux analysis method is to compute the flux of probability for the wavepacket in the outgoing channel along an analysis line (Balakrishnan *et al.* [47], Neuhauser *et al.* [52], Meijer *et al.* [66]). From the flux of probability of the scattered wavepacket we can extract directly the reaction probability

$$P_R(E) = \frac{\hbar}{\mu} Im[\langle \Psi(R, r_0, E) | \frac{\partial \Psi(R, r_0, E)}{\partial r} \rangle]. \tag{155}$$

In the expression above we define

$$\Psi(R, r_0, E) = \psi(R, r_0, E)/A_e, \tag{156}$$

where

$$\psi(R, r_0, E) = \frac{1}{\sqrt{2\pi}} \int_{-\infty}^{\infty} \psi(R, r, t) e^{\frac{iEt}{\hbar}} dt|_{r=r_0}, \tag{157}$$

is the Fourier transform of the time-dependent wavefunction $\psi(R, r, t)$ at a given analysis line $r = r_0$, located in the products region. The potential energy in the analysis region is assumed to be a constant. The A_e factor is

$$A_e = (\mu/\hbar k_{n0})^{(1/2)} A_{n0}(k_{n0}), \tag{158}$$

μ is the reduced mass in the exit channel and k_{n0} is the average wavenumber of the plane waves in the entrance channel ($k_{n0} = \sqrt{2\mu(E - \epsilon_0)/\hbar}$, E is the total energy of the wavepacket and ϵ_0 is the energy of the initial state of the diatomic). The expression of $A_{n0}(k_{n0})$ is

$$A_{n0}(k_{n0}) = \frac{1}{\sqrt{2\pi}} \int_0^{\infty} \int_0^{\infty} \Psi(R, r, t = 0) \phi(r) e^{-ik_{n0}R} dr dR. \tag{159}$$

The final expression for the reaction probabilities in term of flux becomes

$$P_R(E) = \frac{\hbar^2 k_{n0}}{\mu^2 |A_{n0}(k_{n0})|^2} Im[\langle \Psi(R, r_0, E) | \frac{\partial \Psi(R, r_0, E)}{\partial r} \rangle]. \tag{160}$$

For $J > 0$ the relation becomes

$$P_R^J(E) = \frac{\hbar^2 k_{n0}}{\mu^2 |A_{n0}(k_{n0})|^2} \sum_{\Omega=0}^{J} Im[\langle \Psi_\Omega(R, r_0, E) | \frac{\partial \Psi_\Omega(R, r_0, E)}{\partial r} \rangle], \tag{161}$$

where $\Psi_\Omega(R, r_0, E)$ and $\partial \Psi_\Omega(R, r_0, E)/\partial r$ are computed, as explained above, for the given Ω channel.

5 Implementation

5.1 Scalar implementation

For 1D systems several test-programs were implemented. This concerns both the simple propagation of wavepackets described in the two sections before, and advanced features like non-adiabatic coupling of two potential energy curves and the filter diagonalisation method for computing resonance states in the scattering processes.

After a description of these tests the full 3-D, $J > 0$ implementation program is described. There exists two versions of the program: a) scalar ("usual implementation") and b) parallel implementation.

5.2 1D propagation

The implementation follows the usual features of the wavepacket propagation:

- Chebyshev expansion of the evolution operator
- DVR representation for the wavefunction in order to compute the contributions of the kinetic (rotational part) and potential energy to the Hamiltonian
- For the kinetic energy (translational part), FFT back and forth transformation of the wavefunction (kinetic energies are computed in momentum representation)

Several tests were made concerning the stability of the propagation when the wavepacket includes very large, respectively very small energies. The mean value of the wavenumbers included in the wavepacket is printed at each run

$$k_{mean} = \sqrt{2\mu E_{mean}}, \tag{162}$$

where E_{mean} is the mean energy of the wavepacket and μ is the mass.

The extreme values of momentum allowed by the grid are printed

$$k_{max} = \frac{\pi}{2dx}, \quad k_{min} = \frac{\pi}{2\Delta x}. \tag{163}$$

dx is the distance between two grid points and Δx is the length of the complete grid.

When the mean value of the wavenumbers included in the wavepacket k_{mean} is $k_{mean} \approx (k_{min} + k_{max})/2$, the propagation is correct. When this value is close to the maximum allowed by the grid, $k_{mean} \approx k_{max}$, some components of the wavepacket are propagated backward with respect to the interaction region. For $k_{mean} \approx k_{max}$ there is practically no propagation (the wavepacket decomposes itself in forward and backward components).

When $k_{mean} > k_{max}$ the whole wavepacket is "correctly" propagated backward with respect to the interaction region.

The same scenario occurs when k_{mean} is close to the minimum allowed by the grid ($k_{mean} \approx k_{min}$).

This information is useful for calculation of "heavy systems" (e.g. molecules heavier than the H_2 molecule) or "light systems" (like scattering of electrons).

5.2.1 Two potential energy surfaces propagation

The Born Oppenheimer approach is the basic assumption for the most of the dynamical calculations. Because the nuclei are heavier than the electrons, their velocities can be considered small compared to those of electrons. The complete wavefunction can be separated as a product

$$\psi(\mathbf{Q_i}, \mathbf{q_j}) = \psi_1(\mathbf{Q_i})\psi_2(\mathbf{q_j})$$

where $\psi_1(\mathbf{Q_i})$ is the nuclear wavefunction of nuclear coordinates $\{\mathbf{Q_i}\}$ and $\psi_2(\mathbf{q_j})$ is the electronic wavefunction of electronic coordinates $\{\mathbf{q_j}\}$. For a given nuclear configuration $\{\ \mathbf{Q_i}\ \}$, different electronic wavefunctions lead to different total energies of the molecular system, hence to different potential energy curves (for diatomics) or surfaces (for molecules with more than 3 atoms). In the Born-Oppenheimer approach, there is no coupling between different potential energy surfaces, and the total wavefunction is the product between nuclear and electronic wavefunctions.

More realistic models consider that a coupling between different potential surfaces is possible. The way how the couplings between potential energy surfaces can be computed in the adiabatic or diabatic representation was discussed in Eqs. (115) - (123).

In this section we discuss a simple 1D implementation model for the propagation of a wavepacket using two potential energy curves in the diabatical representation.

Technical details. The 2-PES propagation is performed using an appropriate storage of the wave function and the potential. In order to apply the Hamiltonian on the array vector optimally, all the vectors have to be stored in the following manner

$$\psi(nx, npot),$$

where nx is the number of grid points and $npot$ the number of PES. All the usual 'do loop' according to number of points in a vector are given twice: one for the nx variable and one for the $npot$ variable.

We use a Gaussian-type coupling,

$$H_{coupl} = z_0 e^{(x-x_0)^2}, \tag{164}$$

where z_0 is the amplitude of the coupling (we set $z_0 = 0.1$ E_h for present tests). Alternatively, we have implemented an electric dipole type coupling

$$\hat{H}_{coupl} = z_0(x - x_0). \tag{165}$$

For our tests we defined a coupling that acts between x_0 and $x_0 + 2$ a_0. x_0 defines where the coupling is located in space. The complete Hamiltonian matrix for a 2 level coupling has the following form:

$$\hat{H} = \begin{pmatrix} \hat{H}_1 & \hat{H}_{coupl} \\ \hat{H}_{coupl} & \hat{H}_2 \end{pmatrix},$$

where $\hat{H}_1$ is the Hamiltonian which describes the dynamics for the first potential surface ($\hat{H}_1 = \hat{p}^2/2\mu + \hat{V}_1$) and $\hat{H}_2$ is the Hamiltonian which describes the dynamics for the second potential surface ($\hat{H}_2 = \hat{p}^2/2\mu + \hat{V}_2$).

The implementation of the coupling in the Hamiltonian is shown in the **Appendix 3**.

Results. Test calculations were made for the first two levels of the Cl_2 molecule. The first two potential curves are simulated by a Morse potential

$$V_{Morse} = d_0(1 - e^{-a(x-x_0)^2}), \tag{166}$$

where d_0 is the potential well, $a = (\frac{\mu}{2d_0})^{1/2}\omega$, with μ the mass of oscillator and ω its frequency. x_0 is the position of the minimum of the potential energy.

The realistic equilibrium distances and dissociation energy (0.091 E_h and 3.78 a_0 - for the first potential curve, and 0.013 E_h and 4.42 a_0 - for the second curve) were taken from ab initio calculation [67]. The gaussian coupling was centered at $x_0 = 4.0$ a_0 close to the minima of both potential curves.

For the first potential curve 98 bound states exists, for the second 34. Initially the wavepacket was located only on the first curve. The mathematical expression of the wavepacket is

$$\psi(x, t = 0) = \sqrt{\frac{\sqrt{2}}{\pi\sigma}} e^{-ik_0 x} e^{-\frac{(x-x_0)^2}{\sqrt{2}\sigma}}, \tag{167}$$

with σ - the initial width of the wavepacket and k_0 its mean wavenumber.

During the propagation, the population of the second component of the wavefunction increases progressively. It reaches a maximum when the wavepacket is located entirely in the interaction region (e.g. after 50 time steps Δt (Δt=200 a.u.)).

The dynamics of the wavepacket for two coupled potential energy curves is plotted in Figures 8 and 9. In the first case, (see Figure 8), the initial position of the wavepacket was $x_0 = 8.5$ a_0. This scenario corresponds to a collision between the two Cl_2 atoms, at the mean energy of $E_{mean} = 1$ eV. The two potential energy curves couple and the wavepacket has a different dynamics on each of them. A small part of the wavepacket is "trapped" as a stable bound state (see the Figure 8, last row).

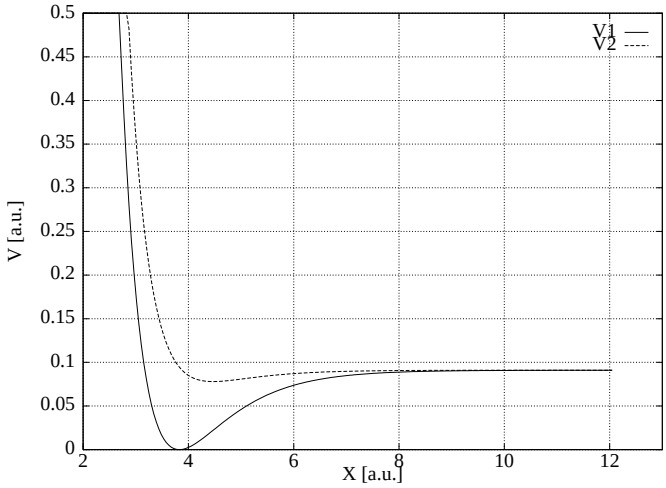

Figure 7: The first 2 potential energy curves for the Cl_2 molecule, simulated by a Morse potential. The parameters are extracted from ab initio calculations.

In the second case, the evolution of the two atoms starts near the equilibrium distance (see Figure 9). In the beginning the wavepacket rests for a longer time in the interaction region. In this case the values of the wavefunction which populates the second potential energy curve are larger than those in the first case (see Figures 8 and 9, second column). This happens because the wavefunction spend a longer time in the region where the coupling is located. The coupling was

$$V_{coupling} = z_0 e^{-(x-x_0)^2}, \tag{168}$$

where $z_0 = 0.1\mathrm{E}_h$, $x_0 = 8.5$ a$_0$ (Figure 8), respectively, $x_0 = 4.0$ a$_0$ (Figure 9). One can see that the second potential energy curve which is not so deep, is used as an "escape channel" by the wavepacket: for time t >2000 a.u. and $x > 6$ a$_0$ the norm of the wavepacket on the upper surface is larger than the norm of the wavepacket for the lower surface.

5.2.2 Bound states from wavepackets

In case of a sparse matrix Hamiltonian, it is inefficient to calculate bound states by using direct full matrix diagonalisation techniques. Several methods were proposed to solve the problem of sparse matrices eigenvectors [68] (e.g. the relaxation method of Tal-Ezer and Kosloff [69], the Lanczos algorithm [70] etc.). A general characteristic of these methods is that they are iterative methods, which allow the study of eigenvalues within a given energy range.

Filter diagonalisation [71, 72, 73] is an iterative method which we tested by using the 1D implementation of the wavepacket propagation. The present implementation follows the paper of Neuhauser [71] and is based on the time-energy resolution of the wavepacket. It

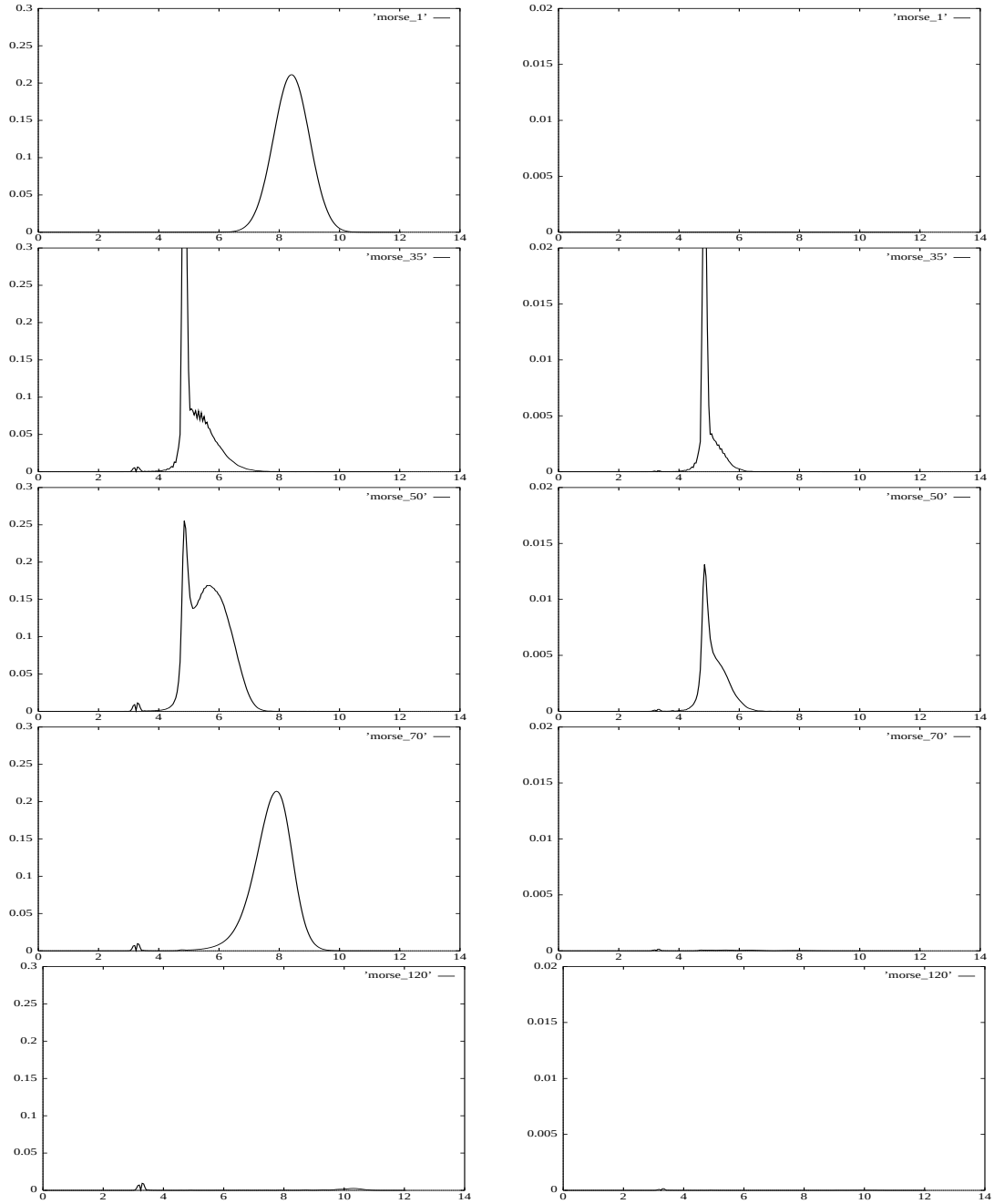

Figure 8: Propagation of a wavepacket on two coupled potential energy curves. A collision between two Cl atoms is simulated: the initial wavepacket is located at the 8.5 a_0. In this region the potential between the Cl atoms is a constant. From top to bottom snapshots at several time-steps are presented (t =70, 2450, 3500, 4900 and 8400 a.u.) The parameters of the initial wavepacket were: mean energy $E_0 = 0.33$ eV, center at $x_0(t = 0) = 8.5$ a_0. Left: lower potential curve. Right: upper potential curve. After a long propagation time the wavepacket is absorbed by the imaginary potential (see Eq. (76)).

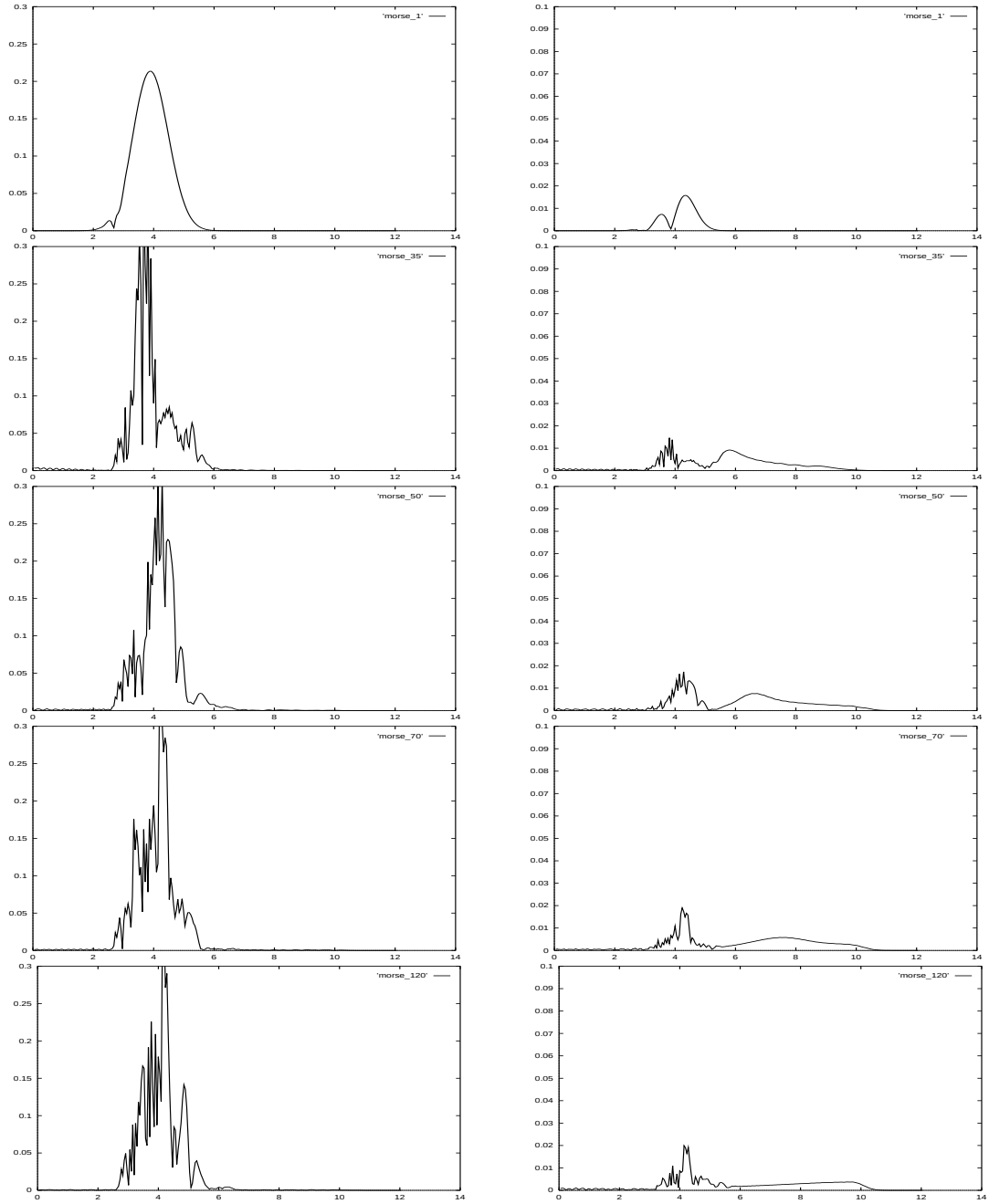

Figure 9: Propagation of a wavepacket on two coupled potential energy curves of Cl_2 molecule. The initial wavepacket is located at 4.0 a_0, close to the bottom of both potential curves. From top to bottom snapshots at several time-steps are presented (t =70, 2450, 3500, 4900 and 8400 a.u.) The parameters of the initial wavepacket were: $E_0 = 0.33$ eV, $x_0(t = 0) = 4.0$ a_0. Left: lower potential curve. Right: upper potential curve. After a long propagation time the wavepacket is absorbed by the imaginary potential (see Eq. (76)).

can be also used to avoid long propagation times in the case of scattering with resonances [74, 75].

The conceptual problem in applying real-time propagation methods to obtain bound-states is that the initial wavefunction remains indefinitely trapped in these states and its norm does not decay. Different states, however, loose their phase coherence rapidly. Therefore, for any chosen energy E the long-time Fourier transform ($\hbar = 1$)

$$|\psi(E)\rangle \approx \int_{-T}^{T} |\psi(t)\rangle e^{iEt} dt, \quad T \to \infty \tag{169}$$

will converge to the bound state closest in energy to E.

The evolution of the wavepacket is described through the evolution operator $e^{-i\hat{H}t}$ as

$$\psi(x,t) = e^{-i\hat{H}t}\psi(x,t=0). \tag{170}$$

We can expand $\psi(x,t)$ in terms of eigenfunctions $\phi(x,\epsilon_n)$ of $\hat{H}$. For a discrete spectrum the expansion is

$$\psi(x,t) = \sum_n a_n \phi(x,\epsilon_n) e^{-i\epsilon_n t}, \tag{171}$$

where ϵ_n are the eigenvalues of $\hat{H}$. The expansion coefficients are

$$a_n = \langle \psi(x,t=0) | \phi(x,\epsilon_n \rangle. \tag{172}$$

For a continuum spectrum, Eq. (171) becomes

$$\psi(x,t) = \int a_\epsilon \phi(x,\epsilon) e^{-i\epsilon t} d\epsilon, \tag{173}$$

with $a_\epsilon = \langle \psi(x,t=0) | \phi(x,\epsilon) \rangle$.

Using the relations above, we can compute the quantity $a_\epsilon \phi(x,\epsilon)$ as back Fourier transform of the propagated wavefunction $\psi(x,t)$

$$2\pi a_\epsilon \phi(x,E) = \int_{-\infty}^{\infty} \psi(x,t) e^{iEt} dt. \tag{174}$$

In practice, the propagation time goes from $t_0 = 0$ up to $t_1 = t_{max}$. t_{max} is the propagation time needed till the norm of the propagated wavepacket decreased to zero (e.g. the order of magnitude which is needed for a required accuracy). The integral in Eq. (174) usually needs a long propagation time to converge. To get a better convergence the wavefunction is multiplied by an artificial damping factor $g(t)$. The filtered wavepacket at energy E will be

$$\psi(x,E) \equiv \int_{-\infty}^{+\infty} \psi(x,t) e^{iEt} g(t) dt. \tag{175}$$

By using the *convolution theorem* [51], which has the general form

$$\int_{-\infty}^{\infty} f(x) p(x) e^{-ikx} dx = \int_{-\infty}^{\infty} F(q) P(k-q) dq \tag{176}$$

with $F(q)$ and $G(q)$ being the Fourier transforms of $f(x)$ and $p(x)$, respectively, we get

$$\psi(x,E) = \int_{-\infty}^{\infty} a_\epsilon \phi(x,\epsilon) G(E-\epsilon) d\epsilon. \tag{177}$$

If we write this in a discretised basis set we get the relation between $\psi(x,E)$ and the eigenfunctions of $\hat{H}$ (Neuhauser [71])

$$\psi(x,E) = \sum_n a_n \phi(x,\epsilon_n) G(E-\epsilon_n), \tag{178}$$

with

$$G(w) = \int e^{iwt} g(t) dt, \tag{179}$$

the Fourier transform of $g(t)$. By comparing the results of Eqs. (175) - (178) it is possible to find the eigenvalues ϵ_n. If $G(w)$ is a narrow band function, each term in Eq. (178) contributes to the sum with a narrow peak. The graphical representation of $\psi(x,E)$ in Eq. (178) looks like an approximate spectrum of eigenvalues.

For a good energy separation the wavepacket must be propagated for a time

$$t \approx \frac{1}{\delta E}, \tag{180}$$

where δE is the energy separation between the analyzed state and its nearest neighbour ($\delta E = \epsilon_n - \epsilon_{\pm 1}$). This simple method will require very long propagation times for closely spaced eigenvalues. A qualitative summary of this discussion is presented in Figure 10, where the shape of $\psi(x,E)$ and $\psi(x = 4\ \mathrm{a_0}, E)$ are given for a Morse type potential (see Eq. (166)) with a well depth $d_0 = 0.091\ \mathrm{E}_h$ and a equilibrium distance $x_0 = 3.78\ \mathrm{a_0}$. The mass of the Morse oscillator was set to 1840 a.u.. This set of parameters leads to 14 bound states.

Initially the wavepacket is defined as a narrow band function centered at $x = x_0$. For the usual Hamiltonian $\hat{H} = \hat{P}^2/2\mu + \hat{V}(x)$ the location of the initial wavepacket should be chosen such that $V(x_0) < E_1$ (where E_1 is the lowest eigenvalue of the spectrum).

The implementation includes the following:

- 1D propagation of the wavepacket: the propagation time is set up by using Eq. (180).
- At each time step two values are stored: $\psi(x,t)$ - the propagated wavepacket and $\chi(x,t) = g(t)\psi(x,t)$ - the filtered wavepacket.
- After finishing the propagation $\psi(x,E)$ and $\chi(x,E)$ are computed from the stored components ($\psi(x,t)$ and $\chi(x,t)$) by using FFT.

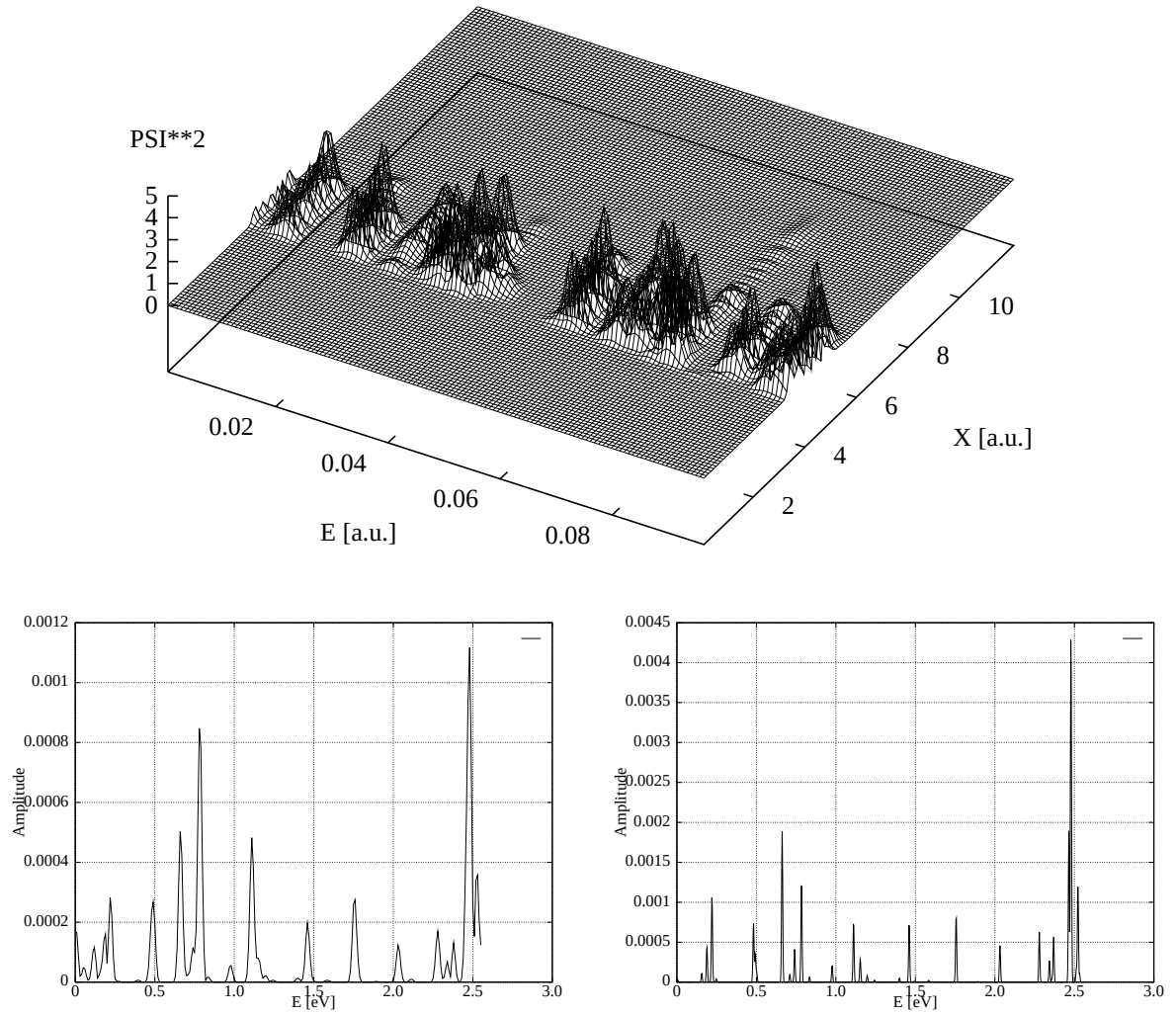

Figure 10: Top: the 3D picture of the Fourier transform of the absolute value of the filtered function $\chi(x,E) = \int_{-\infty}^{\infty} g(t)\psi(x,t)e^{iEt}dt$. Bottom: a cut through the 3D picture (top) at the 14-th grid point (approx. $x = 4$ a.u.). Bottom left: propagation time step was $t = 200$ a.u., number of steps=256. Bottom right: the same time step, but with 1024 steps in the propagation leading to a better resolution for the first 14 energy eigenvalues.

- $\chi(x_0, E)$ is plotted at a value x_0. The plot shows the approximate location of the eigenvalues in energy (according to Eq. (178)) if $G(E-\epsilon_n)$ is a narrow band function in energy space (e.g. Gaussian).

- At the given approximate locations found above a more refined calculation is performed afterwards by using the functions produced by FFT

$$E_n =< \psi(E,x)|\hat{H}|\psi(E,x) > . \tag{181}$$

If the propagation time is shorter than the time indicated by Eq. (180), then each energy peak contains information about several eigenvalues. In this case we have a small Hilbert space associated with the given peak, and the eigenvalues can be recovered by diagonalisation of a $n \times n$ matrix type, where "n" must be larger than the number of eigenvalues contributing to the given peak. The matrix is produced by choosing several positions in the energy grid ("E_n" points of the grid) and computing then the matrix elements $< \psi(E_n, x_i)|\hat{H}|\psi(E_n, x_i) >$, where E_n is a position inside of the peak and x_i a arbitrary space point. The number of energies in the peak must be guessed reasonably before all calculations start.

The code is still in the test phase.

5.3 3D propagation of the wavepackets

The full code can propagate the 3D wavepackets for $J > 0$, using the fully-coupled Hamiltonian given in Eq. (96) and the Chebychev expansion of the evolution operator. The code was developed from an existing version previously tested by Prof. Jaquet's group for $J = 0$ problems. Both short-time and long-time propagation schemes were tested for different absorbing potentials showing good results. The long-time propagation scheme requires the Mandelshtam and Taylor formulation of the Chebychev recursion formula [27, 28].

The next scheme was used in order to include the $J > 0$ quantum numbers in the propagated wavepacket:

- The angular part of the wavepacket was assigned by two indices. The first index labels the projection of the total angular momentum $\hat{J}$ onto the Z body-fixed axis (Ω). The second index describes the Jacobi angle θ (for a given Ω).

- A DVR representation was set up for the wavepacket, using a set of points as described in Eq. (138).

- The complete Hamiltonian has the general matrix form

$$H^J = H_\Omega + H_{coupling}, \tag{182}$$

in the DVR-FFT basis set described in section 3. H_Ω is the part of the Hamiltonian which is diagonal with respect to the Ω quantum number.

$$H_\Omega = H_{\Omega=0} \oplus H_{\Omega=1} \oplus ...H_{\Omega=J} \tag{183}$$

and the coupling term $H_{coupling}$ connects $H_{\Omega=m}$ with $H_{\Omega=m+1}$ and $H_{\Omega=m-1}$ blocks (see the last term in Eq. (96)).

The propagation of the wavepacket follows then the steps described in the 1D implementation part (see **Section 3**).

The output of the propagation part of the program includes information about the wavepacket at each time step during the propagation.

5.4 Analysis

The analysis part of the program uses the files stored during the propagation to produce the reaction probabilities. Three methods have been tested. The grid parameters used in the different calculations are summarized in Table 1.

Calculation	N_t	Δt [a.u.]	N_R	ΔR [a_0]	N_r	Δr [a_0]	N_θ	σ [a_0]	E_0 [eV]	$Type$
Figure 11	230	25	128	14.0	64	7.0	32	0.5	0.8	R
Figure 12	1	6000	128	11.0	64	7.0	32	0.5	0.6	R
Figure 13	1	6000	128	11.0	128	10.0	40	0.25	1	R
Figure 14	1	6000	128	11.0	64	7.0	32	0.5	0.6	P

Table 1: Grid parameters used to compute reaction probabilities given in Figures 11 - 14

The notations are :
N_t - the number of time steps.
Δt - the length of one time step (in atomic units [a.u.]).
N_R - the number of grid points in R direction.
ΔR - the length of the grid in R [a_0].
N_r - the number of points in r direction.
Δr - the length of the grid in r [a_0].
N_θ - the number of points for the θ coordinate.
σ - the initial width of the wavepacket with respect to R [a_0].
E_0 - the initial mean energy [eV] of the wavepacket.
$Type$ - is the type of analysis - in the reactant zone (R) or in the product zone (P).
We compared our results with Zhang and Miller's time-independent results [76].

5.4.1 The split-function method

The split-function method is implemented for the short-time propagation scheme. Within this scheme, the complete propagation (propagation time t $\approx$ 5-10000 a.u.) is simulated by a set of several short time-steps ($\Delta\tau$ = 25-100 a.u.). After each short propagation the wavepacket is splitted into two pieces - the one lying in the interaction region and the one located in the asymptotic region. The second piece is stored (binary) at each time step. When the propagation is finished, the analysis part of the program reads this file and produces the S-matrix according to the Eq. (150).

During the tests this method was found to be not accurate enough. For the D+H_2 $\rightarrow$ DH +H reaction the following behavior occurs:

- For a propagation time smaller than t = 4000 a.u. the reaction probability is underestimated
- For a propagation time $t \approx$ 5000 a.u. the reaction probability is correctly described
- If the propagation time is still increased (more than t = 6000 a.u.) the reaction probability acquires an artificial oscillatory structure. According to Heather and Metiu [59], the final momentum distribution $P_f(k_\mu)$ of the scattered wavepacket

$$P_f(k_\mu) \equiv |\langle k_\mu|\psi(t_f)\rangle|^2 \tag{184}$$

(k_μ are the momenta included in the scattered wavepacket and t_f is the complete time needed for propagation) is not well described when the grid is too short. We can write the expression for the final momentum distribution as a sum over time steps t_α

$$P_f(k_\mu) = |\sum_{\alpha=1}^{S}\langle k_\mu|\hat{W}(t_\alpha,t_f)|\psi(t_\alpha)\rangle|^2. \tag{185}$$

$\hat{W}(t_\alpha,t_f)$ is the evolution operator, and t_α is the moment when the split of the wavepacket is done. The insufficient accuracy in describing $P_f(k_\mu)$ can lead to an interference between the terms of Eq. (185) at late times (large α values). The interference is responsible for the oscillatory structure of the reaction probability in the split method.

5.4.2 The analysis line method

Another possibility to investigate the wavepacket in the "free-force region" is to analyze the wavefunction at the so-called "analysis line" (see Figure 6).

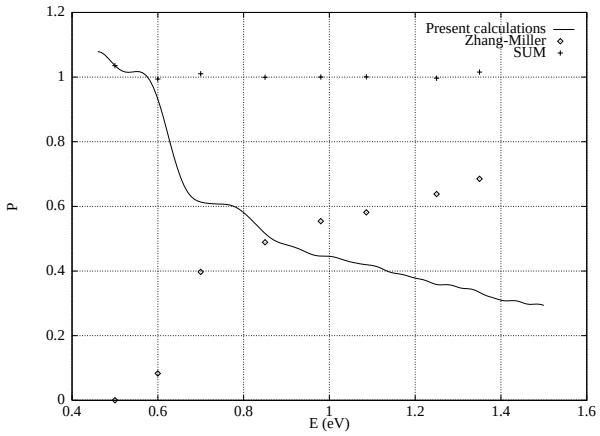

Figure 11: Inelastic transition probabilities, $P(E)$, for the D + H_2 (v =0, j =0)→ DH + H reaction. Analysis method: split function. The symbols ⋄ are the time-independent reactive calculations of Zhang and Miller [76]. The symbols + present the sum of the present inelastic reaction probabilities and Zhang and Miller's reactive results.

The method was tested for long-time propagation schemes. At each iteration in the Chebychev expansion the autocorrelation function is computed for the last term in the recursion scheme and stored until the propagation is finished.

The analysis part of the program reads these data and computes the S-matrix using Eq. (154). Compared to the split-function method the advantage of this method is that during the propagation not so many data have to be stored and that the algorithm for the analysis of these data is fast.

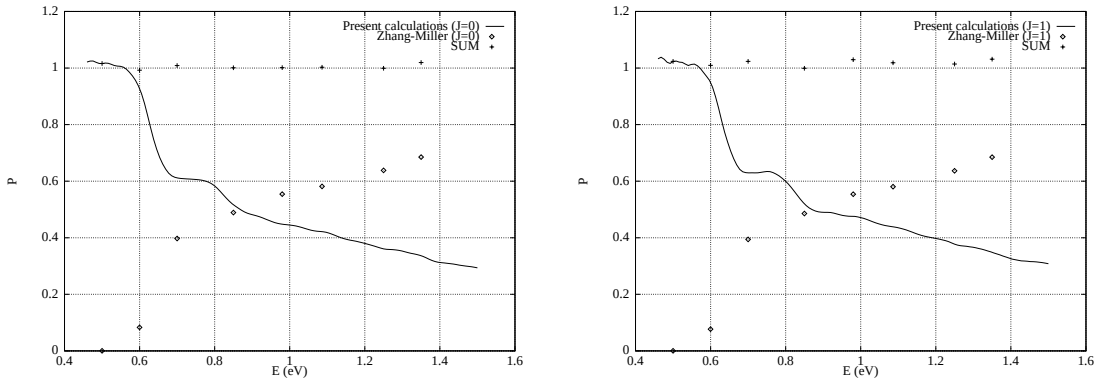

Figure 12: Inelastic transition probabilities for the D+H_2 (v=0, j=0) → DH +H reaction using the analysis line method for $J = 0$ (left) and for $J = 1$ (right). The symbols ⋄ are the time-independent reactive calculations of Zhang and Miller [76]. The symbols + give the sum of present inelastic reaction probabilities and Zhang and Miller's reactive calculations.

The effect of different grid parameters can be seen by comparing Figure 12 with Figure 13. The accuracy in the range of small energies is improved because the new grid can offer more information about the small frequencies included in the wavepacket.

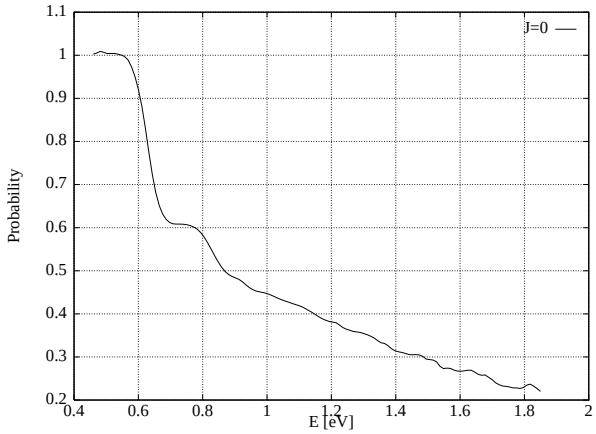

Figure 13: The same method as in Figure 12, but with a different set of numerical parameters (larger grid, more grid points), $J = 0$.

5.4.3 The flux analysis method

The flux analysis method needs information of the wavepacket at the analysis line. The storage requirements are higher since at each iteration a copy of the wavefunction and of its derivative are needed. This method was found to be in our implementation the most stable and accurate one. The analysis line can be placed into the product region, and by that the reaction probability is computed directly without the change of coordinates.

The total reaction probabilities for total angular momentum $J = 0$ and $J = 1$ are given in the Figure 14, together with Zhang and Millers's results [76].

We obtained a good accuracy in small energy regime (E = 0.4 - 1.0 eV). At energies $E_i > 1$ eV the reaction probabilities are not correctly described. For the energies $E_i < 1$ eV the absolute values $|P_{time-dependent}(E_i) - P_{time-independent}(E_i)|$ are less than 0.01 for $J = 0$, respectively less than 0.015 for $J = 1$. For the energies $E_i > 1$ eV these values have a maximum of 0.05 for $J = 0$, respectively, 0.053 for $J = 1$.

The reasons for that are the initial energy and width of the wavepacket. An improved set of parameters is discussed in **Section 6** - "Results".

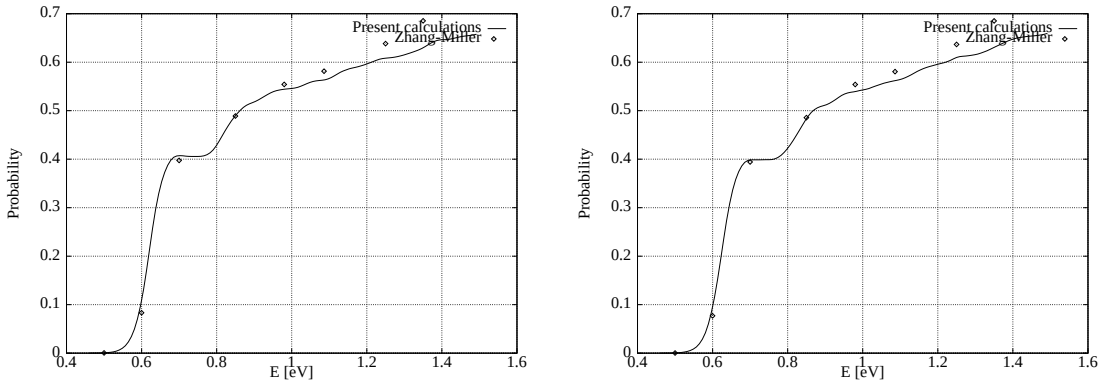

Figure 14: The reaction probability for D+H_2(v=0, j=0)→DH +H reaction using the flux analysis method for $J = 0$ (left) and for $J = 1$ (right). For comparison the Zhang and Miller results are given [76].

5.5 Parallel implementation

The parallel implementation exploits the matrix representation of the Hamiltonian

$$H = \begin{pmatrix} H_{\Omega=0} & H_{\Omega=0,+} & 0 & 0 & 0 & \dots \\ H_{\Omega=1,-} & H_{\Omega=1} & H_{\Omega=1,+} & 0 & 0 & \dots \\ 0 & H_{\Omega=2,-} & H_{\Omega=2} & H_{\Omega=2,+} & 0 & \dots \\ 0 & 0 & \dots & \dots & & \ddots \end{pmatrix}, \tag{186}$$

where, according to Eq. (96), each block is the matrix representation of the operator

$$\hat{H}_\Omega = -\frac{1}{2\mu_{A-BC}}\frac{\partial^2}{\partial R^2} - \frac{1}{2\mu_{BC}}\frac{\partial^2}{\partial r^2} - \frac{1}{2I}(\frac{1}{sin\theta}\frac{\partial}{\partial\theta}sin\theta\frac{\partial}{\partial\theta} - \frac{\hat{j}_z^2}{sin\theta^2})+$$
$$+\frac{1}{2\mu_{A-BC}R^2}(\hat{J}^2 - 2\Omega^2) + \hat{V}(R,r,\theta), \tag{187}$$

and

$$\hat{H}_{\Omega,\pm} = -\frac{1}{2\mu_{A-BC}R^2}(\hat{J}_\pm\hat{j}_\mp). \tag{188}$$

Since the action of $\hat{H}_\Omega$ and $\hat{H}_{\Omega,\pm}$ on the wavefunction is computed independently, and the action of $\hat{H}_{\Omega,\pm}$ on ψ takes $\approx$ 20 times less CPU than the action of $\hat{H}_\Omega$ on ψ, the parallelisation concerns just the "Ω diagonal Hamiltonian" which can be represented as follows:

$$H_{diag} = \begin{pmatrix} H_{\Omega=0} & 0 & 0 & 0 & 0 & \dots \\ 0 & H_{\Omega=1} & 0 & 0 & 0 & \dots \\ 0 & 0 & H_{\Omega=2} & 0 & 0 & \dots \\ 0 & 0 & \dots & \dots & \dots & \ddots \end{pmatrix}. \tag{189}$$

The action of each H_Ω block on the wavefunction can be computed independently on different processors.

5.5.1 General presentation of the parallel scheme

We used the MPMD (Multiple Program Multiple Data) paradigm [77] to parallelise the WAVE program. A graphical representation of this paradigm is given in Figure 15 (one arrow is a sequence of data processing).

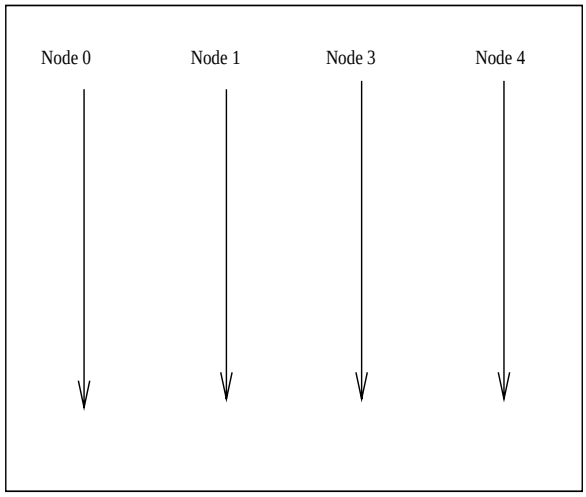

Figure 15: Without communication, a program is running on several nodes of a parallel system.

Each node of the parallel context [8] receives a copy of the program and a set of input data. The data are processed then independently on each node. The benefit of parallelisation comes by splitting a given task of the program (for instance a "do-loop") between different nodes, so that each node does just a part of the complete job. In order to do that a communication between processes is needed: first at the level "A" (see the Figure 16) the pieces of the vector which must be processed in the parallel context are sent to different nodes, then at the level "B" the results of several independent calculations are collected, and a new complete vector has to be formed.

Because this communication process takes time, the complete information about $\psi(t)$ is recovered only in node 0 ("the main node"), while the other nodes keep just pieces of it. The structure of the complete program can be represented as in Figure 17.

"N" programs run on "N" nodes of the parallel context, but only the node 0 produces the complete output. The other nodes are available for those pieces of the program where a parallel calculation is needed (see Figure 17).

It was found by experience that a synchronization between processes which are very different (e.g. when only node 0 does the input-output operations and the other nodes have to wait till the processing starts) is quite difficult to do. There are some subroutines

[8] A collection of processes (group) which may communicate to each other is labeled parallel context.

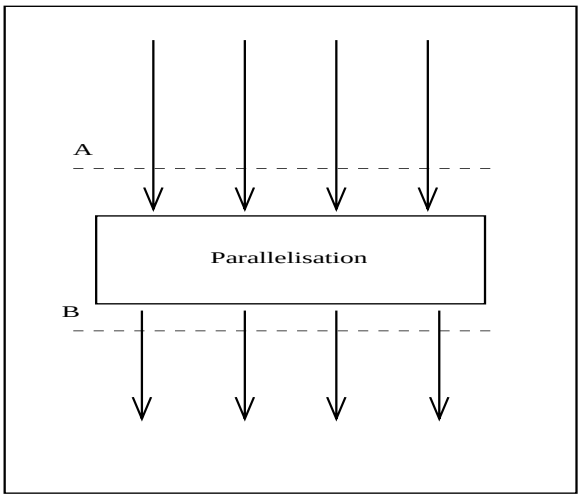

Figure 16: A program runs on several nodes of a parallel system. Between the situation "A" and "B" different nodes communicate.

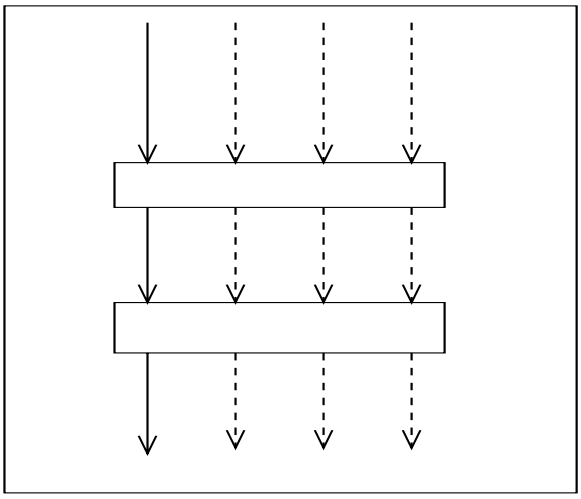

Figure 17: A parallel program runs on several nodes. There are two main steps: the computations done independently on each node and the communication between nodes.

available which helps for synchronization [80]. On the other hand, processes which have almost the same speed can be synchronized easier.

Within the **BLACS library** (Basic Linear Algebra Communication Subprograms) software all the parallelisation tasks are supported. An exact description of all the **BLACS** features can be found in www.netlib.org/blacs. **BLACS** software is designed to make different parallel applications more portables and can manage several message-passing parallel libraries (like MPI, MPL or PVM). The most important calls within **BLACS** are:

blacssetup(icontext, iam) - creates the parallel context (using MPI, in this case) where "icontext" is the parallel communicator [9] process and "iam" is the index of the current node in the parallel context.

blacsgridinit() - initialization of the processor grid required by the actual calculation (number of processors and the way they are ordered by MPI).

blacsbarrier(icontext, iam) - wait until all the processes are reaching this point. It helps in synchronization of the jobs between different processors.

blacsexit() - close the parallel context.

For the communication part we wrote a subroutine which splits the array where the wavefunctions is stored among the nodes of the parallel context. We used the **zgesd2d BLACS** subroutine to send a two-dimensional complex array from node 0 to the other nodes of the parallel context, and the **zgerv2d** subroutine to collect on node 0 the arrays from different nodes. The FORTRAN implementation of the communication subroutines is given in the **Appendix 4**.

5.5.2 Parallelisation with respect to Ω channels

The basic idea of parallelizing the action of the Hamiltonian on the wavefunction is to transform the 'do loop' over the different Ω values:

```
do i=1, omega
.............
enddo
```

into a parallel instruction, executed on several different processors:

```
do i=n1,n2
..........
enddo
```

[9] The communicator is a special feature introduced by MPI. It consist in labeling a set of processes by the same index and creating a group of processes acting synchronic in a parallel context.

All the processors receive successive values of n1 and n2 (processor 1: n1=1, n2=2, processor 2: n1=2, n2=3 etc - for a run on a grid of 'omega' processors).

On the SP2 machines of the University of Karlsruhe, one step of the 'do loop' above takes about 1.0 s. This is much larger than the communication time. In the calculations made for the $D+H_2 \rightarrow DH + H$ reaction, the "scatter" and "gatter" subroutines described above, need around 0.07 s to distribute the whole wavefunction over the nodes. Therefore, because the computing time is small compared to the communication time, the strategy described above can significantly decrease the computing time.

An improved version of the program includes a parallel computation of the DVR to FBR transformation of the wavepacket. The wavefunction, indexed by Ω, can be split into Ω pieces, when the transformation given by Eq. (143), is performed.

For $J = 1$ the program uses 2 processors. We used a grid of $128 \times 64 \times 32$ points in R, r, and θ Jacobi coordinates. In this case the scalar version needs ≈ 0.1 s to compute the action of the potential to the wavefunction, ≈ 0.03 s for the rotational part and ≈ 1.25 s for the kinetic energy part (two times FFT in R and r) of the Hamiltonian. About 1.8 s are needed for the back and forth transformations DVR - FBR. Both kinetic and transformation parts include a "do loop" over the two possible Ω values in the $J = 1$ case. The parallel version needs only ≈ 0.9 s for the transformation and $0.9 - 1.0$ s for the kinetic energy part. In addition, a call of the "scatter/gatter" subroutines takes ≈ 0.05 s, each time when one of them is called. In order to synchronize all the processes in the parallel context, we use

```
call blacs_barrier()
```

before the call of the "gatter" subroutine. The effect of this call is that the fast processes wait until the slowest one calls also the "barrier" subroutine. This waiting time is $\approx 0.1 - 0.2$ s for our test run on 2 processors.

Finally, the parallel version needs about $2.15 - 2.4$ s to compute the action of the Hamiltonian on ψ ($J = 1$, $128 \times 64 \times 32 \times 2$ points, IBM-SP2 machine). The same program needs in a scalar version about $4.6 - 4.8$ s to do the same operations.

For the scalar case the time needed to compute the action of the Hamiltonian on the wavefunction is

$$T_{scalar}(J) \approx T_0(J + 1). \tag{190}$$

T_0 is the time needed to compute the action of the Hamiltonian on the wavefunction for $J = 0$. In the parallel case the scaling relation becomes

$$T_{parallel}(J) \approx T_0(\alpha J + 1), \tag{191}$$

where α is a constant which is close to 0 in the ideal case (no scaling) and to 1 in the scalar implementation.

In Figure 18 the scaling up to $J = 5$ is shown for the IBM-SP2 machine.

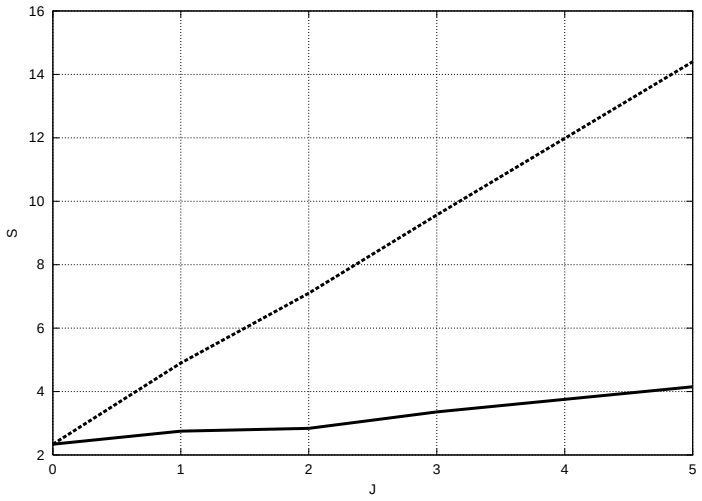

Figure 18: D $+H_2 \rightarrow$ DH +H: time needed to compute $\hat{H}\psi$ for different values of the total angular momentum J (IBM SP-2). Serial (upper line) and parallel (lower line) scalings are plotted.

Using this implementation strategy a scaling factor up to $\alpha = 0.15$ can be reached. $\alpha = 0$ value corresponds to the ideal case, when no scaling with respect to the value of J is present.

Details about how the parallel jobs are submitted using the batch jobs can be found at the web page:

`http:\www.uni-karlsruhe.de/~SP/Handbuch/`

5.5.3 Parallel 2D-FFT implementation

A second version of the parallel program includes the usage of a standard parallel library. We tested the 2D-complex FFT parallel subroutine **PDCFT2** from the **PESSL** library of IBM.

As pointed out in the **Section 4**, the energy is computed for operators as given by Eq. (131) using Eq. (132). If we use a 2D-FFT subroutine we can compute the kinetic energy for both R and r Jacobi coordinates in the same time. Tests were done using the parallel **PDCFT2** routine.

Our tests are not finished. It was found that after 8140 calls of the **PDCFT2** subroutine a warning message is given. It is repeated for each transformations at each point of

the grid where the wavepacket is represented (typical wavepackets are described by using $128 \times 128 \times 50$ grid points). This leads to a tremendous amount of output which makes the subroutine unproper for our purpose. (The existence of this warning message was reported to IBM from Mr. N. Geers of the Rechenzentrum Karlsruhe.)

A **summary** of all the programs developed to compute the reaction cross sections using time-dependent wavepacket methods is given in the Figure 19.

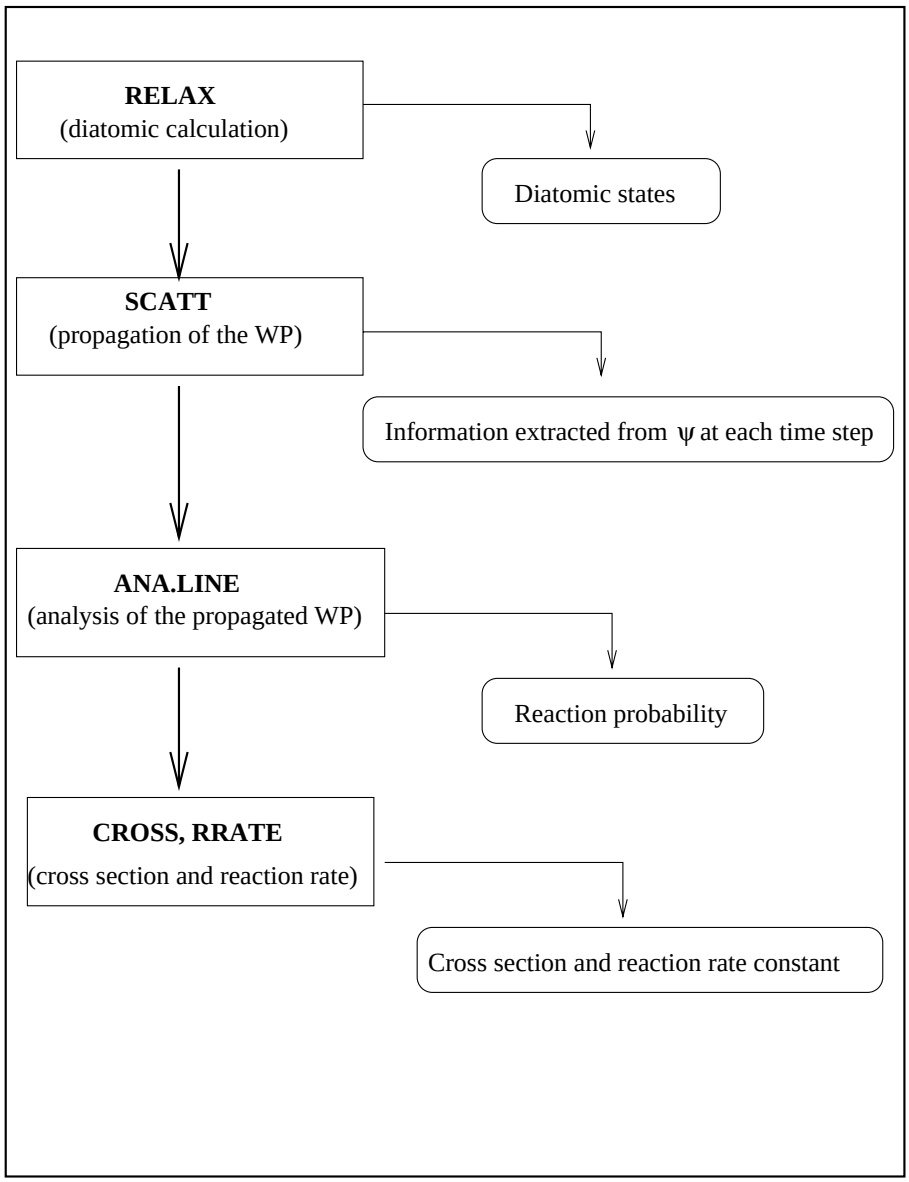

Figure 19: Global scheme of our WAVE program package showing the different modules, the order of execution and the type of output produced by each of them (WP - wavepacket).

6 Results

6.1 The D+H_2 → DH +H reaction

6.1.1 The scenario of the reaction

An elementary bimolecular reaction like D+H_2 → DH +H proceeds not in sequential steps by breaking the "old" bond and subsequent formation of the "new" molecule, but via the concerted motion of the nuclei in a continuous transformation from the reactant valley to the product valley. The potential energy surface serves to mediate between the reactant and the product configuration. According to Zewail *et al.* [5] a **transition state** (TS) is fundamental in defining the region of internuclear separation at which the reagent molecules "pass on" to the products. Closely related to the TS concept can be defined the **reaction path** as the line of minimal energy from reactant to product valley [34]. Properties of the TS and the reaction path are determined by the potential energy surface characterizing the system.

The PES topology gives us information about the preferential orientation of the molecules during the reaction. This defines a "cone of acceptance", as a solid angle surrounding the projectile-target axis where the reaction is highly probable (Levine and Bernstein [34]). A *steric factor* can de defined as the number of molecules which reacts relative to the number of colliding molecules, for a given relative orientation of reactants [81]. The different efficiency of the collision at different angles is caused by the topology of the PES. The most convenient relative orientation of the reactants defines the reaction path.

6.1.2 Effect of vibrational energy of the reagents upon the reaction

D+H_2 → DH + H is a reaction with a symmetric barrier between the entrance and the exit channel. For all exoergic reactions with a barrier along the reaction path and for all endoergic reactions we seek to obtain information on the energy requirements for reaction. Obviously we require a collision energy E_c larger than the threshold (the difference between largest and smallest values along the reaction path) of the PES. Even if the products are oriented according to the angle which defines the reaction path, there is still to discuss the problem of distribution of energy among the degrees of freedom.

Usually the energy inside of a molecular complex is distributed over $3n-6$ vibrational degrees of freedom and 3 rotational degrees of freedom ("n" is the number of atoms in the molecule). When a reaction occurs only the energy of those degrees of freedom which are along the reaction path can be used to overcome the barrier. According to Figure 20 and to the discussion of Polanyi *et al.* [82, 83] translational energy is most effective for passage across an early barrier (e.g. the saddle point in the entrance valley), whereas

vibrational energy of the reactants is more efficient in surmounting a late barrier (in the "exit" valley).

Figure 20 summarizes the classically possible trajectories on a general type of PES.

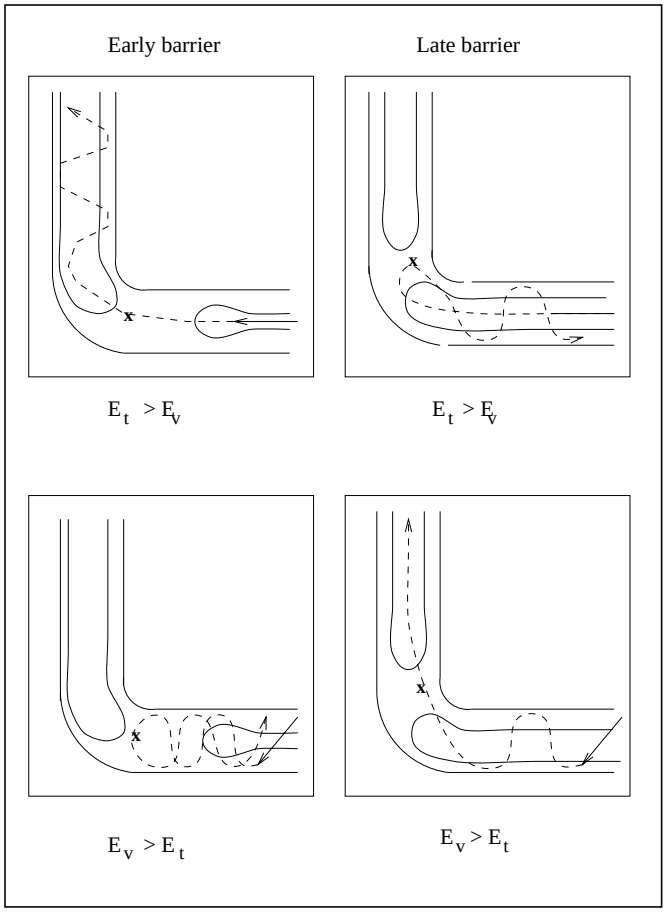

Figure 20: Qualitative discussion of the influence of the topology on the reaction flow, using internal coordinates (r_{AB}, r_{BC}). The trajectories starts in all the cases in the low - right corner of the pictures. Left: early barrier. Right: late barrier. Up: the reactants have mostly translational energy (E_t). Down: the reactants have mostly vibrational energy (E_v).

6.1.3 Effect of rotational energy of the reagents upon the reaction

The effect of the diatomic rotation in the reaction D+H_2 → DH +H was discussed by Sathyamurthy and Toennies [84]. According to their work, the rotational excitation of the reactants plays a significant, often non-monotonic role in bimolecular exchange reactions.

For many reactions of the type

$$A + BC \rightarrow AB + C,$$

the reaction cross section initially decreases with increase in the rotational quantum number j of the diatom and then increases with further increase of j (Sathyamurthy and Toennies [84]). To a large extent the decrease has been identified as an *orientation effect* and the increase as an *energy effect*.

When a reaction has a preferred reaction path (for example a collinear reaction in the case of D+H_2 → DH +H), rotational motion disrupts the preferred orientation and the reactivity decreases. This is reflected in the lowering of the cross section when the rotational quantum number j of the diatomic BC has small values (the *orientation effect*). Beyond a critical value j_i (i is the index of the critical value) the favored orientation is accessible with equal probability, independent of j. The orientation effect plays a non-significant role when $j > j_i$. In such case the increase of j for a given vibrational state v of the diatom and relative translational energy E_{trans} of the reactants provides a larger amount of energy to cross the barrier. This is the *energy effect*, which is reflected in the increase of the cross section with respect to the values of j.

The D+H_2 → DH +H specifics.

As benchmark system for our implementation we used the D+H_2 → DH +H reaction. All the results presented in the following section were obtained by using the LSTH PES of Truhlar *et al.* [85]. New improvements of the PES like those of Bauschlicher *et al.* [86], does not lead to sensible modifications in the theoretical results [91]. With the present implementation investigations for the nonadiabatic PES for the H_3 system of Varandas *et al.* [87] are also possible. Within the Born-Oppenheimer approach the same PES can be used for all isotopic substitutions.

D+H_2 → DH +H is a direct reaction in which the H-H bond is continually extended as the D atom approaches. The switch between bonds occurs in a very short time interval, corresponding roughly to one vibrational period. The barrier of the reaction is about $E_b \approx 10$ kcal/mol, representing $\approx 10\%$ of the dissociation energy of the H_2 molecule. The LSTH value for the barrier is $E_b = 9.802$ kcal/mol.

The most convenient orientation for the reaction is the collinear one. The explanation of this is the following (Levine and Bernstein [34]): molecular orbitals (MO) are constructed as a linear combination of atomic orbitals (AO). For H_2 we use a 1s AO on each H atom, so we have two independent linear combinations: $\sigma_g(1s)$ and $\sigma_u(1s)$. In the σ_g orbital the two 1s functions have the same phase. The MO has no node, hence it is a low-energy bonding orbital. In the σ_u MO (anti-bonding orbital) the two atomic functions have opposite phases, the node between the two nuclei increases the energy of this orbital. So, the ground state of H_2 is $\sigma(1s)^2$.

When the D atom collinearly approaches the H_2 molecule, the following situations can occur (see Figure (21)): three electrons have to be assigned: two go to the lowest bonding

orbital the third is assigned to the orbital of next higher energy. Thus, it is expected to have a small barrier, due to the presence of this electron in the "anti bonding" orbital, which has a larger energy than the energy of the separate system. The "anti bonding" character is given by the node occurring between the $\sigma_g(1s)$ and $\sigma_u(1s)$ orbitals.

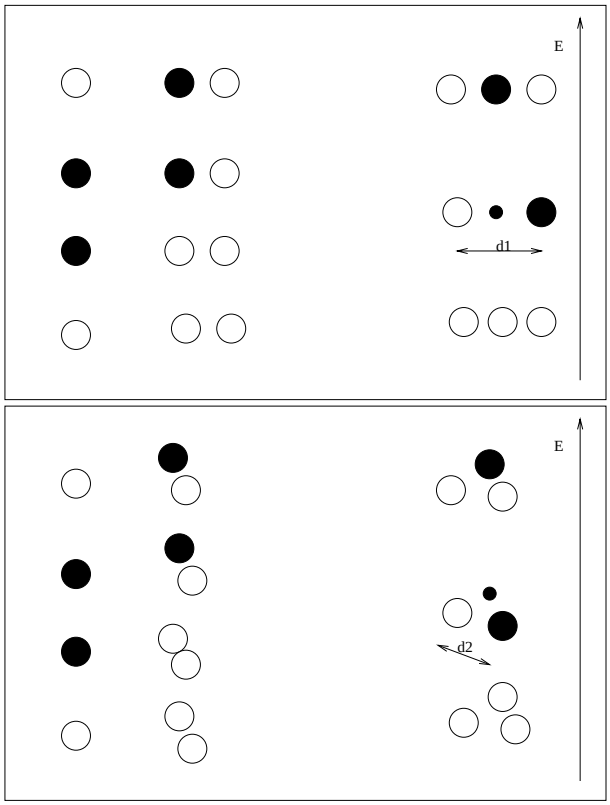

Figure 21: H - H_2 collision. The dark circles are the 1s orbitals, the white ones are of 1s* type. Top: collinear reaction. Bottom: collision at an angle $\alpha \in (0, \pi/2)$. In the left side the atom and the molecule are separated ("free-force region"). In the right side the atom and the molecule are colliding ("interaction region"). The distances between the 1s and 1s* orbitals in the interaction region are changing when the collision angle is changed.

Now let the D atom approach the H_2 at an angle $\alpha \in (0, \pi)$ with respect to the H_2 bond. This situation is described in the Figure (21) - bottom. The energy of the bonding orbital and the strongly anti-bonding are nearly unaffected by the change of angle. The second orbital which is "nearly anti bonding" has a node between the nuclei which are now closer to each another ($d_1 < d_2$ in the figure (21)). The third electron assigned to the "anti-bonding" bent orbital, will have a higher energy than in the collinear case and the barrier will increase (see also the Walsh diagram for the AH_2 systems [88]).

By plotting the opacity for the D + $H_2(v_0, j_0)$ → DH + H reaction, for different initial ro-vibrational states (v_0, j_0) of the H_2 molecule, Neuhauser *et al.* [92] found that

for collision energies $E \approx 2$ eV, the largest opacities are those for $j_0 = 1$ and $j_{0z} = 1$ (where $j_{0z} = 1$ is the projection of the j_0 onto the Z space-fixed axis). By discussing the significance of different quantum numbers that characterize the reaction, they prove that quantum states with $j_{0z} = 1$ cannot have any contribution from collinear geometries, so at collision energies larger than 2.0 eV the collinear configuration is not the most preferred one for the reaction.

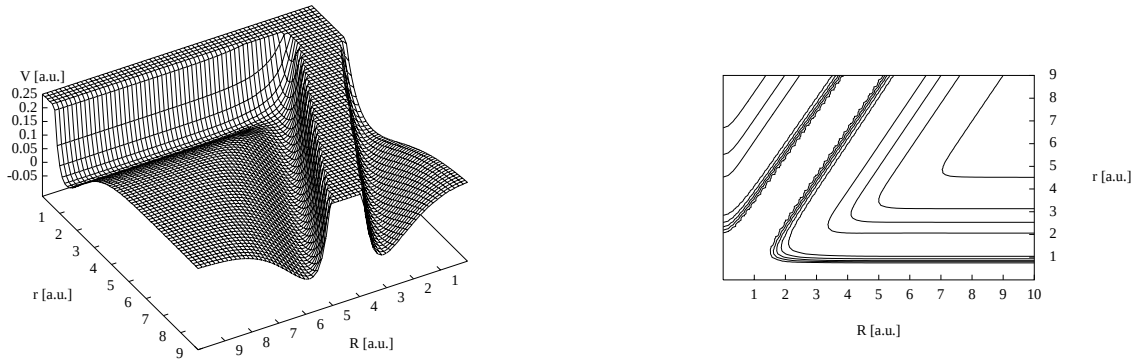

Figure 22: Left: 3-D picture of the LSTH potential energy surface [85] for the linear configuration of the three H atoms. The cutoff for the potential (see Eq. (55)) was set to 0.25 E_h. Right: the same picture, as a contour plot. Energies and distances are given in atomic units.

6.1.4 Investigations with wavepackets

The time-dependent methods have already described in **Sections 2** and **3**. The program described in **Section 4** was used to simulate the dynamics of the D+H_2 → DH +H reaction. Previous theoretical [76, 84, 92, 93, 94, 95, 97, 99, 100] and experimental [89, 90, 91, 101] investigations were compared with present results, as described below.

Initial bound states of the diatomic

50 eigenvalues of H_2 were taken into account during the propagation. The energies together with their vibrational and rotational quantum numbers (v, j) are presented in Table 2.

The initial state for H_2 was $v = 0,\ j = 0$.

Choice of the grid

First, one wants to set up the most convenient grid for the calculation. Jacobi coordinates have been used: R, r and θ (see Figure 4). We used 128 points in the R coordinate,

Nr.	Energy [eV]	Energy [cm^{-1}]	v	j
1	0.270	2179.83	0	0
2	0.285	2298.32	0	1
3	0.314	2534.23	0	2
4	0.358	2885.39	0	3
5	0.415	3348.70	0	4
6	0.486	3920.13	0	5
7	0.570	4594.89	0	6
...	...	...	...	...
48	1.945	15689.82	2	10
49	1.987	16022.48	3	6
50	2.056	16581.03	1	14

Table 2: H_2 eigenstates for given quantum numbers

64 points in the r coordinate and 32 points for the angle θ. We choose for $R = [0.001, 11.0]$ a_0, and for $r = [0.001, 7.0]$ a_0. The analysis line was put at $r = 4.9$ a_0. For comparison, tests with $128 \times 128 \times 40$ points were also performed. The results are summarized in Table 3.

Although the domain $r = [0.001, 7.0]$ a_0 is not so large and the analysis line is not far in the asymptotic region, there are not large differences between the probabilities computed using the $128 \times 64 \times 32$ grid and those computed within a grid of 128×128 points distributed over the 11.0 $a_0 \times$ 10.0 $a_0 \times$ 2π (R, r, θ) domain, with an analysis line at $r = 7.5$ a_0.

The next step was to set up correctly the **parameters for the initial wavepacket**. We wanted to investigate the reaction probabilities between 0.45 eV and 1.65 eV. For comparison we used the time-independent calculations of Zhang and Miller [76]. A first set of calculations was done, by using a gaussian wavepacket with a mean kinetic energy of 0.6 eV and a width of $\sigma = 0.5$ a_0 for $J = 1$. The $J = 1$ value gives us the opportunity to check the behavior of the wavepacket in the simplest case when a coupling between the Ω channels is present. The first set of reaction probabilities was found to be underestimated in the region of energies $E > 1$ eV - see Figure 23 - right.

New calculations were performed with $E_0 = 1$ eV, $\sigma = 0.5$ a_0. In this case the results were overestimated in the low energy region [0.6, 0.8] eV - see Figure 23 - right.

For $J = 1$ and $E_0 = 1$ eV several vales for the initial width σ of the wavepacket where tested. The set of initial parameters $E_0 = 1$ eV, $\sigma = 0.5$ a_0 leads to good results in the high energy area ($E > 0.8$ eV) (see Table 5). However, the reaction probabilities in

E [eV]	P_1	P_2	P_3
0.503	0.812E-03	0.824E-03	0.822E-03
0.600	0.115	0.116	0.114
0.707	0.407	0.407	0.407
0.804	0.441	0.443	0.442
0.901	0.530	0.528	0.530
1.000	0.565	0.565	0.564
1.106	0.593	0.590	0.591
1.203	0.624	0.622	0.625
1.300	0.646	0.647	0.648

Table 3: Reactions probabilities $P(E)$ for different energies E and grid parameters (see Table 4) for the D+$H_2(v = 0, j = 0)$ → DH +H reaction ($J = 0$).

Index	N_R	N_r	N_θ	ΔR [a_0]	Δr [a_0]	r_{ana} [a_0]
P_1	128	128	40	11.0	10.0	7.5
P_2	128	128	40	11.0	10.0	6.5
P_3	128	64	32	11.0	7.0	4.9

Table 4: Grid parameters used to compute the reaction probabilities in Table 3. The notations are the same as those in **Section 4** page 50 for the grid parameters used in D + H_2 reaction.

E_i [eV]	0.600	0.708	0.840	0.977	1.085	1.247	1.354
R_1	0.022	0.001	0.009	0.003	0.003	0.001	0.020
R_2	0.048	0.031	0.011	0.009	0.003	0.003	0.027

Table 5: For the results presented in Figure 23 the absolute values $|P_{time-dependent}(E_i) - P_{time-independent}(E_i)|$ are given at several energies E_i. Two time-dependent calculations are compared with the time-independent results of Zhang and Miller. The initial parameters of the wavepackets were: E_0=1 eV, σ=0.25 (first row R_1) and E_0=1 eV, σ=0.5 (second row R_2).

the energy domain E = [0.45, 0.8] eV are overestimated in this case. The set of initial parameters $E_0 = 1$ eV and $\sigma = 0.25$ a_0 was found to be the best (see Figure 23 - left).

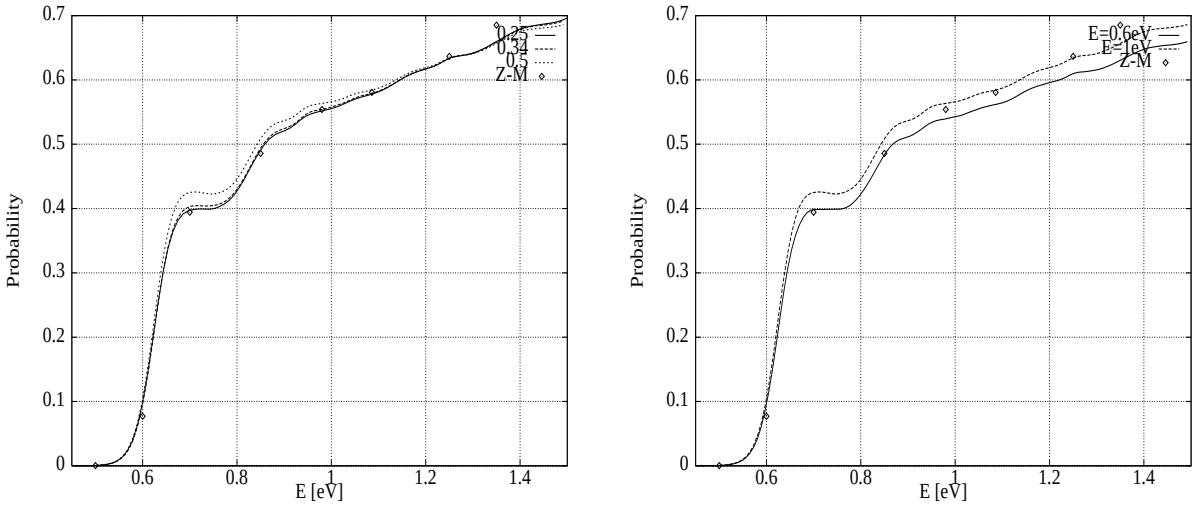

Figure 23: Total reaction probabilities $P(E)$ for the D+ $H_2(v{=}0, j{=}0)$ → DH +H reaction ($J = 1$). Left: reaction probabilities for different initial widths σ of the wavepacket (the value for σ is given in the top-right corner of the picture). The initial energy was $E_0 = 1$ eV. Right: reaction probabilities for initial energies $E_0 = 0.6, 1.0$ eV at $\sigma = 0.5$ a_0. For comparison, time-independent results of Zhang and Miller [76] are plotted with squares ⋄ (Z-M).

For the collinear configuration several **snapshots of the propagation** are plotted in Figure 24. We can briefly resume the dynamics of the reaction as follows: initially, the wavepacket is located in the reactants region of the grid (R is large, $r \approx 1.42$ a_0 (equilibrium distance for H_2)). At later times ($t > 1100$ a.u.), the wavepacket moves into the product region (r is increasing). During this process, there are no significant resonances in the interaction region (where R and r have both values of $\approx 1 - 2$ a_0).

6.1.5 Reaction probabilities for $J = 0, ..., 33$

Total reaction probabilities for the D+$H_2(v{=}0, j{=}0)$ → DH +H reaction were computed for $J = 0$ up to 33 for total energies in the range (0.45 - 1.65) eV. Up to $J = 5$, the fully coupled Hamiltonian was used. For larger values a restricted number of Ω channels was used (8 channels for $J > 9$, 5 channels for $J = [6, 9]$), because the computational cost (CPU-time and memory requirements) become demanding. By using just one channel (e.q. for $J = 0$) the complete propagation takes around 2 hours on an IBM-SP2 machine. The scaling of the calculations with respect to J is linear, with a prefactor close to 1,

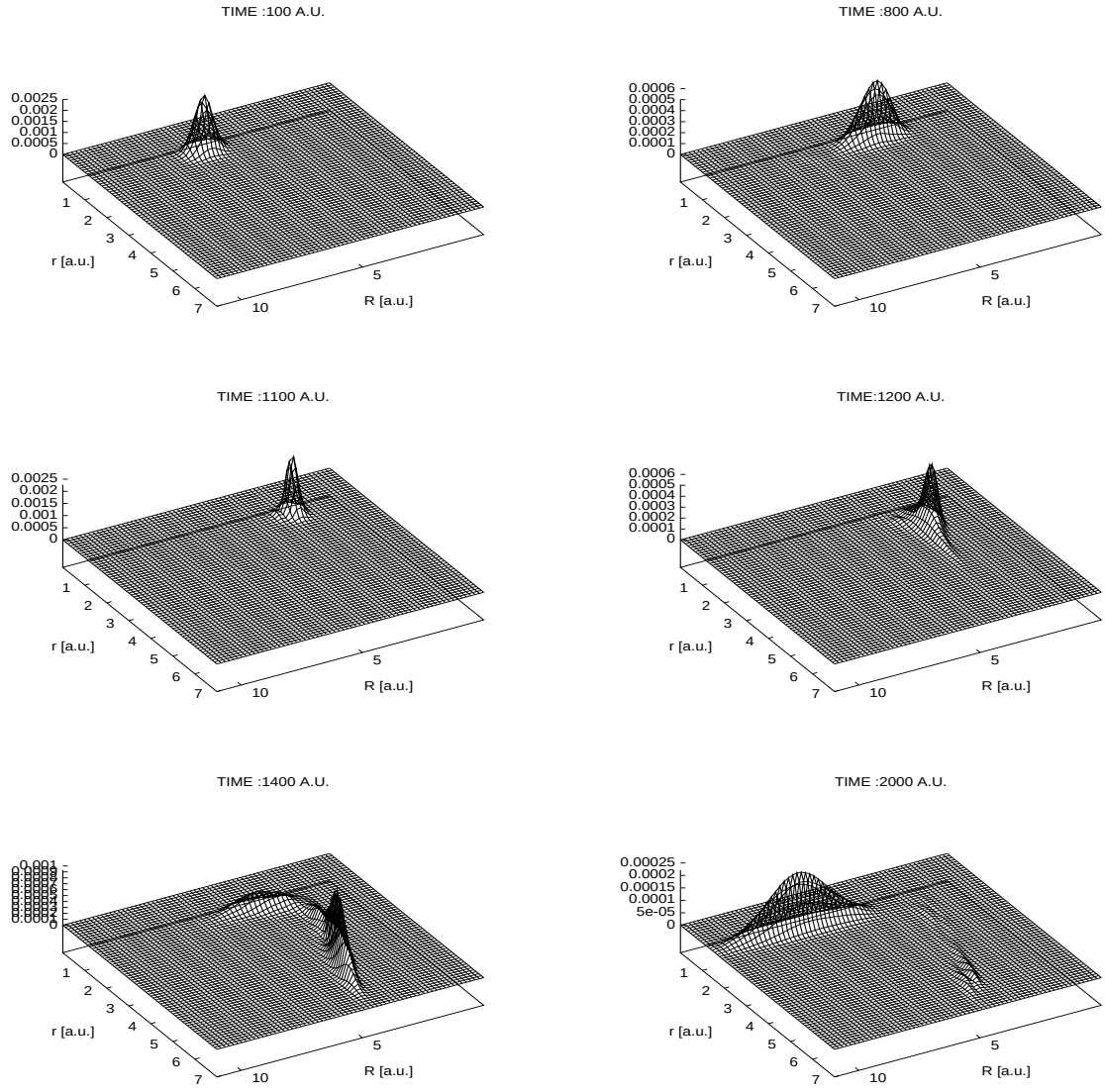

Figure 24: $|\psi|$ during the D+H_2(v=0, j=0)→ DH +H reaction is given (linear configuration D-H-H). Pictures are given at times t = 100, 800, 1100, 1200, 1400 and 2000 a.u.. The initial wavepacket was located at R = 7.0 a_0.

which leads for an 8-channel calculation to more than 16 hours real computing time, keeping the same level of accuracy (e.g. the number of grid points per channel).

The cutoff conditions for the angular kinetic energy operator (see page 16) must be imposed to the effective potential in Eq. (96). This term has the form

$$V_{eff}(j,\Omega) = \frac{1}{2\mu_{A-BC}R^2}[J(J+1) + j(j+1) - 2\Omega^2]. \tag{192}$$

The calculation for $J = 5$ shows the behavior of the reaction probabilities at large energies (about 1.8 eV) when the cutoff is not correctly implemented - see Figure 25.

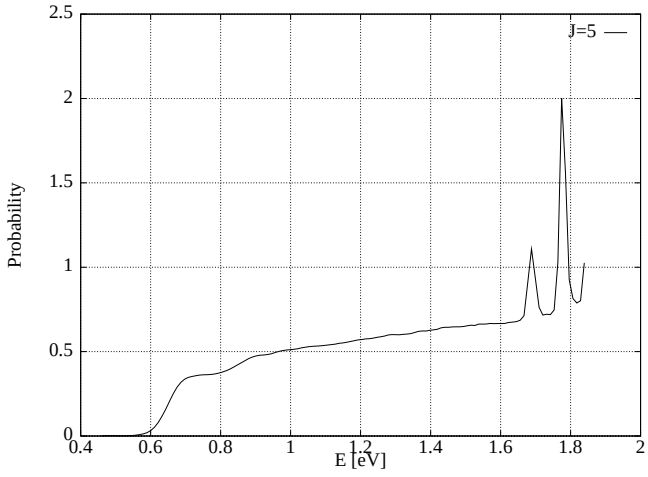

Figure 25: Consequence of the wrong implementation for the cutoff for the effective potential in Eq. (96) onto the reaction probabilities $P(E)$ for the D+H_2(v=0, j=0) → DH +H reaction, $J = 5$. The artificial peaks are located at $E_1 \approx 1.69$ eV and $E_2 \approx 1.76$ eV. Their width is ≈ 0.03 eV.

According to [104] the cutoff must be imposed to the *pairs* of quantum numbers (j, Ω). The cutoff condition is

$$V_{eff}(j,\Omega) < V_{max}. \tag{193}$$

For the pairs (j, Ω) that do not satisfy the relation given in Eq. (193) we take

$$V_{eff}(j,\Omega) = V_{max}. \tag{194}$$

The complete set of reaction probabilities is given in Figure 26, as a 3D-function, and as a contour plot in Figure 27. Details for several reaction probabilities are given in Figure 28.

A detailed comparison of reaction probabilities for several J values with time-independent calculations of Zhang [106] is given in Table 6. The agreement is better in the region around 1 eV, where the center of the wavepacket was located energetically.

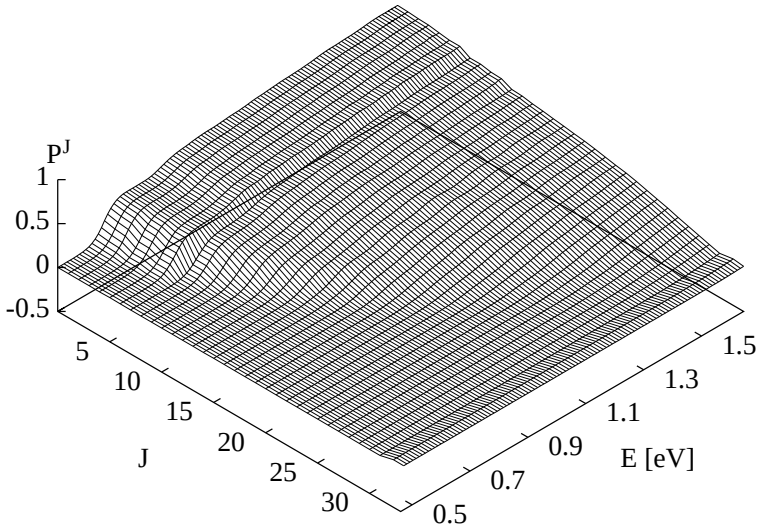

Figure 26: Total reaction probabilities $P^J(E)$ for D+H_2(v=0, j=0) → DH + H. Total angular momentum J = [0, 33] and total energy E =[0.45, 1.6] eV.

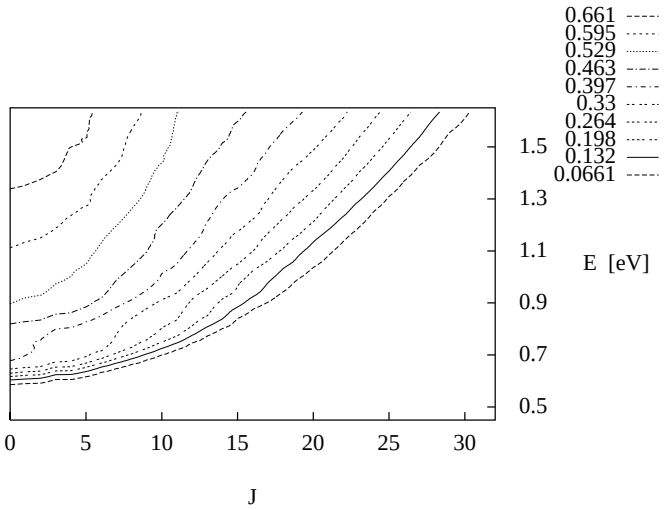

Figure 27: Total reaction probabilities $P^J(E)$ for D+H_2(v=0, j=0) → DH + H, for total angular momentum J = [0, 33] and the total energy E = [0.45, 1.6] eV (contour plot). The values of the contour lines are given in the upper-left corner.

Present calculations				Time-independent calculations [106]			
E [eV]	$J=0$	$J=1$	$J=4$	E [eV]	$J=0$	$J=1$	$J=4$
0.500	0.380E-5	0.347E-5	0.139E-5	.503	0.822E-05	0.660E-05	0.288E-05
0.600	0.832E-3	0.770E-3	0.370E-3	.600	0.114E-02	0.9934E-03	0.509E-03
0.700	0.397	0.394	0.358	0.708	0.407	0.398	0.368
0.850	0.489	0.486	0.459	0.848	0.497	0.488	0.446
0.980	0.554	0.554	0.548	0.977	0.559	0.551	0.523
1.086	0.582	0.581	0.572	1.085	0.584	0.578	0.549
1.250	0.638	0.637	0.635	1.247	0.637	0.633	0.599
1.350	0.686	0.685	0.650	1.354	0.668	0.662	0.624

Table 6: The D + $H_2(v=0, j=0)$ → DH + H reaction probabilities for $J=0$, 1, and 4 are given (left column). For comparison the time-independent total reaction probabilities of Zhang [106] are given in the right column.

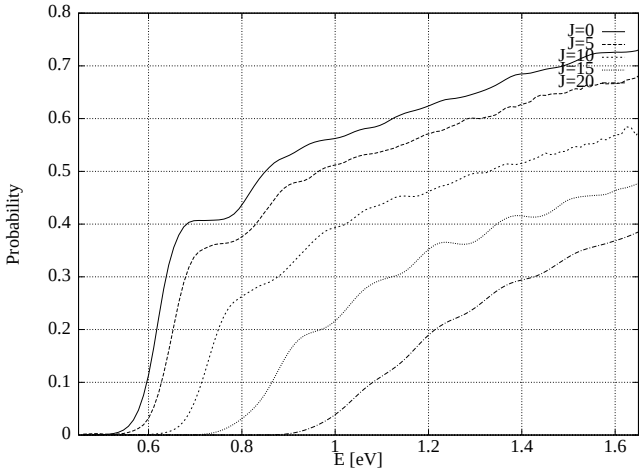

Figure 28: Total reaction probabilities $P^J(E)$ (J=0, 5, 10, 15, 20) for the D+H_2(v=0, j=0) → DH + H reaction. The J-shift effect can be observed: reaction probabilities are shifted to the right.

6.1.6 Total cross sections and reaction rate constants

The **total reaction cross section** was computed using the reaction probabilities presented in Figures 26 and 27 using Eq. (17). The energy domain was $E_1 = [0.45, 1.85]$ eV. The results are compared with Zhang and Miller's time-independent calculations [76] as it can be seen in Figure 29.

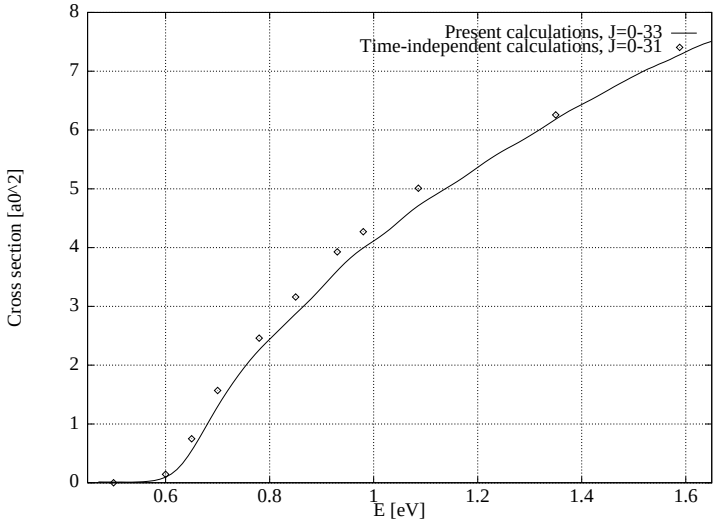

Figure 29: Total reaction cross sections for D+H_2(v=0, j=0) → DH +H reaction. The squares ($\diamond$) represent the time-independent calculations of Zhang and Miller [76].

A list of few values of cross sections compared with the time-independent results is given in Table 7.

To compute the **reaction rate** for the given cross sections, we need an estimation for the temperature range where Eq. (23) can be applied. To determine this temperature range, we used a simple ideal gas model. The correlation between temperature and energy [40] is given by

$$E = \frac{i}{2} k_B T, \tag{195}$$

E is the kinetic energy of the molecules, i are the number of degrees of freedom for the molecule ($i = 3$ for a monoatomic gas, $i = 5$ for diatomic gas), k_B is the Boltzmann constant and T is the temperature of the gas. By comparing the energy domain which is available for our calculations (where we know the values of the cross section) with the energy given by Eq. (195) we can set the temperature range where Eq. (23) can be applied.

The reaction rate $k(T)$ that results from these cross sections is plotted in Figure 30.

For a given reaction barrier $E_{barrier}$ on the potential energy surface the collision energy

Present calculations		Zhang & Miller calculations [76]	
E [eV]	σ_{tot} $[a_0^2]$	E [eV]	σ_{tot} $[a_0^2]$
0.503	0.11E-01	0.500	0.77E-04
0.600	0.94E-01	0.600	0.14E-02
0.707	1.41	0.700	1.57
0.847	2.85	0.850	3.16
0.977	3.97	0.980	4.27
1.080	4.70	1.086	5.01
1.246	5.63	1.250	5.92
1.354	6.20	1.354	6.26
1.451	6.68	-	-
1.602	7.33	-	-

Table 7: Initial state selected total cross sections: D+$H_2(v=0, j=0)$ → DH +H. Time-independent calculations of Zang and Miller [76] - left - compared with our time-dependent calculations - right.

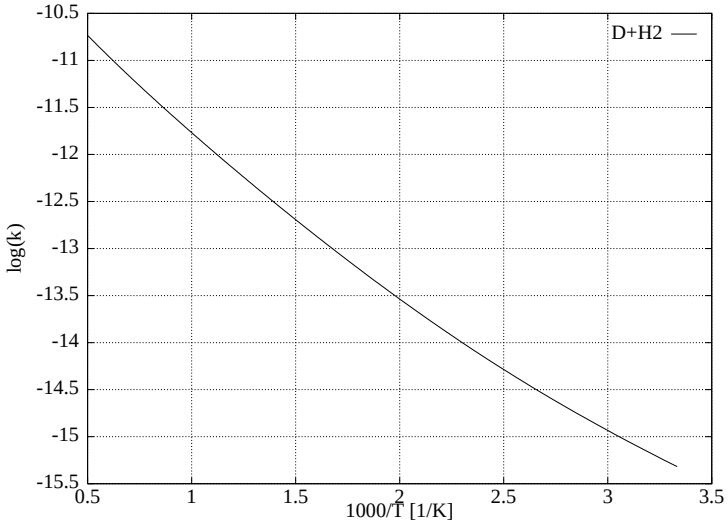

Figure 30: Reaction rate $k(T)$ for the D+H_2(v=0, j=0) → DH +H reaction: $log(k)$ versus inverse temperature T.

at the transition point is $E_{col} = E_0 - E_{barrier}$. E_0 is the total energy of the reactants. In the case of the LSTH potential energy surface this barrier is 0.015 a.u. (0.41 eV).

We plot $logk$ expressed in units of cubic centimeters per mole*second (see Eq. (23)) versus $1000/T$.

We fitted the data, plotted in Figure 30, with an "Arrhenius" type ansatz (see Eq. (22))

$$k(T) = A\sqrt{T}e^{-\frac{E_{col}}{k_B T}}, \tag{196}$$

with A and E_{col} as parameters. For $A = 0.0003$ cm^3/mole*s*K$^{1/2}$ and $E_{col} = 0.29$ eV we get nearly a linear form as seen in Figure 31.

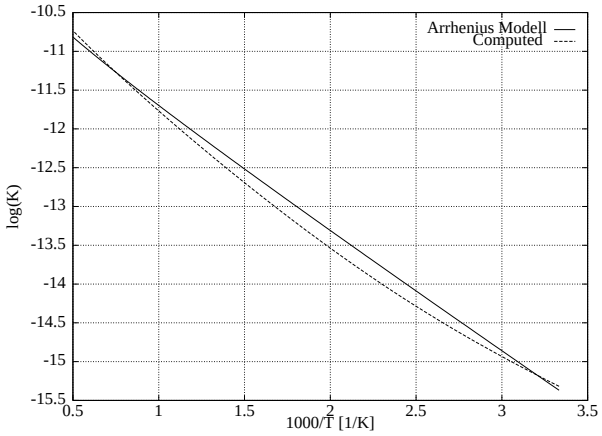

Figure 31: Reaction rate $k(T)$ for D+H_2(v=0, j=0) → DH +H reaction, in comparison to the Arrhenius-type reaction rate (see Eq. (196)).

A comparison with experimental results (Truhlar, Wyatt [96]) for both D+H_2 and H+H_2 systems is shown in Table 8. It can be seen that the J-shift calculations for the H+H_2 system (see the next section) are less accurate then those for D+H_2.

6.1.7 Approximations to reaction probabilities for total angular momentum $J > 0$

The complete wavefunction has the form

$$\psi(R, r, \theta_\Omega) = \psi_1(R) \otimes \psi_2(r) \otimes \psi_3(\theta_\Omega). \tag{197}$$

The angular part includes the degeneracy with respect to Ω. We have to represent the angular part $2J + 1$ times for a given J (or $J + 1$ times if we use the symmetry relation given in Eq. (128)). In principle, each orientation of the total angular momentum J with respect to the BF Z axis (labeled in the following discussion as Ω channel), requires the same number of points in the representation. The storage requirements for a complete

Reaction	Temperature [K]	$k(T)$ [cm^3/mole s K$^{1/2}$] Present calculations	$k(T)$ [cm^3/mole s K$^{1/2}$] Experimental results
A	300.00	4.8×10^{-16}	3.0×10^{-16}
A	425.00	-	1.1×10^{-14}
A	424.66	0.8×10^{-14}	-
B	300.00	3.1×10^{-16}	2.0×10^{-16}
B	425.00	-	3.9×10^{-15}
B	424.66	0.8×10^{-14}	-

Table 8: Reaction rate for the reactions D + $H_2(v = 0, j = 0) \rightarrow$ DH + H (A) and H + $H_2(v = 0, j = 0) \rightarrow H_2$ + H (B).

description of the angular part of the wavepacket increase linearly with $J > 0$; this can lead to major computational problems. Therefore present calculations include in the wavepacket only few Ω channels (corresponding to $\Omega = 0, 1, 2, ..., 8$). A special case of this approach is when we take into account only one Ω channel (see the work of Gray *et al.* [102]). In this approach the coupling between different Ω channels is neglected.

The question we want to answer is: how accurate is the total reaction probability, when a restricted number of Ω channels has been taken into account? It is known from angular momentum theory [35] that the projections of the angular momentum j onto a given axis Z are given as

$$j_Z = -j, -j+1, ..., -1, 0, 1, ...j-1, j \tag{198}$$

(see Figure 33).

For the A-BC system we have in addition the following property (Leforestier [56]): in a body-fixed system, the projection of total angular momentum J onto the Z axis (J_Z) and the projection of the diatomic angular momentum j onto the Z axis (j_Z) are the same. This common value is labeled Ω. Hence, for a given reaction, Ω can take the values: $0 \leq \Omega \leq min(J, j)$.

According to the experimental work of Kliner *et al.* [89, 90, 91], the rotational excitation of the products in the reaction D+H_2 (v =0, j=0) → DH(v' =1, j') +H, at the collision energy $E_{col} \approx 1.05$ eV is important for the first 10 rotational states of the new DH molecule - see Figure 32.

Each rotational state of the DH molecule is $(2j' + 1)$ times degenerate, corresponding to the $2j' + 1$ possible orientations of the rotation angular momentum $\hat{j}$. If no external field is present, all these orientation have the same probability, $p = 1/(2j'+1)$. Hence, we can expect that $n_{j_z} = n_j/(2j' + 1)$ molecules will have the rotational angular momentum oriented parallel with the BF axis ($n_{j'}$ is the number of molecules with the rotational

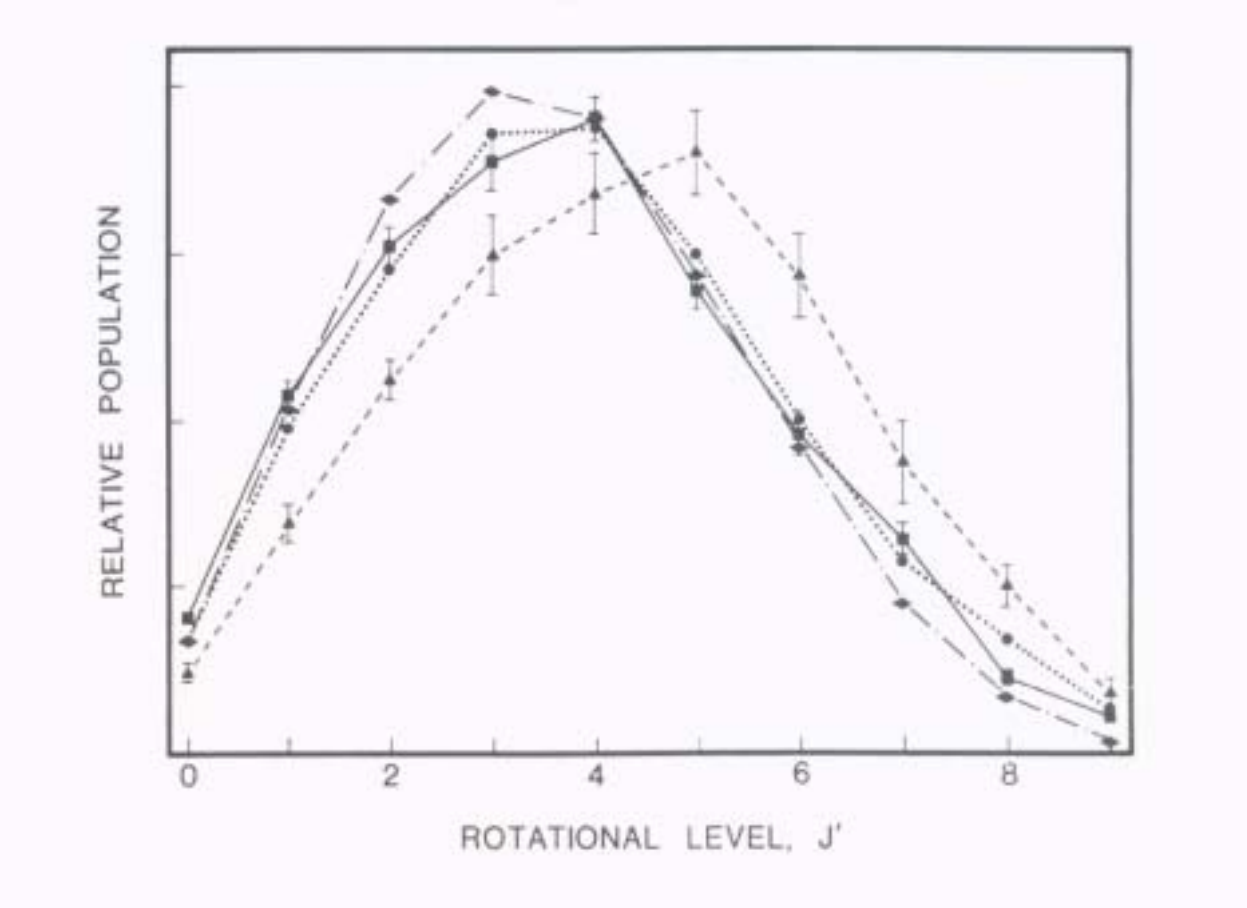

Figure 32: Distribution of rotational level j' in D +H_2 (v =0, j=0)→ DH($v' = 1, j'$) +H. Reaction at a center-of-mass collision energy of about 1.05 eV: experiment (solid curve), where the error bars represent one standard deviation; QM calculation (dotted curve [76] and dash-dotted curve [103]), without error estimacies; QCT calculation (dashed curve [105]), where the error bars represent one standard deviation in the statistics. All four distributions have been normalized to the sum of the common populations. Reproduced from Chem. Phys. Lett., **166** 108 (1990).

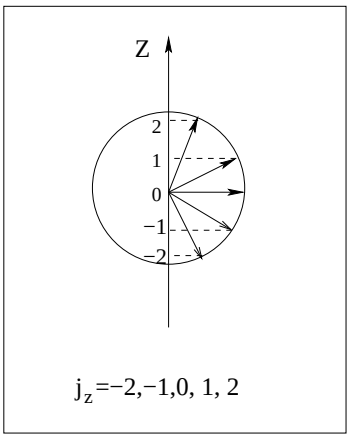

Figure 33: Possible orientations of the angular momentum for $j = 2$.

quantum number j').

In the case of D+H_2 (v =0, j=0) → DH(v' =1, j') +H a truncated number of of Ω channels is a good approximation. For larger collision energies the relative population of the highly excited rotational channels increases. The number of rotationally excited levels of the new DH molecule has a maximum around $j' = 10$ for $v' = 0$ and $E_{col} = 1.5$ eV (Adelman *et al.* [91]). By dividing these populations with the degeneracy factor $2j' + 1$ we can find the relative population of the corresponding Ω channel.

What accuracy can we achieve with an Ω - truncated wavefunction? We can write the total reaction probability as a sum of separate reaction probabilities for each Ω channel,

$$P_{total} = P_{\Omega=0} + P_{\Omega=1} + ...P_{\Omega=\Omega_{max}}, \tag{199}$$

where $P_{\Omega=\Omega_0}$ is the reaction probability that is obtained if we analyze only the given Ω_0 channel of the wavefunction

$$\psi(R, r, \theta_{\Omega=\Omega_0}) = \psi(R, r, \theta_\Omega)\delta_{\Omega,\Omega_0}. \tag{200}$$

We have to analyze the contribution of each channel to the total reaction probability and how the contribution is changing when the number of Ω channels changes. Different Ω channels change their populations because of the presence of the coupling term in the Hamiltonian (see Eq. (96)). Outside of the interaction region the coupling Hamiltonian [37] is rather small

$$H_{coupl} = \frac{1}{2\mu_{A-BC}R^2}[\lambda_\pm(J, \Omega')\lambda_\pm(j, \Omega')\delta_{\Omega'\pm1,\Omega}\delta_{j,j'}]. \tag{201}$$

Higher Ω channels acquire just a small population during the propagation when the prefactor $1/2\mu_{A-BC}R^2$ is small [107]. This is true for the population of each channel. On

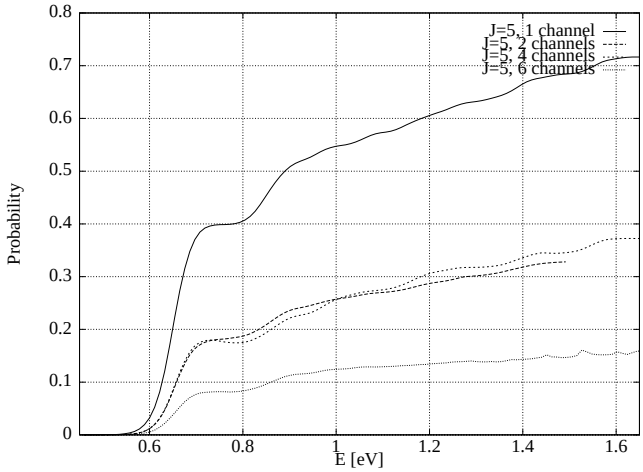

Figure 34: The D+H_2(v=0, j=0) → DH +H reaction, $J = 5$. The contribution of $P_{\Omega=0}(E)$ to the total reaction probability is given. From top to bottom the number of Ω channels in the wavepacket was: 1 ($\Omega_{max} = 0$), 2 ($\Omega_{max} = 1$), 4 ($\Omega_{max} = 3$) and 6 ($\Omega_{max} = 5$), for different calculations including more Ω channels.

the other hand, the dynamics of the different Ω channels is governed by different effective potentials

$$V_{eff} = \frac{1}{2\mu_{A-BC}R^2}[J(J+1) + j(j+1) - 2\Omega^2]. \tag{202}$$

Different effective potentials in each Ω channels, lead to different "velocities" of the wavepacket within each Ω channel. The increased "velocity" of the wavepacket can compensate the small population of the channel, when the flux of the wavepacket is computed.

In the Figures 34 and 35 we plot the contribution of the $\Omega = 0$ channel to the total reaction probability. The total number of channels included in the wavepacket was $N_\Omega =$ 1, 2, 4 and 6 for $J = 5$ respectively $N_\Omega = 1$, 2, 4, 6 and 8 for $J = 20$. Initially the wavepacket populates only the $\Omega = 0$ channel.

From the Figures 34 and 35 it can be seen that there is no convergence for the contribution of the channel $\Omega = 0$ to the total reaction probability. By taking more channels into account the contribution of the $\Omega = 0$ channel decreases. We can conclude that by neglecting the presence of the large Ω channels it is possible to overestimate the contribution of the $\Omega = 0$ channel.

The total reaction probability was computed using the same wavepackets as those we use to plot Figures 34 and 35. We can see that the total reaction probability converges when the number of channels varies (see Figures 36 and 37).

Finally, we can say that a restricted number of channels is a good approximation as long as we want to compute total reaction probabilities and cross sections. If we want to compute the angular dependence of the cross section (see Eq. (18)), a correct evaluation

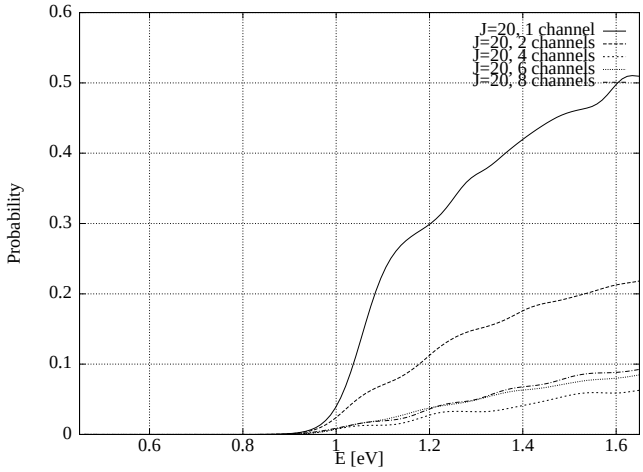

Figure 35: The D+H_2(v=0, j=0) → DH +H reaction, $J = 20$. The contribution of $P_{\Omega=0}(E)$ to the total reaction probability is given. From top to bottom the number of Ω channels in the wavepacket was: 1 ($\Omega_{max} = 0$), 2 ($\Omega_{max} = 1$), 4 ($\Omega_{max} = 3$), 6 ($\Omega_{max} = 5$) and 8 ($\Omega_{max} = 7$), for different calculations including more Ω channels.

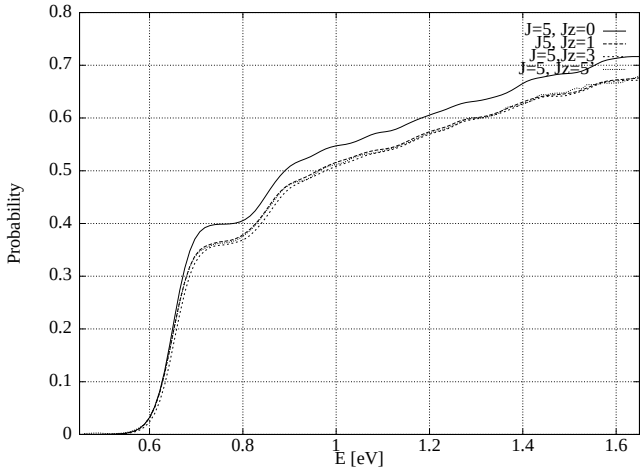

Figure 36: For the reaction D+ H_2 (v=0, j=0) → DH + H, J=5, the comparison between different levels of accuracy calculations is given. The number of channels included in the representation of the wavepacket was set successively to: 1, 2, 4 and 6. The value of Ω_{max} is noted Jz.

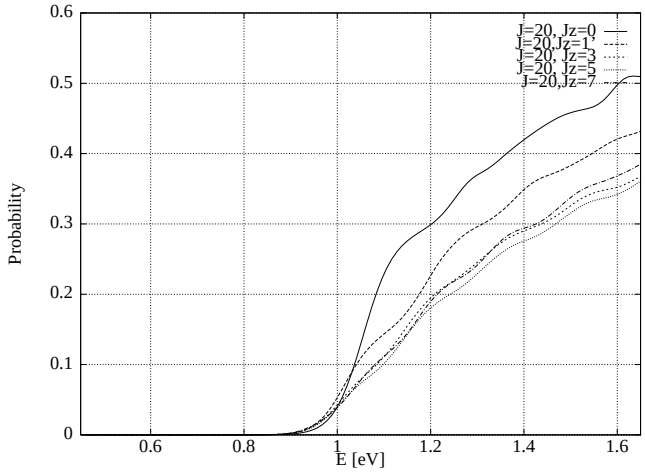

Figure 37: For the reaction D+ H_2 (v=0, j=0) → DH + H, J=20, the comparison between different levels of accuracy calculations is given. The number of channels included in the representation of the wavepacket was set successively to: 1,2,4,6 and 8. The value of Ω_{max} is noted Jz.

of all contributions in Eq. (199) is needed. This cannot be done within the approach of a restricted number of channels (as proved with Figures 34 and 35).

On a scalar machine the computation time for $J > 0$ can be demanding. Within our parallel algorithm (see **Section 5**) the calculations are performed more efficiently.

6.1.8 J-shift calculations

This approach allows us to compute the cross section for a given reaction by using only the reaction probability $P^{J=0}$. The way how the P^J-s for $J > 0$ are produced was described in **Section 2**, Eq. (16).

To compute the centrifugal barrier at the transition state, a classical rigid rotor model was used. First we define the center of mass of the triatomic at the transition state configuration. The moment of inertia of each atom with respect to the center of mass is computed as

$$\mathcal{J}_i = m_i r_i^2, \quad i = 1...3, \tag{203}$$

where r_i is the distance between the atom i with mass m_i and the center of mass of the system, and $\mathcal{J}$ is the moment of inertia with respect to that point. According to [108], the clasical energy for a rotating point is

$$E_{rot} = \mathcal{J}\omega^2/2 = L^2/2\mathcal{J}, \tag{204}$$

where ω is the rotation frequency and L is the angular momentum. For a triatomic

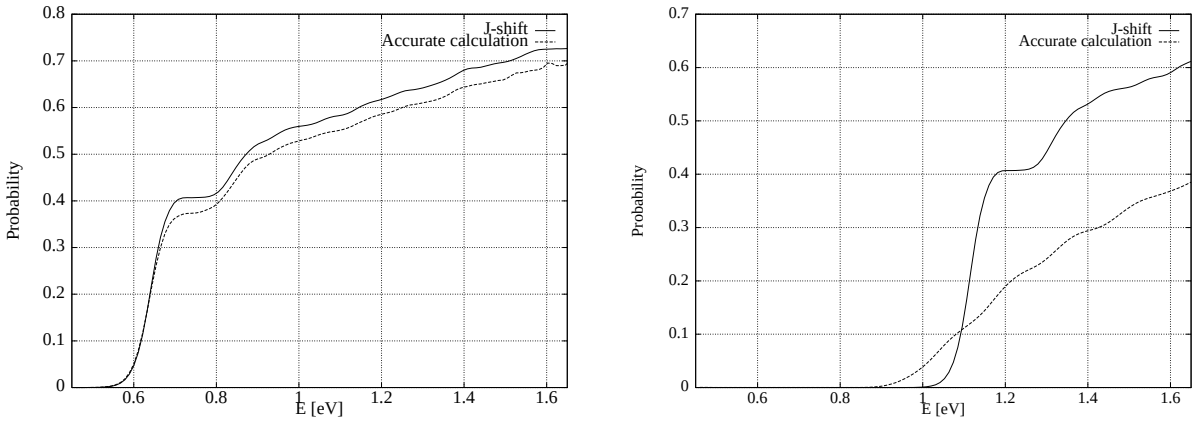

Figure 38: Reaction probabilities $P^J(E)$ for the D+H_2(v=0, j=0) → DH +H reaction: $J = 4$ (left) and $J = 20$ (right). For comparison the J-shift values P^J_{shift} are given in both cases

molecule the complete moment of inertia is given as

$$\mathcal{J} = \mathcal{J}_1 + \mathcal{J}_2 + \mathcal{J}_3. \tag{205}$$

We used this approach to compute the reaction probabilities for $J > 0$, from the reaction probabilities for $J = 0$. At the transition state the distance between the two hydrogen atoms is 1.75 a_0. The D atom is at 3.55 a_0 distance from the first H atom and at 1.8 a_0 from the second.

The total reaction cross section within the J-shift model was computed and the results are presented in Figure 39.

For $J = 4$ and $J = 20$ a comparison between the calculated reaction probabilities and the J-shift values is given in Figure 38. The shift in energy is estimated correctly but the values are overestimated in the high energy regime. In the energy domain $E = [0.85, 1.6]$ eV the same overestimation occurs for the cross section (see Figure 39).

The J-shift reaction rate was computed using Eq. (23). The result is presented in Figure 40.

6.1.9 Summary on the D+H_2 → DH+H reaction

Accurate calculations of the reaction probabilities using the wavepacket method were performed up to $J = 5$. For higher values a restricted number of Ω channels was used to describe the wavepacket. Together with the reaction rates, total reaction cross sections were computed using the total reaction probabilities. For comparison also the J-shift cross sections and reaction rates were computed. For high J the computing time is ca. 30 hours/$P^J(E)$ computation on the IBM-SP2 machines.

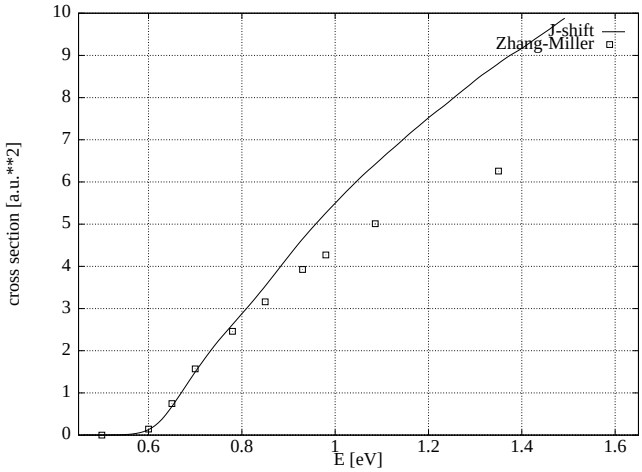

Figure 39: The total reaction cross section for the D+H_2(v=0, j=0) → DH +H reaction computed within a J-shift approximation frame. For comparison the time-independent values of Zhang and Miller [76] are given.

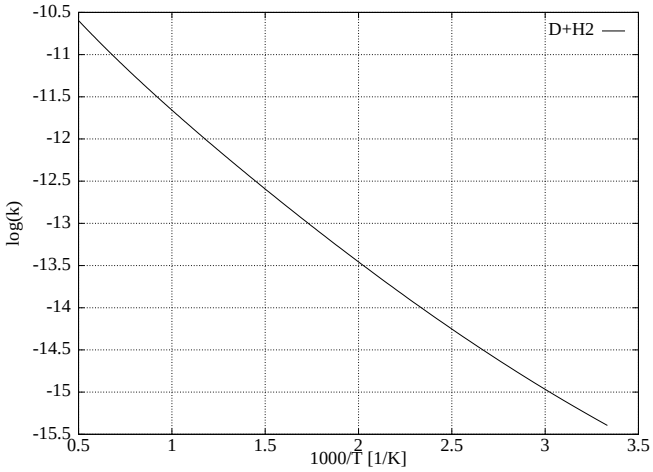

Figure 40: The D+H_2(v=0, j=0) → DH +H reaction. The reaction rate computed within a J-shift approach. We plot the $log_{10}(k)$ versus 1000/T, T is the temperature in K.

6.2 The H+H_2 → H_2 +H reaction

The LSTH potential energy surface [85] was used to describe the reaction H+$H_2(v = 0, j = 0)$ →H_2 +H. Compared with the reaction probability for D+ $H_2(v = 0, j = 0)$ →HD +H reaction, the curve in Figure 41 displays more structure (small resonances about 0.9 eV and 1.2 eV).

6.2.1 *J*-shift calculations

The total reaction cross section for the H+ $H_2(v = 0, j = 0)$ → H_2 +H reaction was estimated by using the *J*-shift approach. As discussed above we expect these results to be overestimated in the high energy regime E = [1.0, 1.65] eV. The results are plotted in Figure 42.

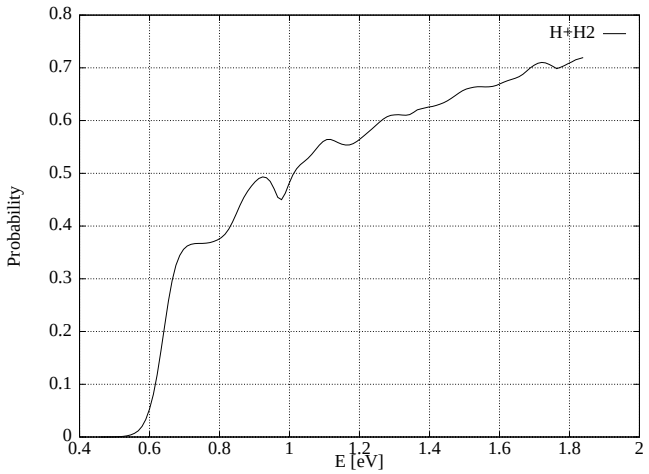

Figure 41: The total reaction probability for the H+H_2(v=0, j=0) → H_2 +H (J = 0) reaction is given.

The reaction rate can be computed by making use of the values plotted in Figure 42 (see Eq. (23)). Figure 43 shows a comparison between the reaction rates of H +H_2(v=0, j=0) → H +H_2 and D+H_2(v=0, j=0) → DH + H. The comparison with the experimental values is given in Table 8. The agreement between the *J*-shift calculations for H + H_2 and the experimental values is not as good as in the case of the D + H_2 calculations.

6.2.2 Summary on H+H_2 → H_2 +H reaction

H+H_2 → H_2 +H is a direct-type reaction for which total cross sections and reaction rates were computed. Although the cross sections are computed within a *J*-shift approach, they give a good qualitative picture of the reaction processes. For the reaction probability $P^{J=0}(E)$ the computing time is rather modest (3 hours for an IBM 43P machine).

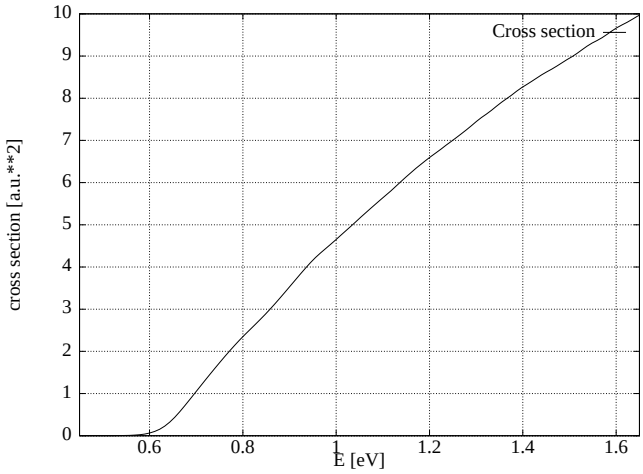

Figure 42: Total cross section for the H+H_2 (v=0, j=0) → H_2 +H reaction computed using the J-shift approach.

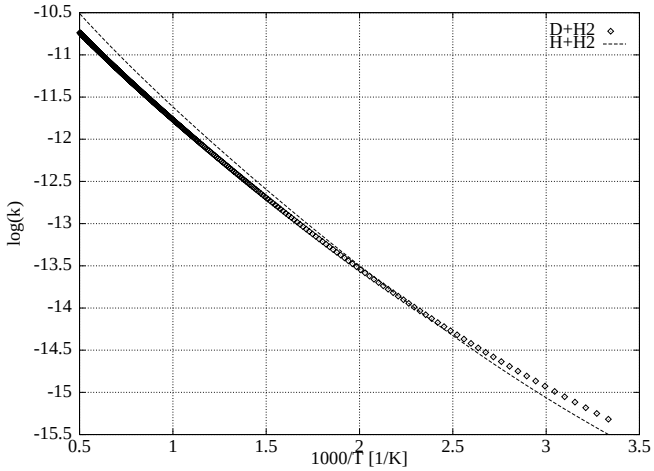

Figure 43: The reaction rate computed using the J-shift approach for the H + H_2 (v=0, j=0) → H_2 + H reaction. The squares (⋄) are the values computed for the D+H_2(v=0, j=0) → DH +H reaction (see Figure 30).

6.3 The $H^+ + H_2 \rightarrow H_3^+ \rightarrow H^+ + H_2$ reaction

6.3.1 Charge transfer and nonadiabatic processes

The foundation of modern quantum chemistry is the Born-Oppenheimer approximation according to which nuclei move on a single adiabatic potential energy surface. However nonadiabatic events are not so rare. Nonadiabatic events occur, for example, in the mechanism of vision and of photosynthesis, and more generally, in photodissociation, predissociation, charge transfer, and spin-changing reactions [65].

Charge transfer belongs to the broader class of collision processes involving transitions between two or more potential hypersurfaces. These transitions usually occur in well defined regions of configuration space where the diabatic potential energy surfaces cross and where the Born-Oppenheimer approximation breaks down. Such crossing processes occur in reactive or nonreactice collisions of open shell systems and in most ion-molecule collisions [109]. For a theoretical study of such systems, a knowledge of the different PES's is required. The dynamics accounts for the transition from one surface to the next.

For the $H^+ + H_2$ system differential cross sections have been determined in a broad energy range [110] . The possible channels are

$H^+ + H_2(v_i = 0) \rightarrow H_3^+ \rightarrow H^+ + H_2(v_f), \ \Delta E = 0,$

$H^+ + H_2(v_i = 0) \rightarrow H_3^+ \rightarrow H + H_2^+(v_f), \ \Delta E = 1.83$ eV.

According to Niedner *et al.* [110], a simplified dynamical model for charge transfer on the collinear H_3^+ can be resumed in two steps:

- Step 1: the reactants ($H^+ + H_2(v_i = 0)$) come close to each other; this leads to vibrationally excited H_2.
- Step 2: vibrational excitation on the lower $H^+ + H_2$ surface is followed by charge transfer for only those H_2 molecules which are excited vibrationally high enough ($v_f \geq 4$) to overcome the reaction barrier ($\Delta E = 1.83$ eV).

6.3.2 The H_3^+ ion

At equilibrium, the H_3^+ molecule is an equilateral triangle. The energy of formation, $H^+ + H_2$, is $E_0 \approx 4.8$ eV. The H_3^+ molecule is with 0.3 eV more tightly bound than H_2.

The infrared spectral line of H_3^+ was measured for the first time by Oka in 1980 [115]. Until 1987 only the fundamental bands of H_3^+ and its isotopomers (D_3^+, H_2D^+ and D_2H^+) had been characterized [116] resulting from experimental difficulties. H_3^+ ions are produced in a discharge cell [115]. Because H_3^+ is a fairly floppy molecule, it undergoes large-amplitude vibrational motions to such an extent that the rovibrational spectrum does not conform to many of the standard rules of spectroscopy. Using the traditional spectroscopic

approach (the harmonic oscillator model) it is difficult to predict rovibrational transitions. Therefore, theoretical studies are needed.

Many people have investigated the ro-vibrational spectrum of H_3^+: Tennyson and Sutcliff [117, 118], Jaquet *et al.* [79], Jaquet [119], Polyansky *et al.* [120] and others.

H_3^+ in the Interstellar Medium

Between visible, hot stars are vast clouds of generally cold, dark gas. Collectively, these clouds are referred to as the interstellar medium (ISM) [116]. The ISM is mainly composed of hydrogen with small amounts of heavier elements. The temperatures are typically between 10 and 100 K. In diffuse clouds the density vary from 100 particles per cubic centimeter, to 10000 particles per cubic centimeter in "dense" clouds [116]. The ISM is continuously subject to ionizing radiation in the form of cosmic rays and photons. These interact initially to ionize molecular hydrogen:

$$H_2 \rightarrow H_2^+ + e,$$

which then reacts rapidly with more hydrogen:

$$H_2 + H_2^+ \rightarrow H_3^+ + H.$$

All this justifies the attempts of detecting the H_3^+ in the interstellar space. In addition, H_3^+ was detected in the atmosphere of Jupiter in 1988-1989 [116].

6.3.3 Investigations with wavepackets

The dynamics has been investigated using the Diatomics In Molecules (DIM) potential of Florescu *et al.* [114].

To compute the PES using the DIM method we have to write the Hamiltonian operator as a sum of operators including only atoms, diatomic molecules, and the interaction terms between them [121]. The Hamiltonian H_{BC} for a diatomic molecule BC is written in its atoms-in-molecules form as

$$H_{BC} = H_B + H_C + V_{BC}. \tag{206}$$

H_B and H_C contain all kinetic energy operators and all intraatomic potential energy terms for atoms B and C. V_{BC} is the term responsible for all the interactions between B and C.

In the same manner, we can write the diatomics in molecules Hamiltonian as

$$H = \sum_i \sum_{i<j} H_{ij} - (N-2) \sum_i H_i, \tag{207}$$

where the indices i and j label the "N" atoms in the molecule (A, B and C in the case of a triatomic molecule). H_{ij} are the Hamiltonians for different diatomics in the system and H_i are the Hamiltonians for the atoms in the system. This expression of the Hamiltonian

contains explicitly no "interaction" operators, but only hamiltonians for the constituent diatomic molecules and atoms.

For an ABC system the DIM method consists in considering the possible products of electronic states of AB with electronic states of C (and similarly of BC with those of A, and of AC with those of B). The resulting set of states is used as a basis set in which the electronic Hamiltonian, given in Eq. (207), is diagonalized.

The "input" in the DIM method are the potential energy curves for all "relevant" AB, BC and AC states. For each nuclear configuration the matrix representation of the DIM Hamiltonian in this basis set is diagonalized. With the resulting set of energies the PES of the ABC system is then build up.

Initial states of the diatomics

In order to do the analysis we have to take into account the diatomic states of the H_2 and H_2^+ molecules. The propagation is performed using the diabatic representation of the two PES. The autocorrelation function of the propagated wavepacket with the diatomic states of the H_2^+ molecule (Eq. (152)) can be used to compute the charge transfer probability (see Eq. (154)). The analysis is done in the reactant channel - see Figure 6.

To test the implementation a set of rather modest grid parameters were chosen in the beginning (see Table 10). By following the mechanism of the reaction described by Niedner *et al.* [110] (see the introduction of this subsection) we included in the initial wavepacket 60 eigenfunctions of the H_2 molecule to describe the $v = 4, j = 0$ ro-vibrational state. 50 eigenfunctions of H_2^+ were taken into account. The value of the zero point energy level and those for the first 4 ro-vibrational excited levels for H_2 and for H_2^+ are given in Table 9. For comparison, the same 5 levels of the LSTH potential are given. For the DIM - PES the difference between the zero points energy levels of (H_2 + H^+) and (H_2^+ + H) in the asymptotic region (e.g. R large) is about 0.067074 a.u. = 1.825 eV.

If we plot the potential energies corresponding to H_2 (for distant H^+) and to H_2^+ (for distant H) we have the situation presented in Figure 44. These curves cross at $r \approx 2.5$ a_0 in the diabatic representation. In the adiabatic representation we have an avoided crossing at this point. Due to strong coupling in the interaction region (see Figure 45 D) a charge transfer reaction $H^+ + H_2 \rightarrow H_2^+ + H$ (Tully and Preston [113]) can happen.

The grid parameters used in the calculations are given in Table 10. The values $R_{min} =$ 0.5 a.u. and $r_{min} = 0.5$ a.u. are the smallest values where the fit is accurate. The values R_{max} and r_{max} given in Table 10 were set to values which allows us to obtain a qualitative description of the wavepacket dynamics, when the number of grid points is not to large. The notations are the same as those in **Section 4** - for the grid parameters used in D + H_2 reaction. In addition, ΔR_{abs} and Δr_{abs} define the width of the absorbing area at the end of the grid.

H_2^{LSTH}		H_2^{DIM}		$H_2^{+\ DIM}$	
E_n^1 [eV]	E_n^1 [cm^{-1}]	E_n^2 [eV]	E_n^2 [cm^{-1}]	E_n^3 [eV]	E_n^3 [cm^{-1}]
0.270	2179.83	0.286	2309.40	2.111	17030.28
0.285	2298.32	0.301	2427.59	2.119	17088.23
0.314	2534.23	0.330	2662.97	2.133	17203.27
0.358	2885.39	0.374	3013.52	2.154	17375.17
0.415	3348.70	0.431	3476.63	2.182	17602.02

Table 9: The zero point energy and the first 4 excited levels for the H_2 and H_2^+ molecules are given. The results are presented as follows: first and second columns - the energies E_n^1 for the H_2 molecule using the LSTH potential; third and fourth columns - the energies E_n^2 for the H_2 molecule using the DIM potential; fifth and sixth columns - the energies E_n^3 for the H_2^+ molecule using the DIM potential.

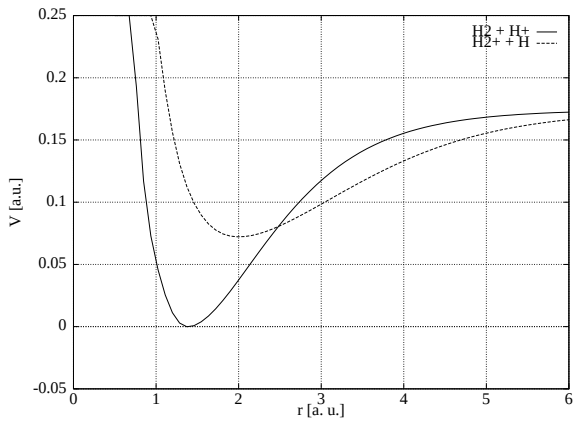

Figure 44: Potential curves of the ground states of H_2 and H_2^+ showing the crossing at $r \approx 2.5\ a_0$.

$R =$	0.5 - 10.5 a_0
$r =$	0.5 - 6 a_0
$N_R =$	64
$N_r =$	64
$N_\theta =$	32
$\Delta R_{abs} =$	2.0 a_0
$\Delta r_{abs} =$	2.0 a_0
$\sigma =$	0.25 a_0

Table 10: Grid parameters used for the test calculations on the $H^+ + H_2$ charge transfer reaction.

The 3D representations for the ($H^+ + H_2$) and the ($H + H_2^+$) PES and for the coupling V_{12} are given in Figure 45. The 3D representations of the potential surfaces in the adiabatic representation are given in Figure 46. The adiabatic results are calculated by diagonalising the matrix

$$\begin{pmatrix} V_1^{diabatic} & V_{12} \\ V_{12} & V_2^{diabatic} \end{pmatrix}$$

at each grid point R_i, r_j, θ_k. $V_1^{diabatic}$, $V_2^{diabatic}$ are the values of the two diabatic potentials at the given grid point and V_{12} is the coupling term. The lower eigenvalue was assigned to $V_1^{adiabatic}$ and the upper one to $V_2^{adiabatic}$.

At time $t = 0$ a.u. the wavepacket was located on the ($H^+ + H_2$) PES (diabatic representation). The collision energy was set to $E_{col} = 2$ eV, to allow energetically the transfer of the wavepacket from the ($H^+ + H_2$) surface to the ($H + H_2^+$) surface.

For the collinear configuration of the three atoms several pictures showing the dynamics of the wavepacket are given in Figures 48 and 50. For the collision angle $\theta_{col} = \pi/2$ the pictures showing the dynamics of the wavepacket are given in Figures 49 and 51. Figures 48 and 49 depict the evolution of the wavepacket on the lower surface (corresponding to $H^+ + H_2$). For both configurations we see no significant components of the wavepacket in the reactive channel. After the collision the wavepacket loses his coherency. At later time ($t > 1500$ a.u.) small resonances are present in the interaction region.

Figures 50 and 51 depicts the evolution of the wavepacket on the upper surface ($H + H_2^+$). Reactive and inelastic components of the wavepacket exist. Some resonances are present after time $t = 1500$ a.u.. After time $t \approx 400$ a.u. the wavepacket is located in the interaction region and the norm of the upper component of the wavepacket (($H + H_2^+$) potential) reaches a maximum of ≈ 0.35 (see Figure 47). After time $t = 1000$ a.u. the norm decreases, caused by absorption (see Figure 47). The norm of the wavefunction on

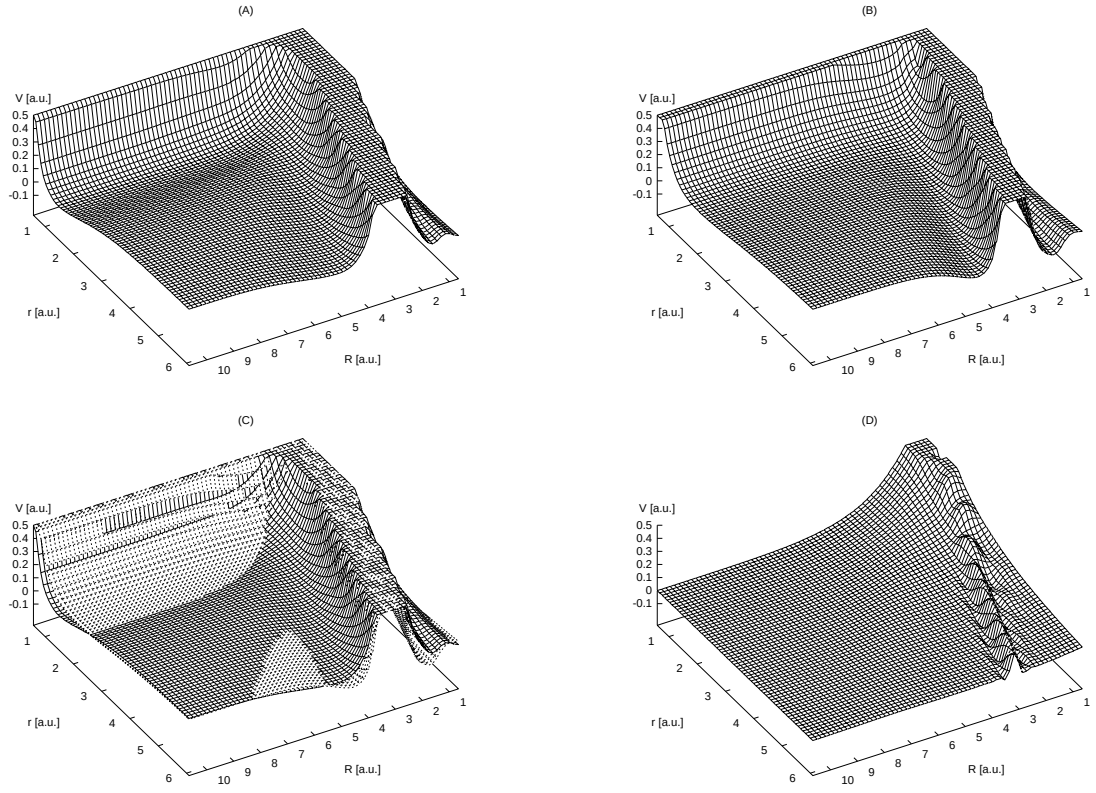

Figure 45: For collinear geometry the potential energy surfaces for the $H^+ + H_2$ (A) and $H + H_2^+$ (B) systems are plotted. The negative values of $V_{coupling}$ are given in picture D. Picture C shows the crossing of the first two PES. The cutoff for the potential (see Eq. (55)) was 0.5 E_h.

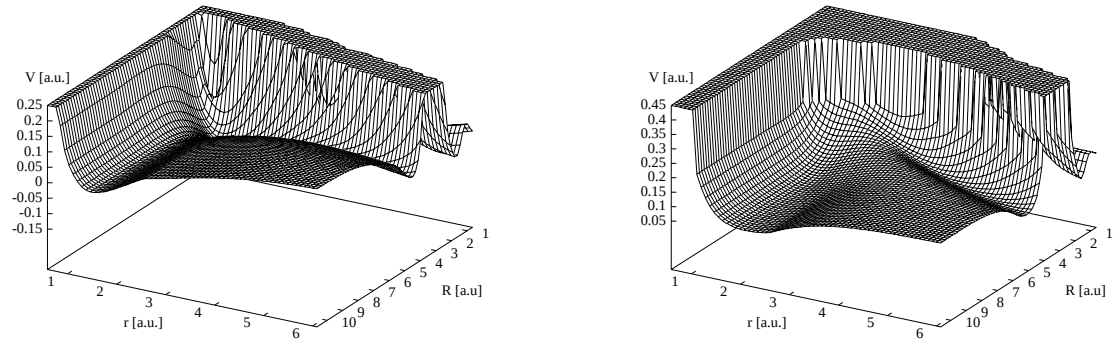

Figure 46: For collinear configuration the potential energy surfaces for adiabatic representation of the $H^+ + H_2$ (left) and $H + H_2^+$ (right) reactions are shown. V_{cutoff} ($H^+ + H_2$) = 0.25 E_h; V_{cutoff} ($H + H_2^+$) = 0.45 E_h.

the upper surface is always smaller than on the lower surface.

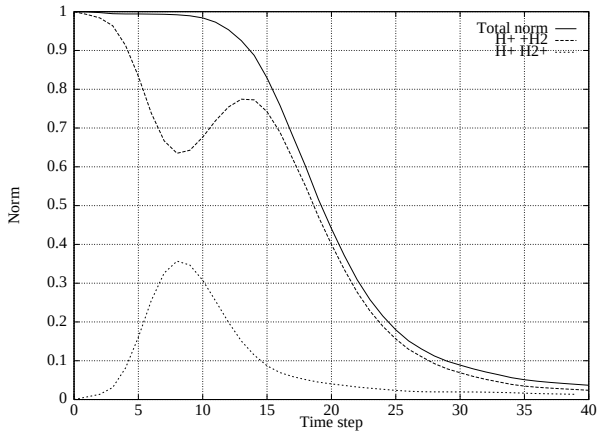

Figure 47: The evolution of the norm for the wavepacket is given, describing the $H^+ + H_2$ (v=0, j=0) $\rightarrow$ H + H_2^+ charge transfer reaction. The norm for the two components of the wavefunction (($H^+ + H_2$) PES and (H + H_2^+) PES, respectively) and the total norm of the wavepacket are given. The time step of the propagation was t =50 a.u..

By comparing the Figures 48 and 50 or 50 and 51, respectively, we can see that the shape of the wavepacket at different moments during the propagation is roughly independent of the collision angle. This is in agreement with the fact that (Levine, Bernstein [34]) there is no preferential orientation for the $H^+ + H_2 \rightarrow H_3^+ \rightarrow H + H_2^+$ reaction.

6.3.4 Summary on H_3^+

Wavepacket investigations were performed for the charge transfer reaction ($H^+ + H_2$) (see page 87).

For the simulation of the wavepacket dynamics the DIM PES of Florescu, Sidis and Sizun [114] was used. The simulation of the dynamics was done at E_{col} = 2 eV. The CPU-time for the complete simulation (J = 0) is $\approx$ 10 hours on an IBM 43P work station.

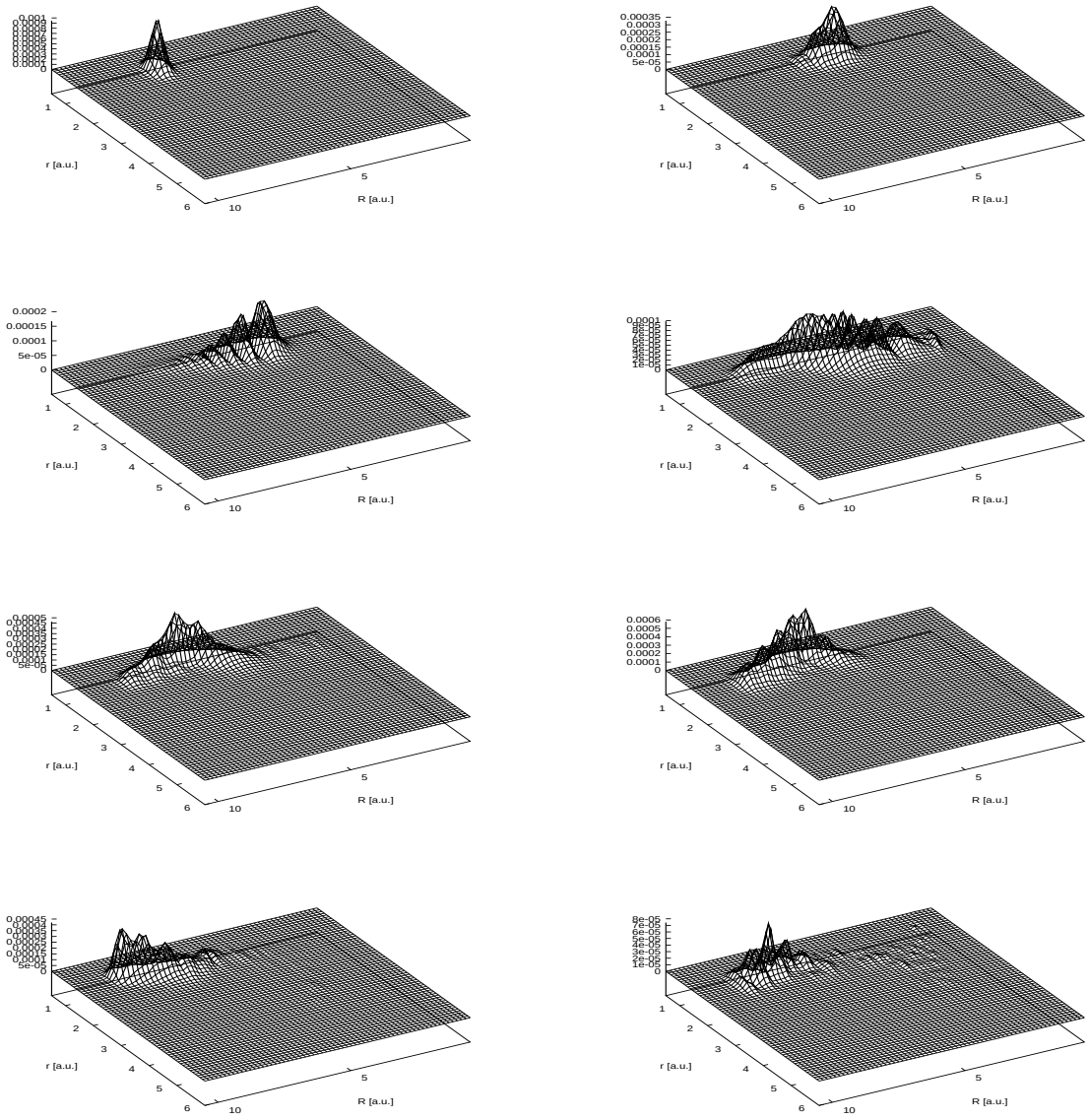

Figure 48: $|\psi|$ during the $H^+ + H_2$ (v=0, j=0) $\rightarrow H^+ + H_2$ scattering is given for the collision angle $\theta_{col} = 0$. Pictures are taken at time t = 50, 250, 400, 550, 700, 800, 1100, 1500 a.u. (E_{col} = 2 eV, DIM potential energy surface [114]). The initial position of the wavepacket was at R_0 =8 a_0.

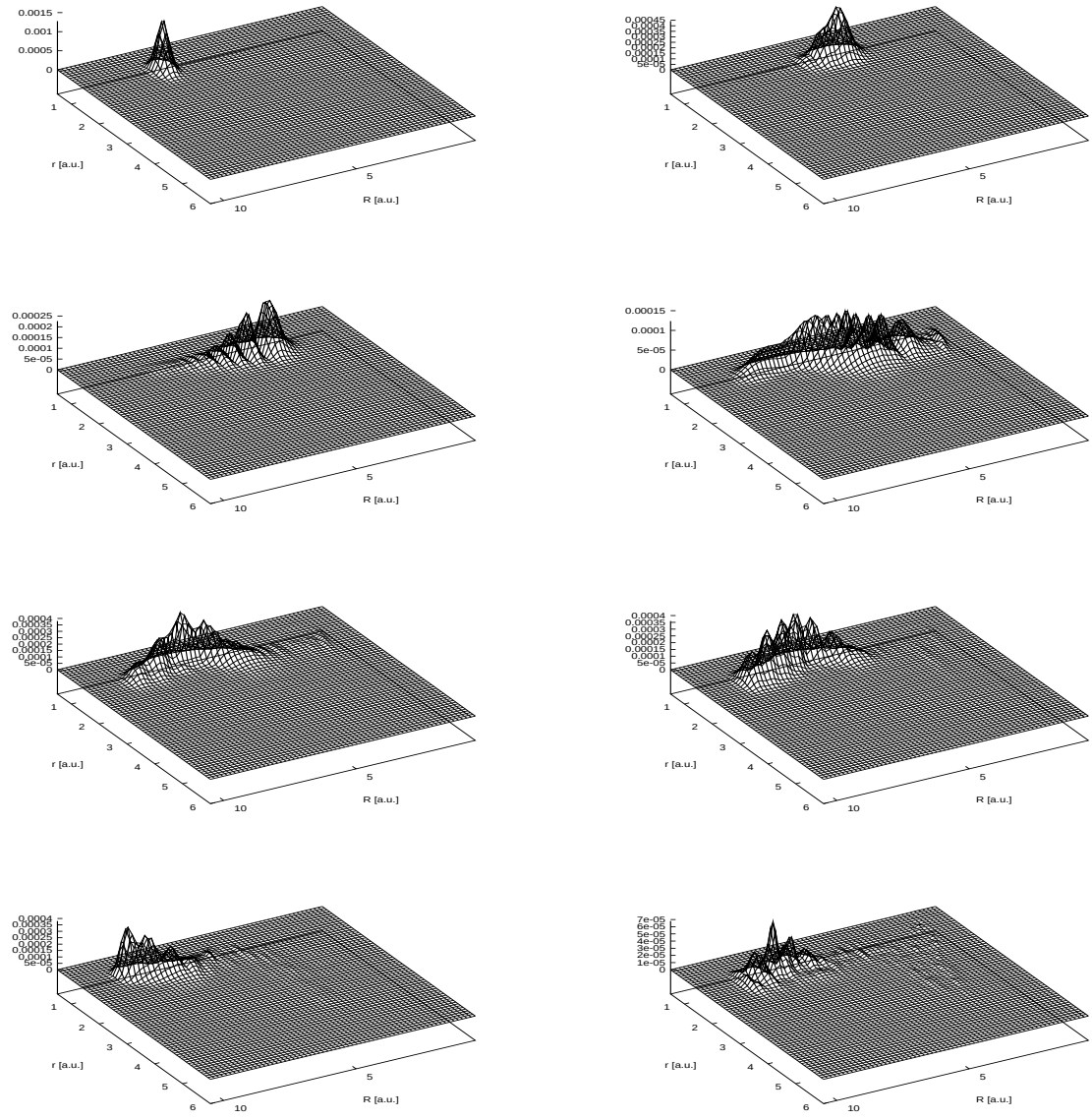

Figure 49: The same information as in Figure 48 is presented ($\theta_{col} = \pi/2$, DIM potential energy surface [114]).

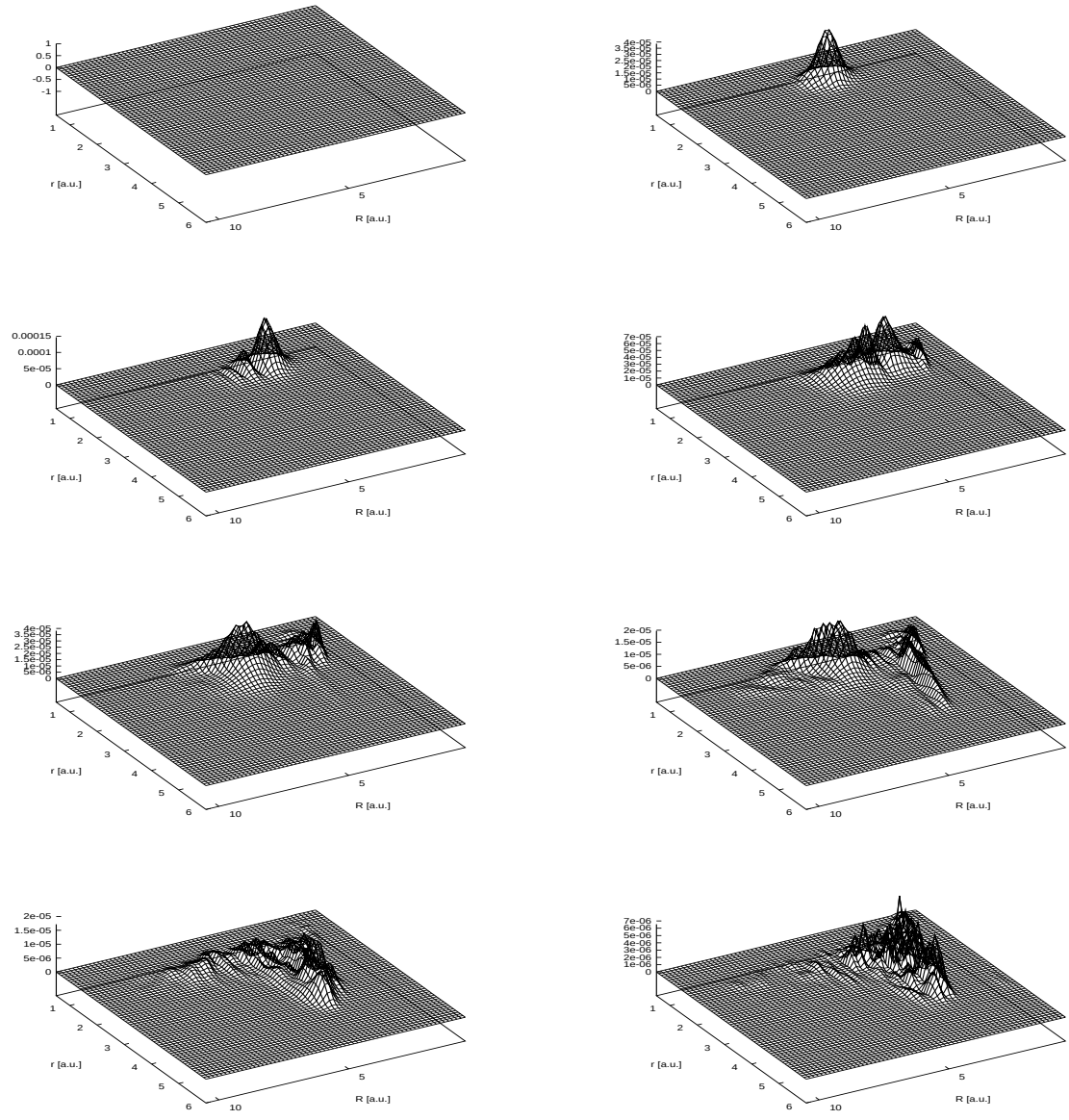

Figure 50: $|\psi|$ during the $H^+ + H_2(v{=}0,\ j{=}0) \rightarrow H + H_2^+$ scattering is given ($\theta_{col} = 0$). Pictures are taken at time t =50, 250, 400, 550, 700, 800, 1100, 1500 a.u. ($E_{col} = 2$ eV, DIM potential energy surface [114]).

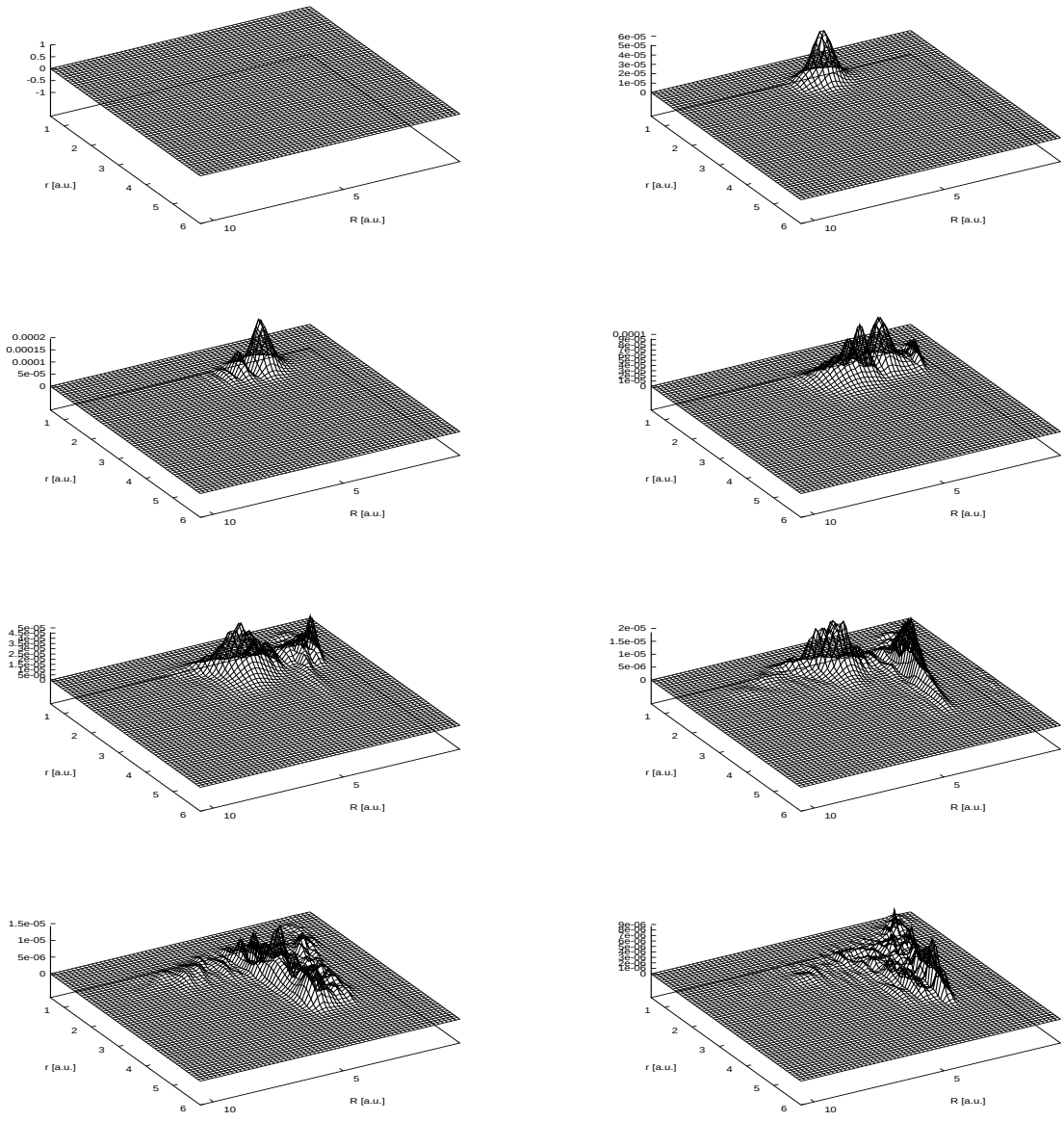

Figure 51: The same information as in Figure 50 is presented ($\theta_{col} = \pi/2$, DIM potential energy surface [114]).

7 Summary

The chemical dynamics of A-BC type reactions has been investigated using time-dependent methods. The purpose was to compute reaction cross sections and reaction rates starting from ab initio potential energy surfaces.

According to **Section 2**, these calculations involve computations of the reaction probabilities for different total angular momenta J of the system. Since J is a good quantum number in this case, the problem can be devided into separate "J" independent calculations of reaction probabilities.

The formalism for time-dependent methods for the investigation of scattering processes was presented in **Section 3**. The particular form of these methods for A-BC systems is exposed in **Section 4** together with a discussion of several possible implementations.

Section 5 describes the implementation of the code. Optimization includes a parallel version of the program. The computer system used for the implementation was an IBM-Power-PC. The parallel version was used on the IBM-SP2 cluster of the Computer Center of Karlsruhe University. The test reaction was D+$H_2(v = 0, j = 0)$ →DH +H using the LSTH potential [85].

Accurate and approximate calculations of cross sections are presented in **Section 6**. Comparison of calculations with different levels of accuracy lead to the following conclusions:

(a) - the time-dependent methods are well suited for systems which do not involve a strong, attractive interaction.

(b) - for ionic systems [79] a special treatment of the propagation may be required (filter diagonalisation).

(c) - a parallel implementation may be required in the $J > 0$ calculations when the propagation time can be very long.

The dynamics of systems - with a small well or barrier - can be relatively easy described up to $J = 5$ resulting in a good accuracy (no approximations). The limitation to $J = 5$ comes mainly from the restrictions imposed by the amount of core memory needed for high J calculation. Approximations like truncating the number of Ω channels can be accepted as long as only the total cross section is computed. If one wants to compute the total differential cross section, the coupling between low and high Ω channels cannot be neglected. Also the J-shift approach of Bowman [38] can be used successfully to compute reasonable accurate cross sections and reaction rates starting only with the reaction probabilities for the $J = 0$ case.

Total reaction cross sections for D+$H_2(v = 0, j = 0)$ → DH +H were computed at

a level of accuracy comparable with previous time-independent calculations [76] (see **Section 6** for details). From these cross sections reaction rates were computed for the temperature range T = 300 - 2000 K. Together with the animation of the wavepackets plotted at different time steps during the propagation, cross sections and reaction rates can mediate a *simulation* of scattering experiments.

A new computer program was set up; it performs the simulation of chemical dynamics for A-BC systems. The only "input" data needed for these simulations are the basic physical constants (the masses of atoms, the collision energy) and its potential energy surface. The results of the simulation include information about the flow of the reaction, reaction probabilities, cross sections and reaction rate constants.

8 Appendix

1. Chebyshev polynomials [51]

The real Chebyshev polynomials [10] $\Phi_n(x)$ can be defined through the *generating function*

$$\frac{1-t^2}{1-2xt+t^2} = \Phi_0(x) + 2\sum_{n=1}^{\infty} \Phi_n(x)t^n, \quad |x| \leq 1,\ |t| < 1.$$

The $\Phi_n(x)$ satisfy the recurrence relation

$$\Phi_{n+1}(x) - 2x\Phi_n(x) + \Phi_{n-1}(x) = 0$$

with initial conditions

$$\Phi_0 = 1, \ \ \Phi_1 = x.$$

The orthogonality is given by

$$\int_{-1}^{1} \Phi_m(x)\Phi_n(x)(1-x^2)^{-1/2}dx = \begin{cases} 0, & m \neq n \\ \pi/2, & m = n \neq 0 \\ \pi, & m = n = 0 \end{cases}$$

The first five polynomials are

$$\Phi_0(x) = 1,$$

$$\Phi_1(x) = x,$$

$$\Phi_2(x) = 2x^2 - 1,$$

$$\Phi_3(x) = 4x^3 - 3x,$$

$$\Phi_4(x) = 8x^4 - 8x^2 + 5x.$$

2. Associated Legendre functions [51]

The associated Legendre functions $P_n^m(x)$ can de defined through the *generating function*

$$\frac{(2m)!(1-x^2)^{m/2}}{2^m m!(1-2tx+t^2)^{m+1/2}} = \sum_{s=0}^{\infty} P_{s+m}^m(x)t^s.$$

The recurrence relation for the associated Legendre functions is

$$(1-x^2)^{1/2}(P_n^m)' = \frac{1}{2}P_n^{m+1} - \frac{1}{2}(n+m)(n-m+1)P_n^{m-1}.$$

The orthogonality is given by

$$\int_{-1}^{1} P_p^m(x)P_q^m(x)dx = \frac{2}{2q+1}\frac{(q+m)!}{(q-m)!}\delta_{p,q}$$

[10] These are the definitions for the Chebyshev polynomials of first kind.

$$\int_{-1}^{1} P_n^m(x) P_n^k(x)(1-x^2)^{-1}dx = \frac{(n+m)!}{m(n-m)!}\delta_{m,k}$$

First few associated Legendre functions are

$$P_1^1(x) = (1-x^2)^{1/2} = sin(\theta),$$

$$P_2^1(x) = 3x(1-x^2)^{1/2} = 3cos(\theta)sin(\theta),$$

$$P_2^2(x) = 3(1-x^2) = 3sin^2(\theta),$$

$$P_3^1(x) = \frac{3}{2}(5x^2-1)(1-x^2)^{1/2} = \frac{3}{2}(5cos^2(\theta)-1)sin(\theta),$$

$$P_3^2(x) = 15x(1-x^2) = 15cos(\theta)sin^2(\theta),$$

$$P_3^3 = 15x(1-x^2)^{3/2} = 15sin^3(\theta).$$

The relation with Legendre polynomials ($P_l(x)$ $(x = cos(\theta))$) is given by

$$P_l^0(x) = P_l(x),$$

$$(1-x^2)^{\frac{m}{2}}(P_l(x))^{(m)} = P_l^m(x), \quad m > 0.$$

3. The 1D Hamiltonian FORTRAN code for the 2-PES coupling

```
      subroutine ham1(psi,w3,v,akx2,iham,npoinx,npprd,idim3,rw1,rw2,
     +                idim4,icount,work, npot)
c
      implicit          double precision (a-h,o-z)
      include 'common.h'
      common/asbs/as,bs,emaxg,dele,eming
c
c This subroutine computes the action of hamiltonian on psi.
c psi - initial wavefunction
c w3 - the hamiltonian of psi (H|psi>) for a given PES
c work - work field with the same dimension as psi
c npot - number of PES
c npoinx - nr. of grid points in x
c npprd - total nr of grid points (if 2d or 3d problems are computed)
c----67--1---------2---------3---------4---------5---------6---------7-2--c
c
      integer           npoinx,npoiny,npprd,npnz,iham,icount
      integer           idim3,idim4,bigj, i,ind,idl,itime
```

```
      double precision  v(npprd, npot), v1(npprd), wnorm(omega)
      complex*16        psi(npprd,npot), psi1(npprd),w31(npprd)
      complex*16        work(npprd, npot), akx2(npoinx)
c
      data              idl/1/
      save idl
c
c Main loop on all the PES:
c
      do 1234 J=1, npot
c
C 'Diagonal' terms: hampsi on each independent PES
c (hamil3 subroutine= 1D FFT + potential action on the w.f.)
c
      do i=1, npprd
        v1(i)=v(i,j)
        psi1(i)=psi(i,j)
      enddo
      call hamil3(psi1,w31, v1,akx2,npoinx,
     +            npprd,
     +            work, as,bs)
c
c The coupling subroutine between psi and w3:
c
       call coupl(psi,w3,as,npoinx, npot,j)
c
c Scaling for the Chebychev recursion:
c
       do 350 i=1, npprd
          w31(i)=as*w31(i)
350    continue
c
      do i=1, npprd
        w3(i,j)=w3(i,j)+w31(i)
      enddo
1234   continue
c
```

```
      idl=0
 9090 format (1x,A)
      return
      end
c
      subroutine coupl(psi,w3,as,npoinx,npot,j)
      include 'common.h'
      implicit double precision(a-h, o-z)
      complex*16 psi(npoinx, npot), w3(npoinx, npot)
c
c psi - wavefunction, with two components
c w3 - collect the action of the coupling on the psi
c npoinx -nr. of points in 'x' grid
c npot - nr. of PES
c j - index of the PES which is coupled (1 or 2)
c
c Test 1: gaussian coupling between psi and w3
c
        if(j.eq.1) k=2
        if(j.eq.2) k=1
c
c To choose gausian coupl. comment this line, else, dipol coupling
c
       goto 500
       x0=4.d0
       x=xanf-dx
c
      do i=1, npoinx
        x=x+dx
        dtx=x-x0
        hcp=zcemax*exp(-dtx*dtx)
c      write(17, *) i, hcp, x
        w3(i,j)=hcp*psi(i,k)
      enddo
      goto 1000
500   continue
c
```

```
c TEST 2: electric field coupling  E=zmax*x between psi and w3
c
      x0=4.d0
      x=xanf-dx
      x1=6.d0
      do i=1, npoinx
         x=x+dx
         if(x.gt.x0.and.x.lt.x1) then
         hcp=zcemax*(x-x0)
         else
         hcp=0.d0
         endif
       w3(i,j)=hcp*psi(i,k)
      enddo
1000  continue
c
        return
        end
```

4. The subroutines used for communication between nodes in the parallel version of WAVE program

```
        subroutine gatter(xfeld, nx,ny,ipoint, icontext, nnodes, iam)
        implicit double precision (a-h, o-z)
        complex*16 xfeld(nx,ny)
c
c This subroutin collects the array from processor having the ID larger than
c 1, to the processor 0 in the parallel context
c      xfeld - 2d array, dimensions are nx and ny
c      icontext, nnodes, iam - define the paralle context: index of context
c               total number of nodes and the node of this processor
c      ipoint - is the pointer were the array must be collected
c
        do ii=1, nnodes-1
        if(iam.eq.ii) then
        iii=ipoint*ii+1
c
c This line sends the vectors from node 0 to all nodes. xfeld(1,1)
```

```
c is the starting point of sending from node zero
c nx is the length  of the transmitted vector
c first zero - is the index of array in the processor grid - in this case
c we have a linear processor grid with just a single line
c last zero is the index of precessor who send the vectors to other
c processors
c
        call zgesd2d(icontext,nx,ipoint,xfeld(1,1),nx,0,0)
        endif
        enddo
c
        if(iam.eq.0) then
        do ii=1, nnodes-1
        iii=ipoint*ii+1
c
c This line receives the vectors from the node zero, on all other nodes
c (index 1,2, up nnodes). The array is stored at the pointer 'iii'
c and it is received on the processor index 'ii' -last parameter in the call
c
        call zgerv2d(icontext,nx,ipoint,xfeld(1,iii),nx,0,ii)
        enddo
         endif
        return
        end

        subroutine scatter(xfeld, nx,ny,ipoint, icontext, nnodes, iam)
        implicit double precision (a-h, o-z)
        complex*16 xfeld(nx,ny)
c
c
c This subroutin scatter the arrays from processor having the ID=0 to those
c having the ID.gt.1 in the parallel context
c      xfeld - 2d array, dimensions are nx and ny
c      icontext, nnodes, iam - define the paralle context: index of context
c                total number of nodes and the node of this processor
c      ipoint - is the pointer were the array must be collected
c
```

```
        if(iam.eq.0) then
        do ii=1, nnodes-1
        iii=ipoint*ii+1
c
c This line send the vectors from node 0 to all nodes. xfeld(1,1)
c - is the starting point of sending from node zero
c nx - is the length  of the transmitted vector
c zero - is the index of array in the processor grid - in this case
c we have a linear processor grid with just a single line
c ii -is the index of processor who send the vectors to other
c processors
c
        call zgesd2d(icontext,nx,ipoint,xfeld(1,iii),nx,0,ii)
        enddo
        endif
c
        do ii=1, nnodes-1
        if(iam.eq.ii) then
        iii=ipoint*ii+1
c
c This line receives the vectors on the node zero, form all other nodes
c (index 1,2, up nnodes). The array is stored at the pointer 'iii'
c and it is received on the processor index '0' -last parameter in the call
c
        call zgerv2d(icontext,nx,ipoint,xfeld(1,1),nx,0,0)
        endif
        enddo
        return
        end
```

References

[1] R.Kosloff, "Time-dependent quantum-mechanical methods for molecular dynamics", J. Phys. Chem., **92** 2087 (1988)

[2] D. M. Neumark A. M. Wodtke, G. N. Robinson, C. C. Hayden, K. Shobatake, R. K. Sparks, "Molecular beam studies of the F + D_2 and F +HD reactions", J. Chem. Phys., **82** 3067 (1985)

[3] D. M. Neumark, A. M. Wodtke, G. N. Robinson, C. C. Hayden, Y. T. Lee, "Molecular beam studies of the F +H_2 reaction", J. Chem. Phys., **82** 3045 (1985)

[4] P. Casavecchia, N. Balucani, G.G. Volpi, "Crossed-beam studies of reaction dynamics", Annu. Rev. Phys. Chem., **50** 347 (1999)

[5] M. Dantus, M.Rosker, A.H. Zewail, "Real-time femtosecond probing of "transition states" in chemical reactions", J. Chem. Phys., **87** 2395 (1987)

[6] S. Ruhman, A. Joly, K. Kohler, K.A. Nelson, "Time-resolved observations of coherent molecular vibrational motion and the general occurence of impulsive stimulated scattering", J. Chem. Phys., **86** 6563 (1987)

[7] S. Mukamel, "Multidimensional femtosecond correlation spectroscopies of electronic and vibrational excitations", Annu. Rev. Phys. Chem., **51** 691 (2000)

[8] R. Wyatt, "Quantum wave packet dynamics with trajectories: Application to reactive scattering", J. Chem. Phys., **111** 4406 (1999)

[9] J.D. Doll, "Semiclassical theory of atom-solid-surface collisions: Application to the He-LiF diffraction", J. Chem. Phys., **61** 954 (1974)

[10] R.Massel, R.P. Merril, W.H. Miller, "A semiclassical model for atomic scattering from solid surfaces - He and Ne scattering from W(112)", J. Chem. Phys., **64** 45 (1976)

[11] D. J. Tannor, S. Garashchuk, "Semiclassical calculation of chemical reaction dynamics via wavepacket correlation functions", Annu. Rev. Phys. Chem., **51** 553 (2000)

[12] M. Thoss, WH Miller, G. Stock, "Semiclassical description of nonadiabatic quantum dynamics: application to the S-1-S-2 conical intersection in pyrazine", J. Chem. Phys., **23** 10282 (2000)

[13] E.J. Heller, "Time-dependent approach to semiclassical dynamics", J. Chem. Phys., **62** 1544 (1975)

[14] E.J. Heller, "Wigner phase space method: Analysis for semiclassical applications", J. Chem. Phys., **65** 1289 (1976)

[15] S.Sawada, H. Metiu, "A multiple trajectories theory for curve crossing problems obtained by using a Gaussian wavepacket representation of the nuclear motion", J. Chem. Phys., **83** 227 (1986)

[16] D. E. Manolopoulos in "Encyclopedia of Computational Chemistry", Willey, New York 1998

[17] J. Z. H. Zhang, "Theory and application of quantum molecular dynamics", World Scientific, Singapore 1999

[18] R.D. Levine, "Quantum mechanics of molecular rate processes", Clarendon, Oxford 1969

[19] G. Nyman, H-G. Yu, "Quantum theory of bimolecular chemical reaction", Rep. Prog. Phys., **63** 1001 (2000)

[20] J.Mazur, R.Rubin, "Quantum-mechanical calculation of the probability of an exchange reaction for constrained linear encounters", J. Chem. Phys., **31** 1395 (1959)

[21] E.A. Mc Cullogh Jr., R.E. Wyatt, "Quantum dynamics of the collinear (H,H_2) reaction", J. Chem. Phys., **51** 1253 (1969)

[22] D. Kosloff, R. Kosloff, "A Fourier method solution for the time-dependent Schrödinger equation as a tool in molecular dymanics", J. Comput. Phys., **52** 35 (1985)

[23] J.C.Light, I.P.Hamilton, J.V.Lill, "Generalised discrete variable representation in quantum mechanics", J. Chem.Phys., **82** 1400 (1985)

[24] J.V. Lill, G.A. Parker, J.C. Light, "Discrete variable representations and sudden models in quantum scattering theory", Chem. Phys. Lett., **89** 481 (1982)

[25] A.S. Dickinson, P.R. Certain, "Calculation of matrix elements for one-dimensional quantum mechanical problems", J. Chem. Phys., **49** 4209 (1968)

[26] H. Tal-Ezer, R. Kosloff, "An accurate and efficient scheme for propagating the time-dependent Schrödinger equation", J. Chem. Phys., **81** 3967 (1984)

[27] V. Mandelshtam, H.S. Taylor, "Spectral projection approach to the quantum scattering calculations", J. Chem. Phys., **102** 7390 (1995)

[28] V. Mandelshtam, H.S. Taylor, "A simple recursion polynomial expansion of the Green's function with absorbing boundary conditions. Application to the reactive scattering", J. Chem. Phys., **103** 2903 (1995)

[29] S.K. Gray, G.G. Balint-Kurti, "Quantum dynamics with real wavepackets, including application to three-dimensional ($J = 0$) D + H_2 $\rightarrow$ DH + H reactive scattering", J. Chem. Phys., **108** 950 (1998)

[30] U. Manthe, T. Seideman, W. Miller, "Full-dimensional quantum mechanical calulation of the rate constant for the H_2 + OH $\rightarrow$ H_2O + H reaction", J. Chem. Phys., **99** 10078 (1993)

[31] D. Neuhauser, "Fully quantal initial-state-selected reaction probabilities ($J = 0$) for a four-atom system: H_2 (v=0,1, j=0) +OH(v=0,1, j=0) $\rightarrow$ H +H_2O", J. Chem. Phys., **100** 9272 (1994)

[32] D. Luckhaus, "6D vibrational quantum dymanics: Generalised coordinate discrete variable representation and (a)diabatic contraction", J. Chem. Phys., **113** 1329 (2000)

[33] J.J. Sakurai, "Modern Quantum Mechanics", Addison-Wesley Publishing Company, Inc. (1994)

[34] R.D. Levine, R.B. Bernstein, "Molekulare Reaktionsdynamik", Teubner Studienbücher, Stuttgart (1991)

[35] R.N. Zare, "Angular momentum", John Wiley & Sons, Inc. (1988)

[36] R.G. Newton, "Scattering theory of waves and particles", Springer 1982

[37] R.S. Judson, D.J. Kouri, D. Neuhauser, M. Baer, "Time-dependent wavepacket method for the complete determination of S-matrix elements for reactive molecular collisions in three dimensions", Phys. Rev. A, **42** 351 (1990)

[38] J.M. Bowman, "Reduced dimensionality theory of quantum reactive scattering", J. Phys. Chem., **95** 4960 (1991)

[39] S.K. Gray, C.Petrongolo, K.Drukker and G.C. Schatz, "Quantum wave packet study of nonadiabatic effects in O (^{1}D) + H_2 $\rightarrow$ OH + H", J. Phys. Chem., **103** 9449 (1999)

[40] Kerson Huang, "Statistical Mechanics" (Second edition), John Willey & Sons, Inc. 1987

[41] R. Jaquet, A. Kumpf, M. Heinen, "S-matrix version of the Hultén-Kohn variational principle for quantum reactive scattering using finite elements", J. Chem. Soc. Faraday Trans., **93** 1027 (1997)

[42] R. Jaquet, 'Time-independent scattering theory', Mariapfarr 1999

[43] M. Abramowitz, I. Stegun, "Handbook of Mathematical Functions", Dover Publications Inc.

[44] R.T. Pack, "Space-fixed vs body-fixed axes in atom-diatomic molecule scattering. Sudden approximations", J. Chem. Phys., **60** 633 (1974)

[45] D.J. Kouri, M. Arnold, D.K. Hoffman, "Time-to-energy transform of wavepackets using absorbing potentials. Time-independent wavepacket-Schrödinger and wavepacket-Lippmann-Schwinger equations", Chem. Phys. Lett., **203** 166 (1993)

[46] Y. Huang, W. Zhu, D.J. Kouri, D.K. Hoffman, "A general time-to-energy transform of wavepackets. Time-independent wavepacket-Schrödinger and wavepacket-Lippmann-Schwinger equations", Chem. Phys. Lett., **206** 96 (1993)

[47] N. Balakrishnan, C.Kalyanaraman, N. Sathyamurthy, "Time-dependent quantum mechanical approach to reactive scattering and related processes", Physics Reports, **280** 79 (1997)

[48] R. Kosloff, "Propagation methods for quantum molecular dynamics", Annu. Rev. Phys. Chem., **45** 145 (1994)

[49] A. Erdelyi (Ed.), "Tables of integral transforms", Mc Graw-Hill Book Company, Inc., 1954 (Vol. I)

[50] Brigham, Elbert Oran, "FFT : schnelle Fourier-Transformation", Oldenbourg, 1995

[51] G.B. Arfken, H.J. Weber, "Mathematical Methods for Physicists" - 4-th ed., Academic Press, 1995

[52] D.Neuhauser, M.Baer, R.S.Hudson, D.J. Kouri, "The application of time-dependent wavepacket methods to reactive scattering", Comp. Phys Comunn., **63** 460 (1991)

[53] A.Vibok, G.G.Balint-Kurti, "Parametrization of complex absorbing potentials for time-dependent quantum dynamics", J. Phys. Chem., **96** 8712 (1992)

[54] W.H. Miller, "Recent advances in quantum mechanical reactive scattering theory", Annu. Rev. Phys. Chem., **41** 245 (1990)

[55] A.M. Arthurs, A. Dalgarno, "The theory of scattering by a rigid rotator", Proc. R. Soc. Lond. A, **256** 540 (1960)

[56] C.Leforestier, "Grid representation of rotating triatomics", J. Chem. Phys., **94** 6388 (1991)

[57] H. Margenau, G.M. Murphy, "Die Mathematik für Physik und Chemie", Verlag Harri Deutsch, Frankfurt a.M. und Zürich, 1965

[58] R. L. Whetten, G. S. Ezra, E. R. Grant, "Molecular dynamics beyond the adiabatic approximation: new experiments and theory", Ann. Rev. Phys. Chem., **36** 277 (1985)

[59] R.Heather, H.Metiu, "An efficient procedure for calculating the evolution of the wavefunction by fast Fourier transform methods for systems with spatially extended wavefunction and localized potential", J. Chem. Phys., **86** 5009 (1987)

[60] D. J. Kouri, T. G. Heil, Y. Shimoni, "On the Lippmann-Schwinger equation for atom-diatom collisions: A rotating frame treatment", J.Chem. Phys., **65** 226 (1976)

[61] Y.Sun, R.S.Judson, D.J.Kouri, "Body frame close coupling wavepacket approach to gas phase atom-rigid rotor inelastic collisions", J. Chem. Phys., **90** 241 (1989)

[62] W.H. Miller, "Coupled equations and the minimim principle for collisions of an atom and a diatomic molecule, including rearrangements", J. Chem. Phys., **50** 407 (1969)

[63] G.G. Balint-Kurti, R.N. Dixon, C. C. Marston, "Time-dependent quantum dynamics of molecular photofragmentation processes", J. Chem. Soc. Faraday Trans., **86** 1741 (1990)

[64] A.R. Offer, G.G. Balint-Kurti, "Time-dependent quantum mechanical study of the photodissociation of HOCl and DOCl", J. Chem. Phys., **101** 10416 (1994)

[65] D.Yarkony, "Current issues in nonadiabatic chemistry", J. Phys. Chem., **100** 18612 (1996)

[66] A. J. Meijer, E. M. Goldfield, S. K. Gray, G. G. Balint-Kurti, "Flux analysis for calculating reaction probabilities with real wavepackets", Chem. Phys. Lett., **293** 270 (1998)

[67] A.S. Bracker, E.R. Wouters, A.G. Suits, "Imaging the alignment angular distribution: State symmetries, coherence effects, and nonadiabatic interactions in photodissociation", J. Chem. Phys., **110** 6749 (1999)

[68] G. Golub (Editor), "Recent advances in iterative methods ", Springer, 1994

[69] R. Kosloff, H. Tal-Ezer, "A direct relaxation method for calculating eigenfunctions and eigenvalues of the Schrödinger equation on a grid", Chem. Phys. Lett., **127** 223 (1986)

[70] J. K. Cullum, R. A. Willoughby, "Lanczos Algorithm for Large Symmetric Eigenvalue Computations", Birkhäuser, Boston MA, 1985

[71] D. Neuhauser, "Bound state eigenfunctions from wavepackets: Time $\rightarrow$ energy resolution", J. Chem. Phys., **93** 2611 (1990)

[72] S-W. Huang, T. Carrington Jr., "A comparison of filter diagonalisation methods with the Lanczos method for calculating vibrational energy levels", Chem. Phys. Lett., **312** 311 (1999)

[73] V.A. Mandelshtam, H.S. Taylor, "A low-storage filter diagonalisation method for quantum eigenenergy calculation or for spectral analysis of time signals", J. Chem. Phys., **106** 5085 (1997)

[74] G.J. Kroes, D. Neuhauser, "Performance of a time-independent scattering wavepacket technique using real operators and wavefunctions", J. Chem. Phys., **105** 8690 (1996)

[75] G.J. Kroes, M.R. Wall, J.W. Pang, D. Neuhauser, "Avoiding long propagation times in wavepacket calculations on scattering with resonances: A new algorithm involving filter diagonalization" J. Chem. Phys., **106** 1800 (1997)

[76] J.Z.H. Zhang, W. Miller, "Quantum reactive scattering via the S-matrix version of the Kohn variational principle: Differential and integral cross sections for D $+H_2 \rightarrow$ HD + H", J. Chem. Phys., **91** 1528 (1989)

[77] Johannes Grotendorst (Editor), "Modern methods and algorithms of quantum chemistry", Winterschool 21-25 Feb. 2000 Forschungszentrum Jülich, Germany. Proceedings

[78] W. Cencek, J. Rychlewski, R. Jaquet, W. Kutzelnigg, "Sub-microhartree accuracy potential energy surface for H_3^+ including adiabatic and relativistic effects. I. Calculation of the potential points", J. Chem. Phys., **108** 2831 (1998)

[79] R. Jaquet, W. Cencek, W. Kutzelnigg, R. Rychlewski, "Sub-microhartree accuracy potential energy surface for H_3^+ including adiabatic and relativistic effects. II. Rovibrational analysis for H_3^+ and D_3^+", J. Chem. Phys., **108** 2837 (1998)

[80] Home page of BLACS library: http://www.netlib.org/blacs

[81] P.W. Atkins, "Einführung in die physikalische Chemie", VCH, 1993

[82] J.C. Polanyi, W.H. Wong, "Location of energy barriers. I. Effect on the dynamics of reactions A +BC", J. Chem. Phys., **51**, 1439 (1969)

[83] M.H. Mock, J.C. Polanyi, "Location of energy barriers. II. Correlation with barrier height", J. Chem. Phys., **51** 1451 (1969)

[84] N. Sathyamurthy, J.P. Toennies, "Effect of reagent rotation on the reaction D + $H_2(v = 1) \rightarrow$ DH + H", Chem. Phys. Lett., **143** 321 (1987)

[85] D.G. Truhlar, C.J. Horowitz, "Functional representation of Liu and Siegbahn's accurate ab initio potential energy calculations for H + H_2", J. Chem. Phys., **68** 2456 (1978)

[86] C.W. Bauschlicher Jr., S.R. Langhoff, H.Partridge, "A reevaluation of the H_3 potential", Chem. Phys. Lett., **170** 345 (1990)

[87] A. J. Varandas, F.B. Brown, C.A. Mead, D.G. Truhlar, "A double many-body expansion of the two lowest-energy potential surfaces and nonadiabatic coupling for H_3", J. Chem. Phys., **86** 6258 (1987)

[88] A. D. Walsh, "The electronic orbitals, shapes, and spectra of polyatomic molecules. Part I. AH_2 molecules.", J. Chem. Soc., 2260 (1953)

[89] D.A.V. Kliner, D.E. Adelman, R.N. Zare, "Comparison of experimental and theoretical integral cross sections for D + $H_2(v = 1, j = 1) \rightarrow$ HD$(v' = 1, j')$ +H", J. Chem. Phys., **95** 1648 (1991)

[90] D.A.V. Kliner, K.-D. Rinnen, R.N. Zare, "The D + H_2 reaction: comparison of experiment with quantum-mechanical calculations", Chem. Phys. Lett., **166** 107 (1990)

[91] D.E. Adelman, N.E. Shafer, D.A.V. Kliner, R.N. Zare, "Measurement of relative state-to-state rate constants for the reaction D+ $H_2(v, j) \rightarrow$ HD(v', j') +H", J. Chem. Phys., **97** 7323 (1992)

[92] D. Neuhauser, R.S. Judson, M. Baer, D.J. Kouri, "State-to-state time-dependent wavepacket approach to reactive scattering: State-resolved cross-sections for D + $H_2(v = 1, j = 1, m) \rightarrow$ H + DH(v, j)", J. Chem. Soc. Faraday. Trans., **93** 727 (1997)

[93] A. Jäckle, M.C. Heitz, H.D. Meyer, "Reaction cross sections for the H+ $D_2(v = 0, 1)$ system for the collision energies up to 2.5 eV: A multiconfiguration time-dependent Hartree wavepacket propagation study", J. Phys. Chem., **110** 241 (1999)

[94] S.M. Auerbach, W.H. Miller, "Efficient polynomial expansion of the scattering Green's function: Application to the D + $H_2(v = 1) \rightarrow$ DH +H rate constant", J. Chem. Phys., **100** 1103 (1994)

[95] N.C. Blais, M. Zhao, M. Mladenovic, D. J. Truhlar, D. V. Schwenke, Y. Sun, D. J. Kouri, "Comparison of quasiclassical trajectory calculations to accurate quantum mechanics for state-to-state partial cross sections at low total angular momentum for the reaction D + $H_2 \rightarrow$ DH +H", J. Chem. Phys., **91** 1038 (1989)

[96] D.G. Truhlar, R. E. Wyatt, "History of H_3 kinetics", Ann. Rev. Phys. Chem., **27** 1 (1976)

[97] R.D. Levine, S. Wu, "Resonances in reactive collisions: computational study of the H+ H_2 collision", Chem. Phys. Lett., **11** 557 (1971)

[98] N. Markovic, G.D. Billing, "The coupled three-dimensional wavepacket approach to reactive scattering", J. Chem. Phys., **100** 1083 (1994)

[99] B.C. Garrett, D.G. Truhlar, R.G. Grev, "Comparison of variational transition state theory and the unified statistical model with vibrationally adiabatic transmission coefficients to accurate collinear rate constants for T + HD $\rightarrow$ TH +D", J. Chem. Phys., **73** 235 (1980)

[100] B.K. Kendrick, "Geometric phase effects in the H + $D_2 \rightarrow$ DH + D reaction", J. Chem. Phys., **112** 5679 (2000)

[101] R. Götting, H.R. Mayne, J.P. Toennies, "Molecular beam measurements of differential cross sections for the reaction D+$H_2 \rightarrow$ DH + H at $E_{cm} = 1.0$ eV", J. Phys. Chem., **80** 2230 (1984)

[102] S.K. Gray, E.M. Goldfield, G.C. Schatz, G.G. Balint-Kurti, "Helicity decoupled quantum dynamics and capture model cross sections and rate constants for O (^{1}D) + $H_2 \rightarrow$ OH + H", Phys. Chem. Chem. Phys., **1** 1141 (1999)

[103] Calculations of M. Zhao, D. G. Truhlar, D. W. Schwenke, D. J. Kouri (see [90])

[104] S. C. Althorpe, "Quantum wavepacket method for state-to-state reactive cross sections", J. Chem. Phys., **114** 1601 (2001)

[105] N. C. Blais, D. G. Truhlar, "The final state and velocity distribution of the reaction D + H_2 → DH + H as a function of scattering angle", J. Chem. Phys., **88** 5457 (1988)

[106] John Zhang, private communication, Oct. 2000

[107] A.Aguado, M.Paniagua, M. Lara, O. Roncero, "Quantum study of the Li +HF → LiH + H reaction", J.Chem. Phys., **107** 10085 (1997)

[108] H. Kuhling, "Taschenbuch der Physik". 16 Auflage, Fachbuchverlag Leipzig, 1999

[109] M.Baer, G. Niedner-Schattenburg, J.P. Toennies, "A three-dimensional quantum mechanical study of vibrationally resolved charge transfer processes in H^+ + H_2 at E_{cm} = 20 eV", J. Chem. Phys., **91** 4169 (1989)

[110] G.Niedner, M.Noll, J.P. Toennies, "Observation of vibrationally resolved charge transfer in H^+ + H_2 at $E_{cm} = 20eV$", J. Chem. Phys., **87** 2685 (1987)

[111] A. Ichihara, O. Iwamoto, R.K. Janev, "Cross sections for the reaction H^+ + H_2 (v=0-14) → H + H_2^+ at low collision energies", Journal of Physics B, **33** 4747 (2000)

[112] T.Kusakabe, K. Asakiwa, J.P. Gu, G. Hirsch, R.J. Buenker, M. Kimura, H. Tawara, Y. Nakai, "Charge-transfer processes in collisions of H^+ ions with H_2, D_2, CO and CO_2 molecules in the energy range 0.2-4 keV", Phys. Rev. A, **6206** 2714 (2000)

[113] R.K. Preston, J. C. Tully, "Effects of surface crossing in chemical reactions: The H_3^+ system", J. Chem. Phys., **54** 4297 (1971)

[114] A. Florescu, M.Sizun, V. Sidis, "Theoretical investigations of differential cross sections for vibrational excitation and vibronic charge transfer in H^+ + H_2 collisions", J. Chem. Phys., **99** 7277 (1993)

[115] T. Oka, "Observation of the infrared spectrum of H_3^+", Phys. Rev. Lett., **45** 531 (1980)

[116] S. Miller, J. Tennyson, "H_3^+ in space", Chem. Soc. Rev., **21** 281 (1992)

[117] J. Tennyson, J. R. Henderson, "Highly excited ro-vibrational states using a discrete variable representation. The H_3^+ molecular ion", J.Chem. Phys., **91** 3815 (1989)

[118] J. Tennyson, B. Sutcliffe, "Rovibrational levels of H_3^+ and H_2D^+", Mol. Phys., **51** 887 (1983)

[119] R. Jaquet, "The influence of non-adiabaticity on the nuclear motion in the H_3^+ molecule", Chem. Phys. Lett., **302** 27 (1999)

[120] O.L. Polyansky, J. Tennyson, "Ab initio calculation of the rotation-vibration energy levels of H_3^+ and its isotopomers to spectroscopic accuracy", J. Chem. Phys., **110** 5056 (1999)

[121] F. O. Ellison, " A method of diatomics in molecules. I. General theory and application to H_2O", J. Am. Chem. Soc., **85** 3540 (1963)

[122] C. A. Mead, " The 'nocrossing' rule for electronic potential energy surfaces. The role of time-reversal invariance", J. Chem. Phys., **70** 2277 (1979)

[123] I. N. Levine, "Quantum Chemistry", Prentice Hall, 2000

Acknowledgements

First, I want to express my deep gratitude to Prof. R. Jaquet, my doctor supervisor, for his excellent guidance of my Ph. D. work. I also want to thank Prof. Jaquet for introducing me to the fascinating field of the wavepacket dynamics.

I am grateful to Mr. N. Geers, University of Karlsruhe, for his help during the parallelisation work.

I would like to express my special thanks to Prof. Schwarz and to all his coworkers for the stimulating discussions and for the friendly attitude.

For the financial support I am thankful to the Deutsche Forschungs-Gemeinschaft and to Mr. Moog, Dez. 3 (Graduiertenförderungsgesetz).

I inscribe this modest work to my family and to all the friends I met in Siegen, during the last three years.